REVIEW

Glacial seismology

IOP Publishing Reports on Progress in Physics
Rep. Prog. Phys. **80** (2017) 126801 (39pp) https://doi.org/10.1088/1361-6633/aa8473

Review

Glacial seismology

R C Aster[1] **and J P Winberry**[2]

[1] Department of Geosciences and Warner College of Natural Resources, Colorado State University, CO, United States of America
[2] Department of Geological Sciences, Central Washington University, WA, United States of America

E-mail: rick.aster@colostate.edu and winberry@geology.cwu.edu

Received 18 January 2016, revised 9 July 2017
Accepted for publication 7 August 2017
Published 14 November 2017

Corresponding Editor Professor Michael Bevis

Abstract

Seismic source and wave propagation studies contribute to understanding structure, transport, fracture mechanics, mass balance, and other processes within glaciers and surrounding environments. Glaciogenic seismic waves readily couple with the bulk Earth, and can be recorded by seismographs deployed at local to global ranges. Although the fracturing, ablating, melting, and/or highly irregular environment of active glaciers can be highly unstable and hazardous, informative seismic measurements can commonly be made at stable proximal ice or rock sites. Seismology also contributes more broadly to emerging studies of elastic and gravity wave coupling between the atmosphere, oceans, solid Earth, and cryosphere, and recent scientific and technical advances have produced glaciological/seismological collaborations across a broad range of scales and processes. This importantly includes improved insight into the responses of cryospheric systems to changing climate and other environmental conditions. Here, we review relevant fundamental physics and glaciology, and provide a broad review of the current state of glacial seismology and its rapidly evolving future directions.

Keywords: glaciers, seismology, geophysics, climate change

(Some figures may appear in colour only in the online journal)

1. Earth's cryosphere

Earth's water ice cryosphere is a dynamic elastic component of the solid Earth system. The elastic moduli of water ice at seismic frequencies are similar to those of shallow crustal rocks. Thus, internal and boundary dynamic processes, as well as internal structures, of Earth's glaciers and other cryospheric features, are fully amenable to study via seismological methods. The developing field of glacial seismology has thus been able to leverage seismological developments refined across many decades for studying Earth's crust and mantle, as well as a vibrant and diversified seismological community, e.g. Forsyth *et al* (2009) and strong community geophysical facilities (Aster and Simons 2015). This growth in scientific interest has resulted in a roughly six-fold growth in the cumulative number of scientific papers in the general area of passive glacier seismology between 2000 and mid-2016 (Podolskiy and Walter 2016).

Most generally, we may refer to the seismology of ice or ice-rich Earth materials, structures, and processes as *cryoseismology*, e.g. Podolskiy and Walter (2016). In this review, we focus on seismic sources and wavefields originating and propagating within glacial ice (figure 1), including those associated with valley and mountain glaciers, ice sheets, ice shelves, and icebergs.

Although early exploration of the cryosphere and polar regions included geological and geophysical observations, seismological study of the cryosphere, including glacial

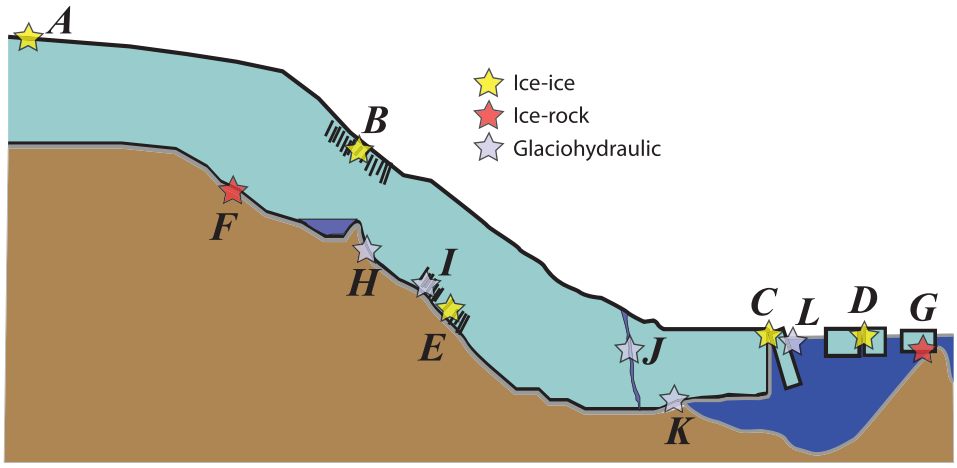

Figure 1. Schematic depiction of a marine-terminating (tidewater) glacial system from icecap source to floating terminus, illustrating seismic source types (stars), identified by source class, and representative citations. (A)–(E): sources associated with ice–ice dynamic processes; (A). Brittle icecap icequakes (Peng *et al* 2014, Lough *et al* 2015); (B). Surface crevasse opening or collapse (Neave and Savage 1970, Colgan *et al* 2016); (C). Calving; (D). Iceberg–iceberg collision, rifting, or fracture (MacAyeal *et al* 2008); (E). Basal crevasse opening or collapse (Harper *et al* 2010). (F) and (G): Sources associated with ice-rock stick-slip; (F). Basal stick-slip (Alley 1993, Winberry *et al* 2009b, Zoet *et al* 2013); (G). Iceberg grounding (Martin *et al* 2010a). (H)–(L): Sources associated with ice-water interactions: (H). Subglacial lake drainage and transport (St. Lawrence and Qamar 1979, Harper *et al* 2005, Winberry *et al* 2009a); (I). Basal crevasse flow and resonance (Walter *et al* 2008, Harper *et al* 2010); (J). Moulin transport and tremor (Röösli *et al* 2016b); (K). Terminus discharge (Glowacki *et al* 2016); (L). Iceberg/Calving impact or other dynamic excitation of hdyroacoustic, gravity, and seismic waves via the water column (Bartholomaus *et al* 2012).

seismology, developed notably during the 1957–1958 International Geophysical Year, e.g. Sullivan (1961). Extensive seismological study of glacial systems has also greatly advanced during the last two decades, driven by expanding and compelling scientific and societal motivations, and facilitated by dramatically improved new instrumentation technologies and seismic methodologies.

1.1. Glacial systems and the global distribution of glacial ice

The vast majority of ice on Earth today exists in the polar regions (figures 2–6). The volume and geographic distribution of ice has varied tremendously over Earth history on time scales ranging from years to millions of years. This variation principally arises from nonlinear feedback processes occurring between the atmospheric, oceanic, and cryospheric elements of the climate system. Earth's current geographical, geological, and climatological state is amenable to dramatic cryospheric changes, and during the past few million years of Earth history the planet has undergone repeated and extensive glacial- interglacial oscillations.

The glacial environment of Earth has exerted profound influence on the evolution of life, and study of glacial conditions and effects across Earth history from recent epochs to deep time is a dynamic field within Earth science, e.g. Macdonald *et al* (2010). To set the stage for the present glacial cryosphere, we characterize the glaciological history to the Quaternary period (composed of the Pleistocene and Holocene epochs) spanning the most recent approximately 2.5 My of Earth history. During the Pleistocene (2.588–0.0117 My before present), the volume and extent of ice on Earth underwent dramatic and repeated glacial/interglacial cycles, each typically lasting between approximately 40 to 100 kYr. These variations are extensively and widely documented by ice core temperature proxy measurements (e.g. oxygen isotope ratios), glacial landforms, marine sediments, and other paleoclimatological proxies. Aspects of glacial/interglacial cycles have been convincingly linked to insolation variations, and associated feedbacks, arising from periodic astronomically forced orbital and axial inclination changes, including eccentricity, obliquity and precession, referred to as Milankovich Cycles. However, the detailed processes controlling glaciation and glacial cycles, which represent a complex and highly nonlinear interaction between astronomical, atmospheric, oceanic, solid Earth, biological, and other forcing mechanisms, remain an active area of investigation.

The maximal extent of glacial ice during the most recent global glacial advance, referred to as last glacial maximum (LGM; e.g. Clark *et al* (2009)), occurred approximately 26.5–19.5 Kyr before present. At LGM, extensive ice sheets, with thicknesses of up to several kilometers, covered much of Fennoscandia and North America and, to a lesser extent, southernmost South America. Significantly greater glacial volumes than today also existed in Antarctica and across high mountain regions. Earth presently resides in the interglacial Holocene epoch (0.0117 My present). The International Commission on Stratigraphy (the entity responsible for official geologic time scale designations) is presently considering whether recent and ongoing anthropogenic changes to the planet, including widespread cryospheric melting due to increasing atmospheric and ocean temperatures primarily attributed to increasing atmospheric CO_2 and other anthropogenic changes warrant the designation of an Anthropocene epoch or age for the latest Holocene. Despite its lack of formal geological designation, the term 'Anthropocene' is currently in wide colloquial, and sometimes scholarly, use to designate the present geological time.

Figure 2. Topographic shaded map showing presently glaciated regions of northwestern North America. Data sources and imagery: U.S. Geological Survey, Scripps Institution of Oceanography, NOAA, U.S. Navy, NGA, GEBCO, PGC/NASA, Landsat, rendered by Google Earth.

Seismically relevant glacial features range from millimeters (e.g. crystal scale) to thousands of kilometers (ice sheets). Large (volume greater that 1 km^3) glaciers are currently present in North America, Asia, South America, Europe, and Antarctica, as well as higher latitude oceanic island landmasses (notably New Zealand and numerous sub-Antarctic and Arctic islands) (figures 2–6). The ice sheets of Antarctica ($\approx 13.5 \times 10^6$ km^2) and Greenland ($\approx 1.74 \times 10^6$ km^2) currently constitute approximately 97% of Earth's glacial area and more than 99% of its volume. Equivalent average global sea level rise for the present land-based Greenland and Antarctic ice masses are approximately 7 and 57 m, respectively (Gregory *et al* 2004, Fretwell 2013). Non-ice sheet glaciers are concentrated in mountainous regions of the higher-latitude southern and (especially) northern hemispheres. Although non-ice sheet glaciers constitute only a small fraction of the global glacial cryosphere, they have large ecological, climate, and hydrological roles in the natural and human resource landscape (Fountain *et al* 2012).

The high elevation topographic regions of the ice sheets are slowly flowing domes that transport ice via sheet flow from ice divides, e.g. Fretwell (2013). The largest glacial systems terminate at the oceans. These marine-terminating systems ultimately deliver ice seaward via outlet glaciers (topographically bounded glaciers) and ice stream (ice-flanked streams of faster moving ice) systems (Bentley 1987). In northern Canada, Greenland and Antarctica, some large marine-extending glacial systems terminate in low-topography floating ice shelves. Many other large glaciers, however, terminate more abruptly at the ocean as grounded or floating calving fronts, which may be abutted by an extensive iceberg mélange of calved ice. In both cases, the ocean can exert strong influences on terminus behavior and stability.

2. Physical and seismological properties of glacial ice

2.1. The phase state of glacial ice

Glacial ice under Earth pressure and temperature conditions (0.1–35 MPa (0–4 km ice thickness) and −80 to 0 °C.) resides exclusively in the ice-I_h (hexagonal) polymorph (figure 7). The melting under pressure (regelation) of ice near 0°C has important consequences for the hydrologic and frictional characteristics of glacial beds, e.g. Weertman (1957) and Clarke (1987) (figure 7). Pure I_h ice at 0 °C and one atmosphere of pressure has a density of 916.79 km m^{-3}, which is 91.69% that of liquid water under identical conditions (Lide 2004). The density of terrestrial *in situ* ice, however, varies widely based on the presence of atmospheric bubbles, rock fragments, and other impurities. The melting-point temperature of ice as a function of pressure can be approximately expressed as a Clausius–Clapeyron relationship

$$T_m = T_0 - \gamma(P - P_0) \tag{1}$$

where T_0 and P_0 are the temperature and pressure of pure water at the triple point (373.16 °K and 611.73 Pa). The constant γ can range appreciably (e.g. 7.42×10^{-5}°K kPa^{-1} for pure water versus 9.87×10^{-5}°K kPa^{-1} for air-saturated water (Harrison 1975).

The density of freshly fallen snow in cold regions is typically 50–70 kg m^3. In the absence of surface or sub-surface melt, snow compacts over tens to hundreds of meters, first into compact snow (firn) and eventually into ice with increasing burial depth and pressure, eventually approaching the density of glacial ice with depth (approximately 820–920 kg m^{-3}).

Figure 3. Greenland, northeastern North America, and northernmost Europe. Data sources and imagery: U.S. Geological Survey, Scripps Institution of Oceanography, NOAA, U.S. Navy, NGA, GEBCO, PGC/NASA, Landsat, rendered by Google Earth.

Glacial ice is a nearly pure to highly impure polycrystalline solid composed of $\mathrm{I_h}$ crystals in varying orientations and sizes (typically from sub-mm to many cm).

At time scales exceeding seismic (elastic) periods (i.e. longer than many minutes), glacial ice viscously deforms under deviatoric stress as a strain rate-softening material. The large-strain deformation of glacial ice at these time scales may be grossly characterized by the Glen-Nye law, e.g. Glen (1955),

$$\dot{\epsilon}_{ij} = \frac{1}{2\eta(T,\ S)} d_{ij} \tag{2}$$

where η is (temperature- and stress-dependent) power law viscosity

$$\eta(T,\ S) = \frac{1}{2C(T)S^{n-1}} \tag{3}$$

with a rate constant $C(T)$ (dependent on both temperature and ice microstructure and impurities), and $n \approx 3$, C exhibits strong temperature dependence, for example, varying from approximately 7×10^{-15} to 4×10^{-18} s^{-1} between 0 and -50 °C (Cuffey and Paterson 2010).

$$d_{ij} = \sigma_{ij} - \sigma_{kk}/3\delta_{ij} \tag{4}$$

is the deviatoric stress tensor (the stress tensor, σ minus the mean isotropic stress), and

$$S = (1/2)(d_{ij}d_{ij}) \tag{5}$$

is the squared maximum shear stress (i.e. the second tensor invariant of d).

While (2) provides a useful formulation for fundamental transport, glacial flow is also influenced by topography, multiple intra- and inter-crystalline creep mechanisms, crystal size distribution, basal or englacial melting, water pathways and inclusions, recrystallization, and temperature profile. Resulting complex strain histories produce spatiotemporally variable, and anisotropic glacial rheology, flow, and fracture structures, e.g. Budd and Jacka (1989). In many cases internal glacial structures can be imaged in substantial detail by land-sited, airborne, or spaceborne ice penetrating radars operating

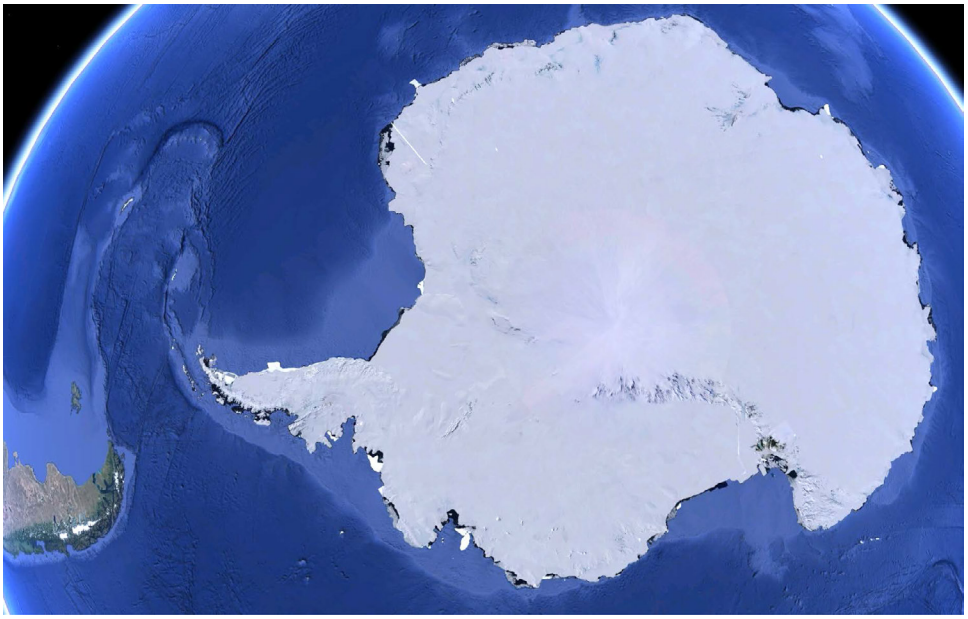

Figure 4. Antarctica and southernmost South America. Data sources and imagery: U.S. Geological Survey, Scripps Institution of Oceanography, NOAA, U.S. Navy, NGA, GEBCO, PGC/NASA, Landsat, rendered by Google Earth.

Figure 5. The European Alpine region. Data sources and imagery: U.S. Geological Survey, Scripps Institution of Oceanography, NOAA, U.S. Navy, NGA, GEBCO, PGC/NASA, Landsat, rendered by Google Earth.

in the MF, HF and VHF frequency bands, e.g. Bogorodsky *et al* (1985) and Kofman *et al* (2010).

The broad thermal structure of glaciers may be usefully categorized into warm, cold, and polythermal cases, e.g. Benn and Evans (2014) . Warm glaciers occur where summer melt rates are sufficiently high. As a result, the entire ice column is close to the freezing point due to a combination of snow insulation in the winter, and melt, infiltration, refreezing, and latent heat release during summer. Cold glaciers are substantially below the freezing point from surface to base, with very limited or no surface or basal melting, and occur in very cold and dry environments, such as the Dry Valleys of Antarctica. Polythermal glaciers include elements of both warm and cold glacial ice, with their heterogeneous thermal structure reflecting surface and basal conductive and advective heat sources and transport processes (Irvine-Fynn *et al* 2011), as well as the influence of strain or frictional heating. The Greenland and Antarctic ice caps are broadly polythermal, and basal thermal condition there may be substantially affected by pressure melting, frictional sliding, and geothermal heat flux, while the surface may be uniformly cold, or experience seasonal melt (especially in Greenland).

2.1.1. Seismic waves in ice. Seismic (elastic) waves in ice, and in solid media generally, are propagating, reversible (or nearly so) elastic strains at frequencies from sub-millihertz to greater than kilohertz. Except in near-source circumstances, seismic strains are usually very small ($<\sim 10^{-6}$). In this case, seismic waves are well characterized by linear elasticity theory described by a Hooke‘s law constitutive relationship of the form

$$\sigma_{ij} = c_{ijkl}\epsilon_{kl} \tag{6}$$

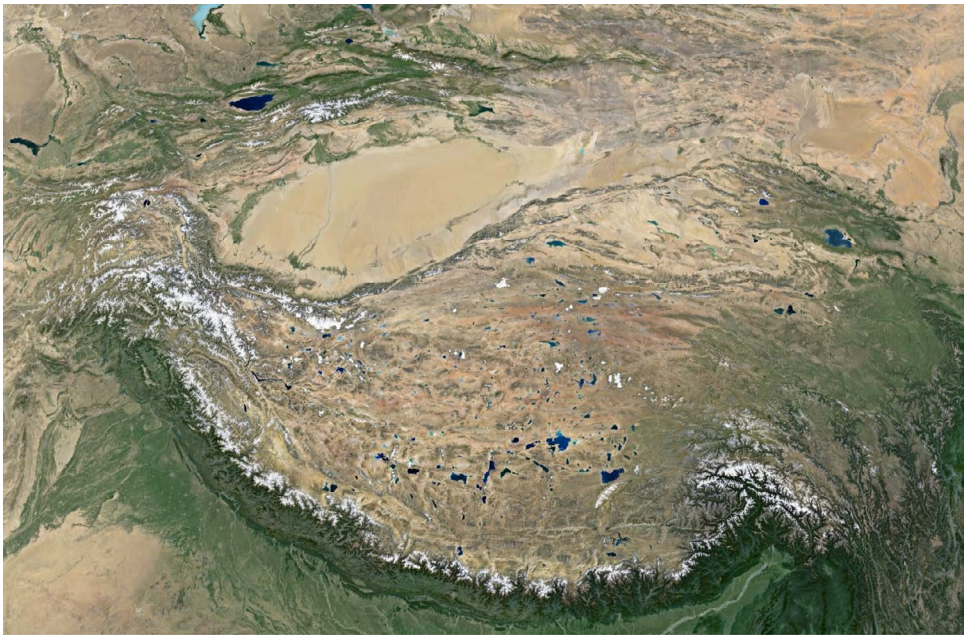

Figure 6. The Himalayan and Tibetan Plateau region. Data Sources and imagery: U.S. Geological Survey, Scripps Institution of Oceanography, NOAA, U.S. Navy, NGA, GEBCO, PGC/NASA, Landsat, rendered by Google Earth: after https://commons.wikimedia.org/wiki/File:Phase_diagram_of_water.svg.

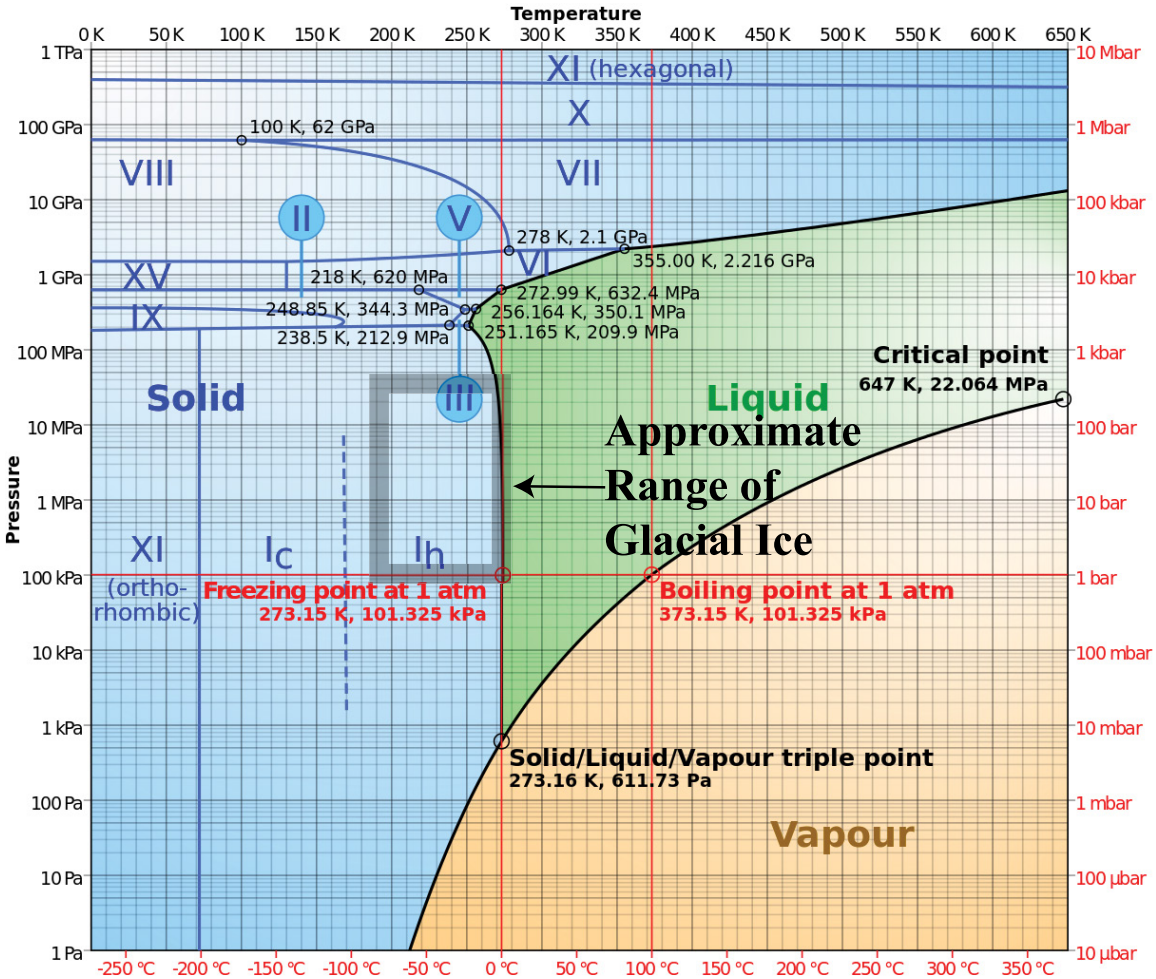

Figure 7. Phase diagram of H_2O (log Pressure versus temperature). The approximate glaciological domain on Earth is indicated by the gray box. Background figure compiled from data in www.lsbu.ac.uk/water/phase.html and http://ergodic.ugr.es/termo/lecciones/water1.html after cmglee; https://commons.wikimedia.org/.

where σ is the (symmetric) stress tensor and ϵ is the corresponding (symmetric, and thus irrotational) strain tensor, both expressed in a common, predefined coordinate system. The stress tensor element σ_{ij} indicates the x_j force component per unit area acting on the x_i face of an infinitessimal cube oriented along $(i,\ j,\ k)$ Cartesian coordinate directions. The force vector per area (traction) on a general cube face defined by a unit normal vector $\mathbf{n}$ is thus given by

$$\tau_i = \sigma_{ij} n_j. \tag{7}$$

Note that seismological convention is for extensional strain (and thus extensional stress) defined as positive. Note that this is the opposite to the convention adopted in some other (e.g. engineering) fields.

The seismic strain tensor is defined in terms of displacement, $\mathbf{u}$, Lagrangian spatial derivatives

$$\epsilon_{ij} = (\partial u_i/\partial x_j + \partial u_j/\partial x_i)/2. \tag{8}$$

Following general seismological practice extensional strain is defined as positive. $\mathbf{c}$ in (6) is the elasticity (or stiffness) tensor, with elements given by the appropriate elastic constants. Once symmetry and thermodynamic conservation considerations are taken into account, the most general physical (triclinic) $\mathbf{c}$ contains 21 independent constants (e.g. Aki and Richards (2002)). For isotropic media, (6) can be expressed using just two elastic constants as

$$\sigma_{ij} = \lambda \Theta \delta_{ij} + 2\mu\epsilon_{ij} \tag{9}$$

where λ and μ are the Lamé (elastic) parameters (where μ is the rigidity and λ approaches the bulk modulus as μ approaches zero), and

$$\Theta = \epsilon_{ii} = \nabla \cdot \mathbf{u} \tag{10}$$

is the trace of the strain tensor (the dilitation).

The hexagonal symmetry of I_h of non-randomly oriented ice crystals and/or thin (relative to seismic wavelength) layering due to deposition, flow, and/or compaction, or aligned inclusions of liquid water (Bradford *et al* 2013) can introduce appreciable bulk elastic rheological anisotropy within glacial ice of up to several percent, e.g. Blankenship and Bentley (1987), Diez *et al* (2014) and Diez and Eisen (2015) (figure 9). If the elastic properties of a bulk medium are azimuthally isotropic (i.e. anisotropic with a vertical rotational symmetry axis), then the associated elastic anisotropy is referred to as vertical transversely isotropic (VTI). The constitutive relationship for linear elasticity in a VTI solid (6) requires five distinct elastic constants. If the ice contains appreciable crystalline heterogeneity or impurities, such as englacial rock, air, or water, seismic wave propagation for wavelengths substantially longer than size scale of the bulk elastic behavior will be governed by effective (e.g. Voigt-, Reuss-, or Hill-averaged; e.g. Man and Huang (2011)) elastic moduli and density.

The existence of seismic waves in general linear elastic media can be deduced from the equation of motion (Navier's equation) for continuous media expressed in terms of stress, displacement, $\mathbf{u}$, and density, ρ

$$\frac{\partial \sigma_{ij}}{\partial x_j} = \rho \frac{\partial^2 u_i}{\partial t^2}. \tag{11}$$

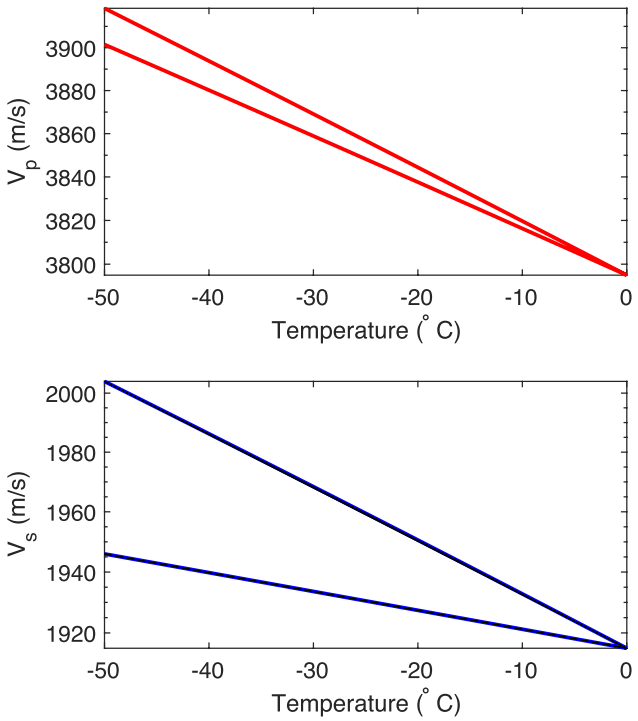

Figure 8. Approximate upper and lower compressional and shear seismic wave velocities in isotropic compact glacial ice, from (14) and (15).

Specific derivation of seismic wave equations arising from (11) requires the adoption of an appropriate constitutive relationship (6). For isotropic media, using (9), wave equations for elastic wave propagation of P (longitudinal) and S (transverse) (body) waves can be readily derived from (11) (appendix). The nondispersive propagation velocities of P and S waves in this situation are

$$v_P = \sqrt{\frac{\lambda + 2\mu}{\rho}} \tag{12}$$

and

$$v_S = \sqrt{\frac{\mu}{\rho}}. \tag{13}$$

where λ and μ are the Lamé elastic moduli of (9), e.g. Stein and Wysession (1991).

The propagation velocities of P and S waves, in ice are temperature dependent, largely reflecting increasing elastic moduli at lower temperatures. Approximate linear regressions for seismic body wave speeds in isotropic compact glacial ice, compiled from laboratory and *in situ* measurements of seismic velocities, are (Kohnen 1974)

$$v_P = -(2.30 \pm 0.17)T + 3795 \text{ m s}^{-1} \tag{14}$$

$$v_S = -(1.2 \pm 0.58)T + 1915 \text{ m s}^{-1} \tag{15}$$

where T is temperature in °C (figure 8).

These velocities are in the general range of shallow crustal rocks. This ensures appreciable elastic wave coupling between the cryospheric and other parts of the solid Earth. However, in

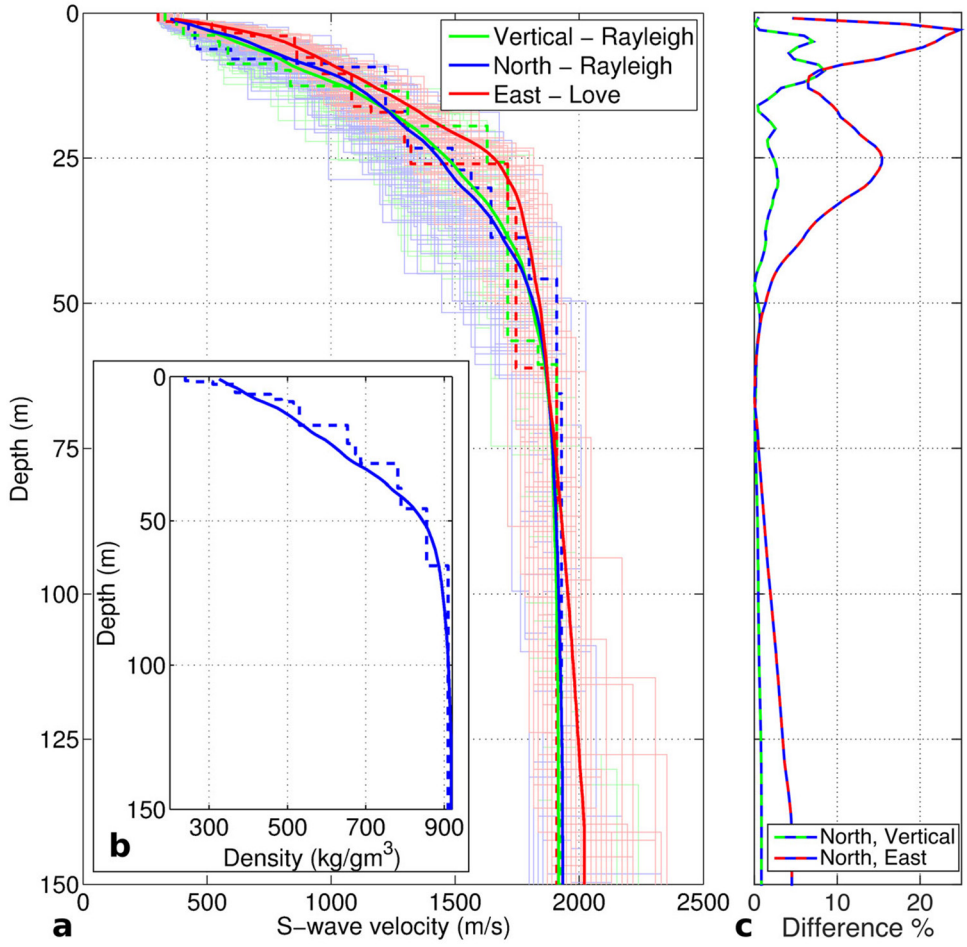

Figure 9. (a) Shear wave velocity of the firn to glacial ice transition for the uppermost 150 m of the Ross Ice Shelf at 79.98°S and 179.9°W, derived from the inversion of Rayleigh and Love surface wave dispersion, using N-S propagating seismic noise recorded by a local seismic array. Green and blue curves indicate Rayleigh wave inversion using data from the vertical and north seismogram components, respectively. Red curve is the velocity inversion from Love waves recorded on the east component. Thin (background) models show 50 representative profiles obtained by fitting surface wave dispersion process using a neighborhood inversion algorithm (Wathelet *et al* 2004, Wathelet 2008). Corresponding colored thick solid lines show the average model. The individual inversion profiles with the best fit are shown as thick dashed lines keyed by color. (b) Corresponding density profile calculated from the north component (blue line in (a) using the shear wave velocity versus density relationship of Diez *et al* (2014)). (c) Percentage difference between the S wave velocity profile derived from the north- and vertical-component (green, blue lines) and the north and east component (red and blue line), respectively, showing seismic anisotropy. Reproduced with permission from Diez *et al* (2016). Copyright © 2016 Oxford University Press.

addition to the significantly lesser density, the Poisson's ratio for glacial ice

$$\nu = \frac{1}{2}\frac{(v_P/v_S)^2 - 2}{(v_p/v_S)^2 - 1} \approx 0.33 \qquad (16)$$

corresponding to $v_p/v_S \approx 2$, is substantially higher than for typical crustal rocks, for which, typically, $\nu \approx 0.25$ and $v_p/v_S \approx 1.73$. Similarly, the bidirectional transmission of elastic wave energy across ice-water interfaces is also significant.

2.2. Snow, firn, and the transformation to glacial ice with depth

The snow-firn-glacial ice transition thickness can exceed 100 m in cold low-accumulation regions (van den Broeke 2008). This transition zone is manifested as a progressive increase in density and elastic stiffness that produces an increasing seismic velocity with depth where v_P and v_S increase from a few hundred m/s near the surface to glacial velocities (14) and (15), e.g. Albert (1998), Albert and Bentley (1998) and Diez *et al* (2016). This strong seismic velocity gradient creates a near-surface waveguide for shallowly dipping higher frequency (i.e. >1 Hz) seismic energy (Anthony *et al* 2015) (figure 9). For glacial systems that are strongly affected by surface melt and ablation, the transition zone will be considerably more complex, or may be absent (in the case of glacial ice exposed by ablation).

2.3. Seismic instrumentation and the seismic noise environment

Seismic sources associated with cryospheric processes exhibit characteristic source durations from thousands of seconds to tens of milliseconds, resulting in seismic radiation across a similar range of periods, e.g. summarized in figure 14 of Podolskiy and Walter (2016). Seismic signals are

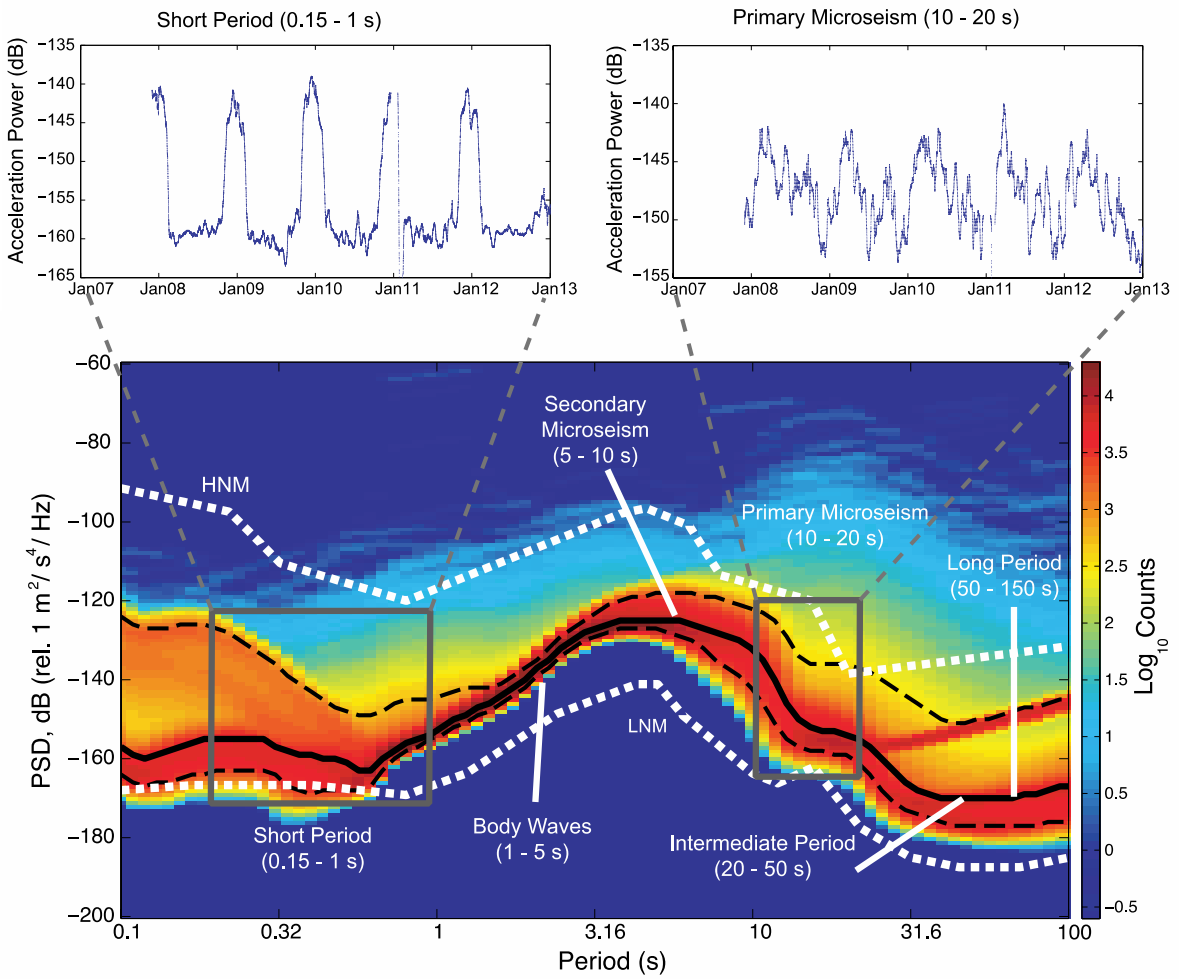

Figure 10. Characteristic seismic signals and noise observed at a broadband seismic station calculated from 1-hour data intervals across five years (December 2007 through December 2012). (a) Probability density function (PDF) of vertical-component seismic acceleration power spectral density (PSD) for global seismographic network (Butler *et al* 2004) station QSPA. The seismometer is located in a 146 m-deep ice borehole 7.8 km from the Amundsen-Scott South Pole Station (U.S.). White curves (HNM and LNM) show characteristic worldwide high- and low-noise spectral levels, respectively (Peterson 1993). Globally detectable earthquakes are infrequent (visible as low probability, high-PSD features). Six period bands of seismological interest are indicated: Short period (local earthquake/icequake signals commonly observed); Body Waves (dominant P and S body wave global earthquake signals); Primary and secondary microseism bands (ocean wave activity), and Intermediate and long period bands (seismic energy generated by longer-period [infragravity] ocean waves, and seismic surface waves from large global earthquakes). Seasonally-varying annual average power levels in two period bands are shown above (b,c). large annual variability in short period noise reflects anthropogenic austral summer activities at the Amundsen-Scott station. Primary microseism band variations reflect storminess of the Southern Ocean and the annual growth and decay of Antarctic sea ice, which strongly buffers the Antarctic coast from ocean waves during the later austral winter (Aster *et al* 2008, 2010, Anthony *et al* 2016). The high probability intermediate to long period PSD swath approaching HNM in this band is from a temporary instrument malfunction. Reproduced with permission from Anthony *et al* (2015). © 2015 by the Seismological Society of America.

most commonly detected and studied using seismographic or strainmeter records of surface or subsurface (borehole) ground motion from seismometers installed at fixed (relative to the ice or land surface) geographic locations. Technologies and scientific analysis methods in general solid-Earth and glacial seismology are highly similar and cross-influential, with modifications for glaciological studies usually reflecting specific environmental and/and logistical considerations. As a result, the seismological and glaciological scientific communities and their geophysical instrumentation and facilities have developed increasing levels of collaboration in recent years (Aster and Simons 2015).

Seismic motion is most commonly detected using an electromagnetic inertial seismometer, which may be passive or incorporate active force feedback, damped mass-spring seismometer that produces a vertical- or three-component time series (seismogram) of ground motion. The (typically) analog seismometer output is digitized, time-stamped (usually to a GPS-synchronized clock), and recorded locally and/or telemetered. Modern portable and observatory-based broadband seismographs have useful ground motion responses that can range from many hundreds of Hz to periods of many hundreds of seconds, with a pass band amplitude response that is typically nearly flat to ground velocity within linear bounds. The instrumental noise floor is commonly designed as much as possible to lie below the natural noise floor for seismically 'quiet' sites on Earth (Peterson 1993). Seismic background noise is highly site-specific, and is dictated by a wide range

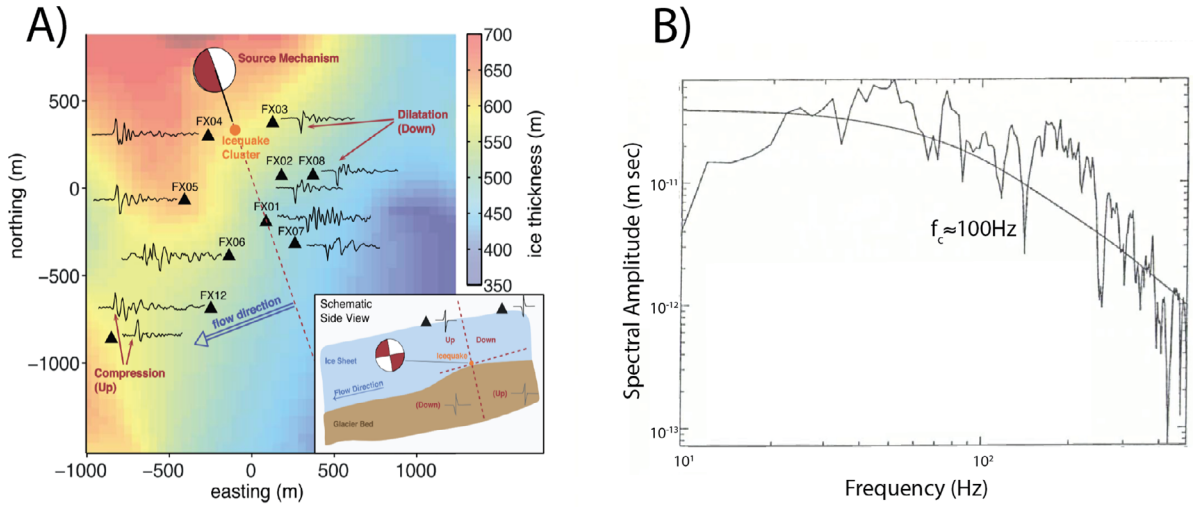

Figure 11. (A) Estimation of source mechanism and slip patch size from seismic measurements for a group glacial stick-slip events on the Greenland Ice Sheet. The compressive down flow events indicate a thrust type source (Reproduced with permission from Röösli *et al* 2016a. © 2016. American Geophysical Union. All Rights Reserved.). (B) Estimation of slip patch size from seismic measurements for Antarctic event from P wave displacement spectrum. Solid line is a fit using a theoretical prediction using equation (17). A corner frequency of 100 Hz indicates fault radius of ≈10 m. (Reproduced with permission from Anandakrishnan and Bentley 1993. © International Glaciological Society 1993.)

of wind, ocean and other environmental processes, e.g. Dìaz (2016) that produce both quasi-continuous and transient seismic wavefield excitation.

The past two decades have produced a remarkable expansion in seismological data from the cryosphere, collected using both portable (typically seasonal to 1- to 2-year) and long term instrument deployments, such as those of the global seismographic network (GSN) (Butler *et al* 2004). Important community instrument pools and networks that have seen wide use in the glacial seismology (and broader seismological) research community notably include Incorporated Research Institutions for Seismology (IRIS) Consortium PASSCAL, Polar Instrumentation and UNAVCO geodetic facilities (Aster *et al* 2005, Nyblade *et al* 2012) (NSF), global seismographic network (Park *et al* 2005), GEOSCOPE (Roult *et al* 2010), GFZ Potsdam GIPP pool (Haberland and Ritter 2016), and SEIS-UK (NERC) facilities. For ground motions at periods beyond the passband of typical seismographic systems (e.g. many hundreds of seconds to thousands of seconds and beyond), larger (e.g. greater than mm-range) surface displacement fields, as well as secular glacial motions may be usefully recorded by geodetic (particularly GPS/GNSS) instruments. Integration of geodetic and seismic observations has been widely utilized to study the full bandwidth of deformation and displacement in seismogenic glaciological processes (Nyblade *et al* 2012).

The detection and analysis of seismic signals depends on the level of seismic background noise arising from a range of environmental processes. At periods between hundreds of seconds and several seconds, Earth's background seismic noise is dominated the oceanic microseism. The microseism consists of both body and, especially, Rayleigh surface waves, and is globally detectable at all suitably quiet seismic sites (Peterson 1993). Microseism excitation results from energy transfer from ocean gravity waves into seismic waves, principally at or near the coasts, via two distinct mechanisms. The 'primary' microseism is excited by direct ocean swell-coastal interactions, while the more powerful, frequency-doubled 'secondary' microseism is generated by standing-wave components of the ocean gravity wave field), e.g. Longuet-Higgins (1950), Douglas (1977), Ardhuin *et al* (2011) and Ardhuin *et al* (2015) that create pressure fluctuations at the ocean floor. Persistent global oceanic excitation of the elastic infrasound field in the atmosphere also occurs, e.g. Ishihara *et al* (2015). The global microseism noise spectrum has a power spectral density mode dictated by secondary microseism energy between approximately 5 and 10 s period, and a secondary peak or shoulder, representing primary microseism energy, at twice this period. At still shorter periods, seismic noise is commonly dominated by more local wind, water wave, and/or anthropogenic processes (Larose *et al* 2015). Figure 10 displays a representative probability density function of noise power spectral density for an Antarctic icecap sited station near the Amundsen-Scott Station (U.S.) near South Pole.

2.4. Detection and source location of glacial seismicity

Seismic signals from impulsive glaciological processes that exhibit clear P and S phases may be detected and located using standard seismological methods that have been extensively developed by the earthquake seismology community. In this case, determining source location and origin time is a well-posed nonlinear problem that may easily be solved using iterative methods provided the seismic velocity structure can be well estimated and the network of recording stations is sufficiently close to the (3-dimensional) source hypocenter. Given a sufficiently large and well-distributed seismographic network, it is feasible and common to jointly estimate both velocity structure and source locations as an inverse problem, e.g. Zhang and Thurber (2003) and Aster *et al* (2013) If seismographs geographically encircle the source region, but none are sufficiently close to lying directly above the source, the

geographic location (epicenter) may be well determined, but source depth many be poorly constrained. If signal-to-noise ratios are high, event detection is commonly and robustly performed by envelope comparison of short-term and long-term energy averages, e.g. Withers *et al* (1998). However, where signal-to-noise ratios are low, or where signals are emergent or otherwise do not show clearly interpretable seismic phases due to an emergent or complex source process, or due to complex wave propagation between source and receiver, more advanced methods may be required to detect and locate a seismic source. In this case, incisive amplitude and timing information to assist with source location and other analysis may be extracted from spectrograms, e.g. Martin *et al* (2010a) and Bartholomaus *et al* (2012). Coherent arrays of seismographs (in conjunction with individual stations or as networks of arrays), when deployed, facilitate powerful beamforming methodologies that can constrain source location (or azimuth), as well as provide local measurements of apparent wave speed, wave type, and local seismic structure (Diez *et al* 2016), even for complex sources, e.g. Richardson *et al* (2012), Köhler *et al* (2016) and Bromirski *et al* (2017). For glacial seismic sources that produce a surface manifestation, camera, video, infrasound, and other ancillary instrumentation has obvious utility, e.g. Richardson *et al* (2010) and Bartholomaus *et al* (2012).

3. Subglacial stick-slip seismicity

Although internal strain (2) strongly affects general glacial behavior, the most significant processes regulating the translation of glaciers under gravitational driving stress occur at or near the ice-bed interface. Substrate conditions and subglacial water-pressure act in concert to regulate the speed at which glaciers and ice sheets may slide over their beds (Clarke 2005). Many processes relevant to understanding this key aspect of the subglacial environment radiate seismic energy, and/or are associated with strong material contrasts, that allow them to be interrogated remotely with seismology in source and imaging studies.

The majority of the ice-bed interface underlying fast moving glaciers and ice sheets is efficiently lubricated, and the coefficient of friction is sufficiently low, to offer only minimal resistance to forward sliding. In such cases, relatively small regions (<10% of the basal area) of increased friction, know as asperities or 'sticky spots', may oppose substantial percentages of the driving stress (Alley 1993) and thus exert large-scale influences on glacial motion. The presence of localized pinning points can produce basal glacial stick-slip behavior at or around such locations that is analogous to earthquake fault slip in solid-Earth settings, e.g. Brace and Byerlee (1966), generating seismic waves that may be observed and analyzed with remote seismographs.

3.1. Seismic signatures of glacial stick-slip

First proposed by VanWormer and Berg (1970) as a mechanism to explain seismic energy originating from glaciers, it is now clear that seismogenic stick-slip is common within the glacial environment. Basal glacial stick-slip processes have been observed on both large ice sheets and on smaller mountain glaciers across the globe. These diverse environments host asperity patches that span several orders of magnitude in scale, ranging from O(1 m) to O(100 km) (figure 12).

Where recorded with sufficient azimuthal coverage to resolve the pattern of seismic radiation (figure 11), the slip mechanism as well as the size of the slip patch can be estimated using earthquake seismological methods. Analysis of polarity or moment tensor inversion has confirmed that energy radiating for these asperities can be modeled as arising from low-angle thrust faulting (double couple mechanism), consistent with topside motion in the down-glacier direction (Anandakrishnan and Bentley 1993, Walter *et al* 2009). The seismic moment (A.15) can be estimated from seismograms using the long-period asymptote of the seismic spectrum, while the fall off in spectral amplitude at higher frequency can be used to constrain the slip patch size, allowing the slip, d, to be calculated from (A.15). The spectrum is often fit using

$$\Omega(f) = \frac{\Omega_0}{1 + (f/f_c)^2} \tag{17}$$

where is f_c is the spectral corner frequency and Ω_0 is the long-period spectral-amplitude at frequencies less than f_c. An estimate of the radius, R, (and thus, the slip area, A) of an assumed circular asperity can be estimated using

$$R = 0.32 v_P / f_c \tag{18}$$

where v_P is the P wave speed for material bounding the fault (Brune 1970).

Smaller events (magnitude 0–1), such as those observed beneath both alpine glaciers (Walter *et al* 2009, Allstadt and Malone 2014, Helmstetter *et al* 2015b) as well as ice streams (Blankenship *et al* 1987, Smith 2006, Winberry *et al* 2013), are most revealingly studied using local (typically up to a few km distant) seismographs due to their small energies. In such cases, dozens to hundreds of distinct bed asperities may be often mapped over relatively small regions (e.g. few square kilometers). Figure 12(a), shows a recent example from the Rutford Ice Stream. Slightly larger slip patches O(100–1000) m, may produce magnitude up to ≈2 events that are readily detectable at regional distances (up to a few hundred km) (Bannister *et al* 2002, Danesi *et al* 2007, Zoet *et al* 2012). Figure 12(b) shows a notable example from the David glacier in Antarctica.

The Whillans Ice Stream in Antarctica is home to largest glacial stick-slip events yet noted (Bindschadler *et al* 2003) (figure 12(c)). During these events, the entire ≈100 km downstream portion of the ice stream moves in approximately twice daily 'slow earthquakes'; 30 min slip events individual seismic moment magnitudes of $M_w \approx 7$. These events were initially detected geodetically via GPS measurements of displacement collected on the glacier surface, but were later found to radiate long-period seismic energy (40–80 s) that can be observed at across Antarctica at distances of up to 1000 km (Wiens *et al* 2008, Winberry *et al* 2011). While a single event, each rupture has subsequently been shown to represent the linked breakage of several distinct large asperities (>5 km radius). This behavior is distinct relative to smaller events, which appear to be isolated asperities that generate several packages of

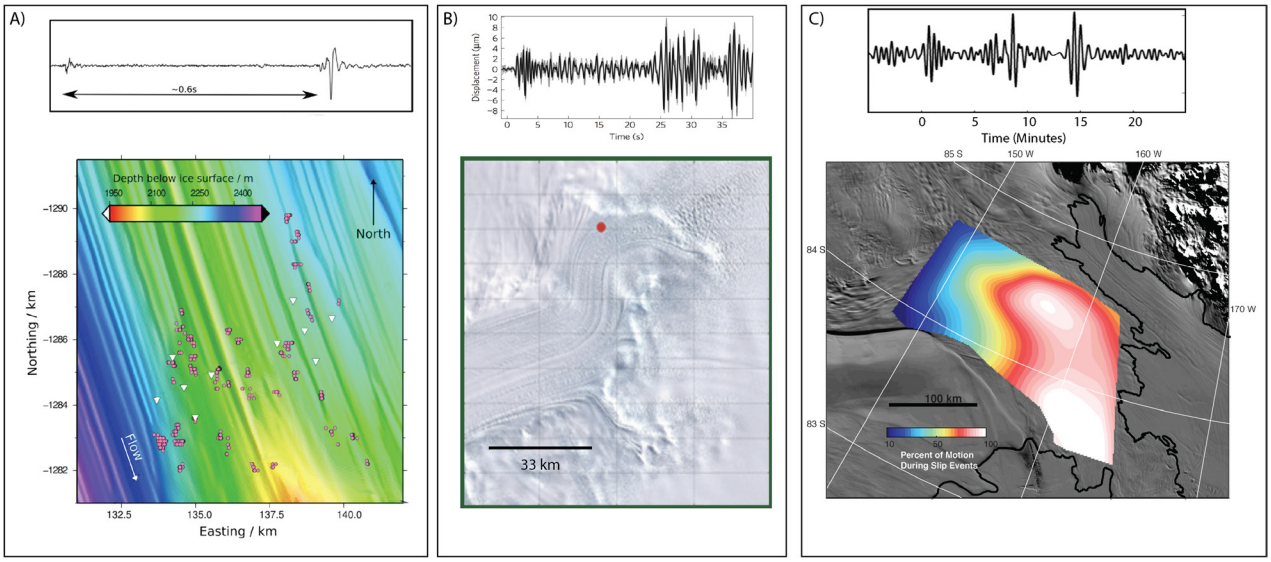

Figure 12. Scales of glacial stick-slip asperities from Antarctica. (A) Top panel shows an example waveform from an ≈1 m asperity, Rutford Ice Stream. Bottom panel shows locations of hundreds of basal icequake events atop high resolution bed topography. Smith *et al* (2015). (B) ≈1 km, David Glacier. Bottom panel shows Landsat image with event location (Zoet *et al* 2012). (C) Top panel shows a seismogram from a Whillans Ice Stream stick-slip event associated with an ≈50 km-scale asperity. Bottom panel displays the percentage of total motion that occurs during a slip event. Reprinted from Winberry *et al* (2011), Copyright (2011), with permission from Elsevier.

energy observed in far-field seismograms (Pratt *et al* 2014). Additionally, the ability to jointly observe the Whillans Ice Stream slip events via GPS and seismic instrumentation deployed directly above the slip surface has revealed more detailed evolution of rupture velocity (Winberry *et al* 2011, Walter *et al* 2011, 2015b).

3.2. Stick-slip in the subglacial environment

While subglacial stick-slip has been documented across a broad range of spatial scales, a relatively simple model of the process is supported by the observations. In particular, the generation of nearly identical waveforms associated with repeating events indicates repeated slip over isolated subglacial asperities (figure 13) (Smith 2006, Zoet *et al* 2012, Winberry *et al* 2013, Allstadt and Malone 2014). We will motivate discussion of subglacial stick-slip mechanics with a relatively simple model that captures its salient features. More detailed and complete summaries of the frictional stick-slip instabilities may be found elsewhere in the seismological literature (Scholz 1998, Marone 1998). We then discuss how the bi-material nature of the subglacial interface (i.e. ice-bedrock or ice-sediment) influences subglacial stick-slip behavior.

As is frequently done, we will utilize a simple spring slider-block analog to discuss the stick-slip process. The spring is extended at constant rate, resulting in a linearly increasing elastic stress σ_e. If the block is initially at rest, motion will be inhibited until σ_e exceeds the frictional strength of the block-surface contact, with frictional strength of this interface defined as

$$\tau = \sigma_n' c \tag{19}$$

where σ_n' is effective normal stress, the applied normal stress σ_n minus pore pressure p, and c is the coefficient of friction, and reflects the sensitivity of basal traction to subglacial hydrologic conditions. This relatively simple relationship between τ and σ_n' can describe basal traction beneath both soft-bedded glaciers (Iverson 2010) and debris laden basal ice sliding over hard beds (Zoet *et al* 2013).

However, c is not generally constant, but is instead a function of sliding speed, with the simplest case being a static value, c_s, while the block is at rest and dynamic value, c_d, once the block is moving. If friction increases at the onset of motion (velocity strengthening behavior), the block will slide smoothly. However, if friction drops at the onset of motion (velocity weakening behavior), an instability summarized in figure 14 may arise.

First consider the case where stress levels at Point A in figure 14 initiate slip of a previously motionless block. At the onset of slip, σ_e will begin to decrease as the spring uncompresses due to motion of the block. However, simultaneously, c will decrease as the system transitions to its dynamic value over some finite distance $\mathcal{L}$. A relatively short time after slip initiation $\sigma_e > \tau$. This force imbalance creates an acceleration of the block. The block will continue to accelerate until Point B, after which $\sigma_e < \tau$, and the block will begin to decelerate. The block will eventually come to rest at Point C, at which point c will return to its static value. Extension in spring will afterwards accumulate until σ_e initiates another slip event. This process will produce periodic slip events with a recurrence interval of

$$\delta t = 2\frac{\sigma_n'(c_s - c_d)}{\dot{\sigma}_e} \tag{20}$$

This relatively simple model has been implemented (with vary degrees of sophistication) to understand glacial stick-slip at all scales (Bindschadler *et al* 2003, Winberry *et al* 2009b, Sergienko *et al* 2009, Lipovsky and Dunham 2016). It is worth noting that in the glaciological literature, the term 'stick-slip' has additionally been used to describe transitions between periods of minimal and relatively fast subglacial motion that are triggered by diurnal subglacial water-pressure fluctuations

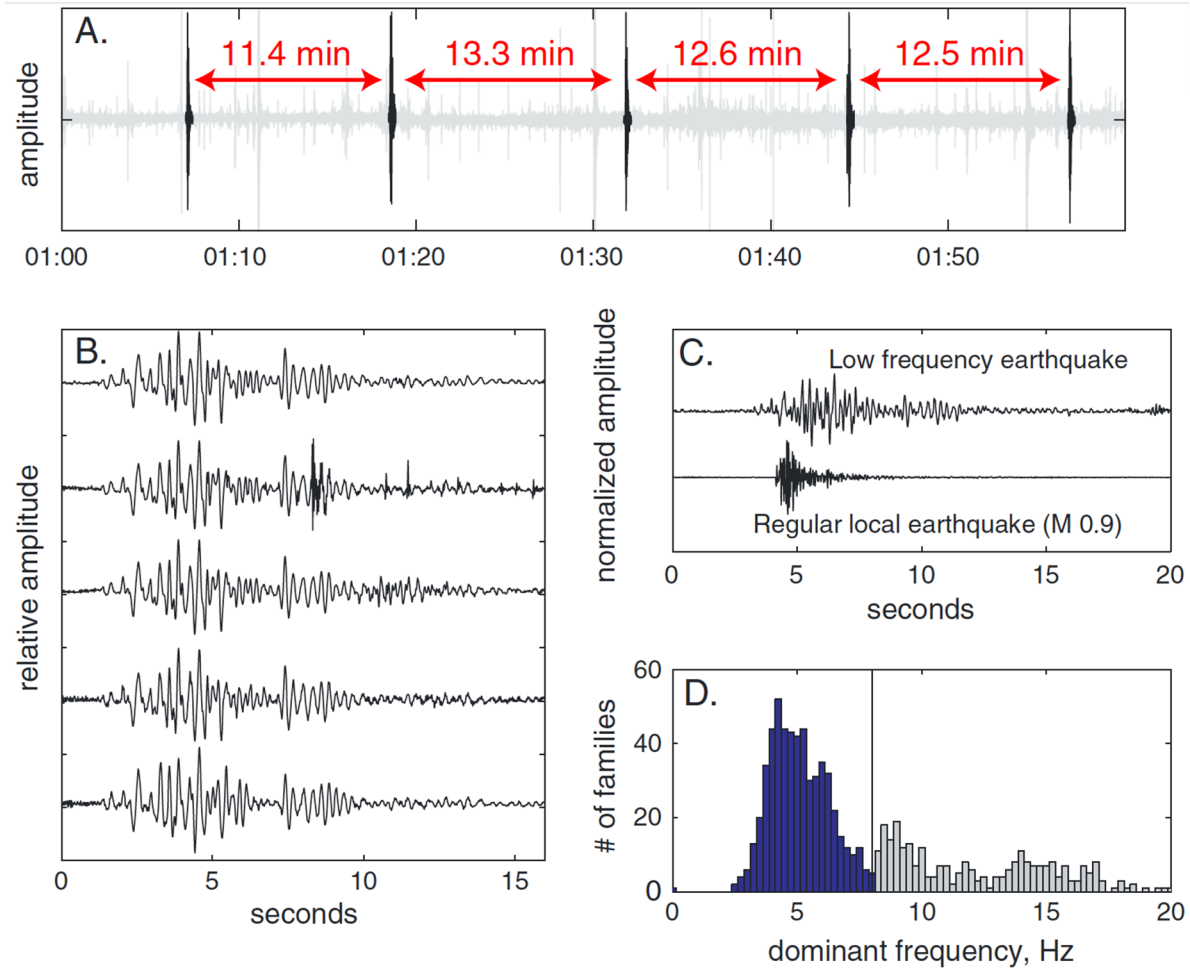

Figure 13. Repeating basal glacial earthquakes from a steep temperate glacier on a dormant volcano (Mount Rainier, Washington, USA). (A). Continuous seismogram showing characteristic near-repeating intervals. (B). Individual (vertical component ground velocity) seismograms from (A). (C). Comparison of glaciogenic events with a tectonic local earthquake, showing unusually low frequency content for an event of this magnitude. (D). Dominant seismogram frequency discriminant developed to separate glacial earthquakes from other seismic events.). Reliable discrimination of glacial, volcanic, and tectonic events on active volcanoes can be a challenge for volcano monitoring (figure 15). Reproduced with permission from Allstadt and Malone (2014). © 2014. American Geophysical Union. All Rights Reserved.

(Fischer and Clarke 1997, Boulton *et al* 2001, Knight 2002, Damsgaard *et al* 2016). This hydrologic mechanism should not be confused with the rapidly-acting frictional mechanism discussed here that is the driver for seismogenic glacial stick-slip systems.

In subglacial systems, variations in pore pressure are known to drive significant variations in σ_n' over time scales ranging from minutes to years. Importantly for stick-slip in glacial systems, the instability of a slip patch with fixed frictional and geometrical properties will be suppressed at effective normal stresses σ_n' below a critical threshold given by

$$\sigma_{\text{crit}}' \leqslant \frac{K\mathcal{L}}{c_s - c_d} \tag{21}$$

where K is the spring stiffness (Scholz 1998).

Consider the stress evolution when $\sigma_n' = \sigma_{\text{crit}}'$ (figure 14). In this scenario, an initially motionless block begins to move in response to stress conditions represented at Point D. As with the previous case, τ will begin to drop, however, due to the value of σ_n', the rate of stress reduction occurs at the same rate as the reduction of σ_e, thus the force balance requires no rapid acceleration between point D and E. When point E is reached, τ remains constant and the block will slide at the rate of spring extension $\mathbf{v}$. However, large perturbations to the background stressing-rate can cause a jump from stable to stick-slip behavior.

In natural systems, the slip behavior is controlled by the elasticity of the materials bounding the slip patch and frictional properties of the interface. We now discuss how the glacial setting influences each of these parameters. From the discussion above, it is clear that the stiffness of system K is fundamental to determining sliding stability. For a slip patch, K dictates the change in stress with slip and is defined as

$$K = \mu/L \tag{22}$$

where μ is the shear modulus of the material bounding the slip interface and L is the length of the slip patch. However, when asperities occur between two strongly contrasting materials μ is not well defined, such as when ice ($\mu_{\text{ice}} \approx 3 \times 10^9$ Pa) moves over either bedrock ($\mu_{\text{rock}} \approx 5 \times 10^{10}$ Pa) or sediment, ($\mu_{\text{sed}} \approx 1 \times 10^6 - 10^9$ Pa) (Iverson *et al* 1999, Lipovsky and Dunham 2016). When the material contrast is significant,

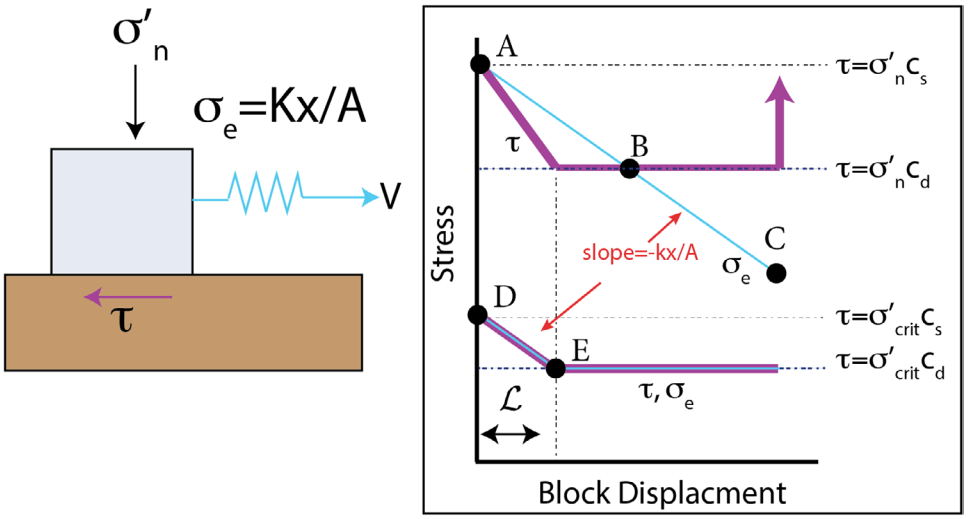

Figure 14. The stick-slip mechanism. The left panel shows a simple spring-slider block system. Extension of the spring, x, applies a force F to the block that is determined by the spring stiffness, K, $F = Kx$ (Hooke's Law). Thus, the applied stress σ_e at the block-surface contact is Kx/A, where A is the contact area between the block and the surface. Motion is resisted by shear stress τ at block-surface contact. σ_n' is the effective normal stress. The right panel shows two stress evolution paths corresponding to unstable (top) and stable (bottom) slip. $\mathcal{L}$ is the distance required for the transition from static friction c_s to dynamic friction c_d.

elastic strain will preferentially be accommodated in the more compliant material (figure 15). Thus, for the case of a hard bed asperity, since ice is more compliant than typical bedrock by about an order of magnitude, strain will preferentially be accommodated within the ice at a bedrock contact. During a slip event under such circumstances, the strain in the ice be released due to elastic rebound during the slip. However, for an asperity atop weak sediments, the situation is less clear. The elasticity of sediment is dependent on the particular properties of the material, and its effective normal stress. However, at levels of σ_n' that promote sliding, μ_{sed} will often be significantly lower than μ_{ice} and the sediment will accommodate the majority of the inter-event strain (Iverson *et al* 1999, Lipovsky and Dunham 2016). For both soft and hard bed cases however, net motion only occurs in the ice.

It is worth noting that due to the length of the central Whillans Ice Stream asperity (>10 km) relative to the ice thickness (≈1 km), this simple model of strain accumulation does not hold. On Whillans Ice Stream, it appears that most inter-event strain is accommodated upstream and downstream of the main sticky-spot (Winberry *et al* 2014).

This material dependence on strain partitioning has a significant implications for seismic estimation of seismic slip and patch size. To convert the long-period component of the seismogram spectrum into the seismic moment an estimate of the shear modulus is required. Similarly, rupture velocity v_r, which controls the duration of the slip event, will be a function of μ, influencing the estimation of slip patch size. Thus, without constraints on material properties of the asperity, authors usually bound estimates for seismic moment, patch size, slip amount with 'hard' and 'soft' bed estimates (Anandakrishnan and Bentley 1993).

Velocity-weakening friction is also a fundamental element for the above stick-slip mechanism. For hard bedded glaciers, insights emerging from limited laboratory studies are showing that the existence of velocity weakening behavior is controlled by ice temperature, basal debris content, and sliding rate (Zoet *et al* 2013, McCarthy *et al* 2017). At relatively high temperatures, near the pressure melting point, the production of meltwater reduces steady-state friction by lubricating contacts and promotes velocity strengthening behavior for both clean and debris-laden ice sliding over bedrock. Below the pressure melting point, velocity weakening behavior is favored by increased basal debris contents, while for relatively debris free basal ice, lower temperatures (<−10 °C) appear to promote slip instabilities. For glaciers overriding a soft bed, basal motion may be accommodated by the glacier sliding over the sediment or dominated by sediment deformation near the ice bottom (<10 m), thus, in many ways similar to gouge in tectonic fault systems. Velocity weakening friction is a common attribute of many granular materials, and significant efforts have been undertaken to constrain the rheological and frictional behavior of subglacial sediments. While these studies reveal that some subglacial sediments display velocity weakening behavior similar to fault gouges, most laboratory results on subglacial sediments tend to display a slight velocity strengthening (or neutral) behavior (Iverson *et al* 1998, Tulaczyk *et al* 2000, Rathbun *et al* 2008). These observations have prompted consideration of velocity-weakening mechanisms associated with pore-pressure reductions in the lee of basal debris as it is dragged through the underlying sediment (Thomason and Iverson 2008) and/or co-seismic pumping and pore pressure change during slip events.

3.3. *Insights into subglacial conditions from stick-slip motion*

In subglacial environments, resistance to motion is controlled by rheological, stress, and hydrologic conditions. Thus, the stick-slip seismicity offers a window into the temporal and spatial variability of subglacial conditions. Below, we highlight a few of the ways in which stick-slip behavior can be used to illuminate subglacial physical conditions.

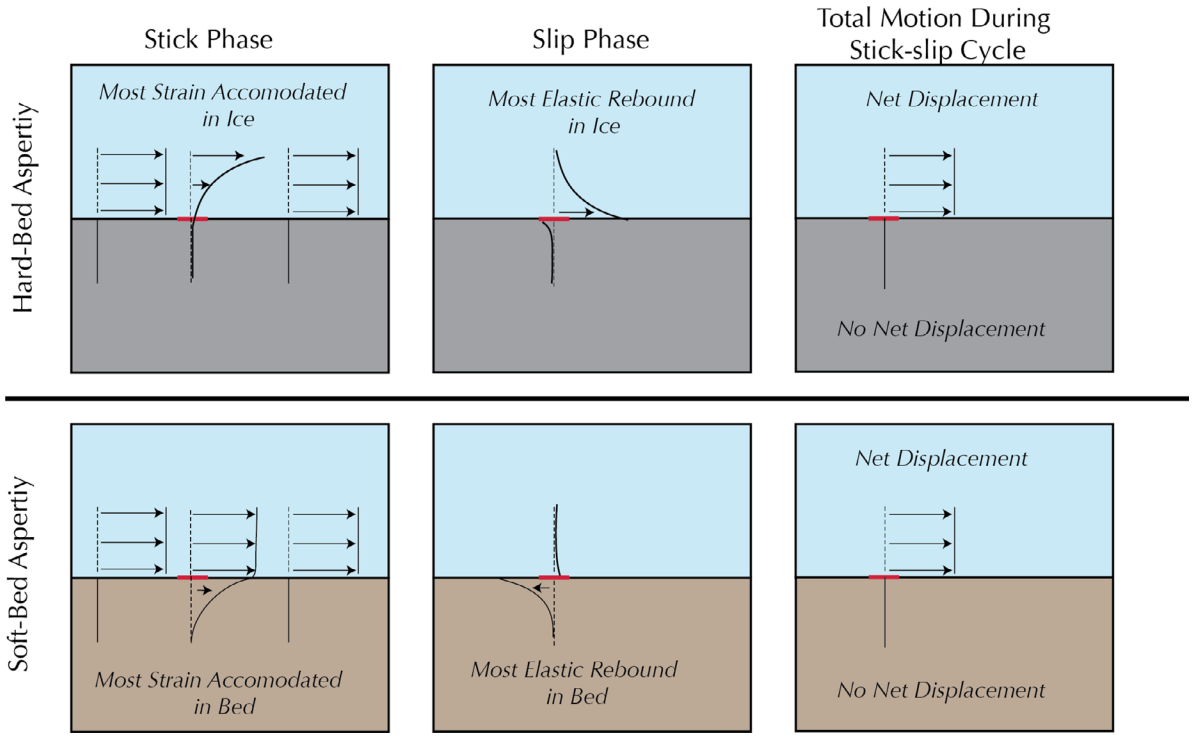

Figure 15. Schematic illustration of asperities on 'hard' and 'soft' beds. When slip is focused on a bi-material interface, strain will preferentially be accommodated in the more compliant material. Thus, for the end-member model of a rigid hard bed asperity, strain is accommodated in ice while the opposite is true for an asperity on a soft bed. As a result, during the slip phase, elastic rebound will primarily occur in the more compliant material. However, irrespective of the materials, net motion only occurs in the overriding ice. Reproduced from Lipovsky and Dunham (2016). CC BY 3.0.

3.3.1. Frictional properties of stick-slip. The generation of stick-slip behavior is dependent on frictional properties (μ_s, μ_d, $\mathcal{L}$). Drivers of this variability may include sediment contrast, basal debris concentration, differing bed types (hard versus soft). As a result, spatial variations in the occurrence of stick-slip behavior may reflect variations in frictional properties.

For example, regions of hard bedded glaciers slightly below their pressure melting point have their sliding stability influenced by basal debris concentration (Zoet *et al* 2013), a parameter that is likely variable in space. Several studies have suggested that asperities may migrate at rate comparable to ice flow (Zoet *et al* 2012, Allstadt and Malone 2014, Helmstetter *et al* 2015b). One potential explanation is that the asperities are generated by regions of high basal debris content that are advected down-glacier. The work of Zoet *et al* (2012), proposed this as an explanation for a sequence of repeating events effectively turning off after a 9-month period of activity. Thus, at any given location, the frictional conditions that give rise to stick-slip behavior may vary through time.

3.3.2. Hydrologic modulation of seismicity. σ_n' is the dominant control on ice-bed coupling and thus sliding speed for both hard and soft bedded glaciers. As a result, fluctuations in subglacial hydrologic conditions driven from either the input of surface melt-water or internal variability may modulate strength of an asperity. In general, for a given set of frictional properties, regions of high seismicity should be associated with relatively elevated levels of σ_n'. The first compelling evidence of this was provided by Anandakrishnan and Bentley (1993). They observed nearly 200 times more seismic events on the now stagnant Kamb Ice Stream when compared to the neighboring fast moving Whillans Ice Stream. This evidence was used to help corroborate the prevailing hypothesis that the Kamb Ice Stream stagnated ≈150 years ago due to elevated σ_n'. On a more local scale, recent work has confirmed that monitoring the spatial distribution of stick-slip seismicity can be used to infer spatial variability in hydrologic conditions. On the Rutford Ice Stream, regions of high seismicity are associated with areas of 'stiff' till determined independently from active source seismic studies. In contrast, regions identified as high porosity showed minimal seismic emissions, as expected from equation (21) (Smith 2006, Smith *et al* 2015).

Recent studies have also demonstrated how the temporal behavior of repeating events may illuminate subglacial hydraulic conditions. It is well known that subglacial water systems are comprised of well connected regions as well as poorly connected regions that are less sensitive to transient inputs (Kavanaugh and Clarke 2001, Clarke 2005). These different regions are usually mapped out by drilling multiple boreholes to directly access a broad region of the ice-bed-interface. However, on the margin of the Greenland ice sheet it was recently observed that neighboring asperities (separated by a few hundred meters) displayed contrasting behavior to a diurnal hydrologic forcing. One cluster was modulated by the transient forcing, indicating a connected region of the bed, while a neighboring cluster (a few hundred meters away) displayed no response that is indicative on a hydraulically

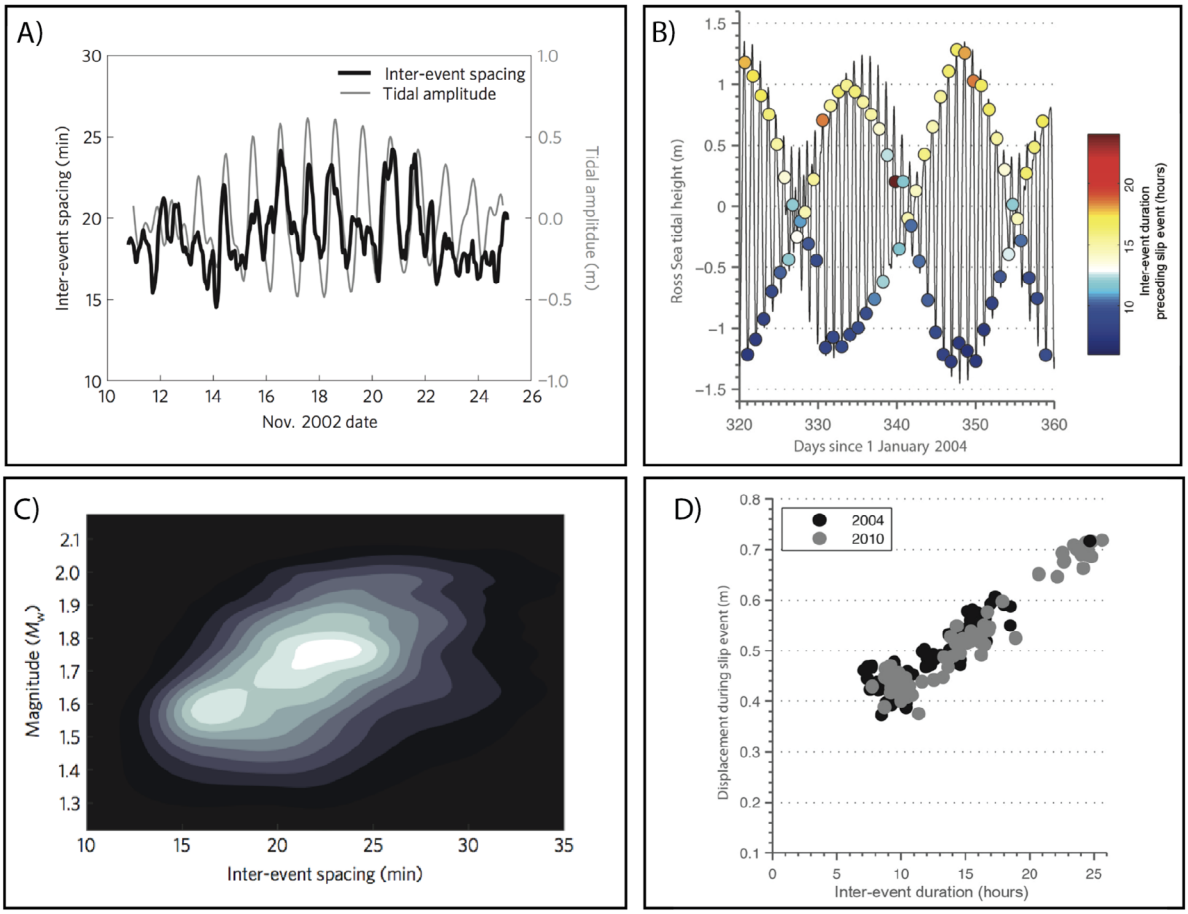

Figure 16. Tidal modulation of stick-slip behavior. (A) Correlation of Ross Sea tides and δt for stick-slip events of David Glacier (Reprinted by permission from Macmillan Publishers Ltd: Nature Geoscience Zoet *et al* (2012), Copyright (2012).). (B) Correlation of Whillans Ice Stream stick-slip events and Ross Sea tides (Reproduced with permission from Winberry *et al* 2014. © International Glaciological Society 2014). (C) δt versus magnitude for David Glacier events. (D) δt versus magnitude for Whillans Ice Stream events.

isolated region of the bed (Röösli *et al* 2016a). These results suggest that monitoring basal asperities can be used to study the spatial structure of subglacial water systems.

Small magnitude ($M < 1$) repeating basal stick-slip events frequently display swarm like behavior, periods of activity followed by quiescence. Allstadt and Malone (2014) observed that the onset of swarms was correlated with relatively modest changes in σ_n', less than $<0.5\%$ of the glacier load, due to snowfall events. They suggested that this small change in normal stress prompted a reorganization of the hydrologic subglacial system, which in turn the spatial distribution of basal shear stresses and instigated the swarm. However, swarm activity has also been observed in Greenland (Röösli *et al* 2016a), Antarctica (Smith *et al* 2015), and other mountain glaciers (Helmstetter *et al* 2015b) with no clear trigger. However, internally driven oscillations are known to occur in subglacial hydrologic systems (Fricker *et al* 2007, Schoof *et al* 2014). Thus, swarm activity may prove useful in tracking spatial and temporal changes in the distribution of subglacial water and stresses (Kavanaugh and Clarke 2001).

3.3.3. Tidal and stressing rate modulation of seismicity. It is clear from equation (20) that stressing rate variations $\dot{\sigma}_e$ will also modulate seismicity patterns. Tidal modulation of the force budget near the grounding lines of marine-terminating glaciers and ice sheets is the best studied driver of variable $\dot{\sigma}_e$. Tides modulate the glacial force budget through a combination of flexural and hydrologic perturbations that propagate upstream. The speed and magnitude with which a grounding line perturbation propagates upstream is dictated to large degree by subglacial conditions and thus, several studies have demonstrated how along flow observations of tidal influences on seismicity and velocity records can be used to infer subglacial conditions, potentially the appropriate sliding laws (Anandakrishnan and Alley 1997, Gudmundsson 2011, Walker *et al* 2013). However, in some regions where the surface velocity is tidally modulated, asperities appear to be unperturbed, indicating that the sticky-spots are strong relative to the size of the tidal perturbation (a few kPa) (Aalgeirsdóttir *et al* 2008, Smith *et al* 2015).

In the Ross Sea region of Antarctica, a semi-diurnal tide results in peak grounding line flow speeds on the falling tide (Anandakrishnan *et al* 2003) (figure 16). Analysis of δt shows a clear modulation by the tide for both the large Whillans Ice Stream events as well as the smaller David Glacier events. Winberry *et al* (2009b) and Zoet *et al* (2012). As expected, higher stressing rates promote a decrease in δt by promoting failure of the asperity earlier in the stick-slip cycle for the David Glacier events. On the Whillans Ice Stream, increasing flow rates near the grounding line on falling tide lead to

shorter δt (Bindschadler *et al* 2003, Winberry *et al* 2014). It is also observed in both settings that event size scales with inter-event time. This implies that c_s is not solely a function on σ_n', but is a time-dependent feature. This well known behavior is called 'healing' in the rock mechanics literature and is consistent with more complex friction laws (Marone 1998). Several mechanism likely control healing rates in the subglacial environment, but potential processes include increasing contact area between either side of the slip patch with time due to creep of the ice (Zoet *et al* 2013, McCarthy *et al* 2017) or pore-pressure diffusion following slip events (Iverson 2010).

4. Brittle failure seismicity in the interiors of glaciers, ice sheets, and ice shelves

Crevasses are one of the most visible indicators of dynamic behavior in glacial setting, and play an essential role in a range of glacial phenomena (Colgan *et al* 2016). While satellite imagery provides the spatial resolution required to study fracture processes in glacial systems, it lacks the temporal resolution to resolve short time-scale (<1 d) processes that characterize fracture evolution. Crevasse formation and expansion in response to glacial stresses generates seismic waves that allow the fracture mechanism to be investigated, providing a complementary tool to other *in situ* observations (such as GPS). At the smallest scales, firn or exposed ice may produce very small seismic events through consolidation, or in response to boundary or thermal stresses, e.g. Chaput *et al* (2015).

Across a broad range of glacial settings, small seismic events (magnitudes −1 to 1) generated by near-surface crevasses are often the most abundant source of seismic activity, allowing development of individual fractures to be monitored, e.g. Neave and Savage (1970) and Rowe *et al* (2005), while larger events (e.g. magnitudes ≈2) may be observed at relatively large distances (>800 km) and to exhibit enhanced Rayleigh wave radiation due to their shallow source depths (Lough *et al* 2015, Mikesell *et al* 2012). While highly conspicuous on the surface, fractures at depth and in basal context play important roles in the glacial hydrologic system (Fountain *et al* 2005, Harper *et al* 2010) as well as in the calving and general stability of ice shelves, e.g. Joughin and MacAyeal (2005) and MacAyeal *et al* (2003).

Thus, locating seismic activity with high accuracy provides a means of identifying fractures not visible at the surface, e.g. Roux *et al* (2008). Subsurface fractures may be distinguished from the stick-slip style events discussed above by their predominately isotropic (volumetric) source mechanism. While, the crack opening mechanism is useful for interpreting fracture sources, a few studies have computed the full moment tensor and consistent with theoretical expectations and other observations these studies have shown that shear failure can also be a significant component of the deformation during fracture in glacial settings (Walter *et al* 2009, Heeszel *et al* 2014a). Thus, the temporal evolution of seismic activity provides insight into both internal and external drivers of fracture propagation across a range of glacial settings.

On grounded ice, fracture seismicity varies over a range of time-scales in response to both external and internal drivers. In regions associated with surface melt, daily fluctuations in meltwater can modulate seismicity rate by introducing strain-rate variations (Mikesell *et al* 2012) or through hydrofracturing (Carmichael *et al* 2012). However, the most significant source of hydrofracturing seismicity is surpaglacial lakes that drain englacially through fractures. During these lake drainage events additional near surface seismicity is driven by glacial deformation as water is redistributed into the sublglacial environment (Roux *et al* 2010, Carmichael *et al* 2015). Deformation associated with a passing glacial surge front can drive significant seismicity variations (Raymond and Malone 1986, Stuart *et al* 2005). At much shorter time-scales it has recently been discovered that transient strain associated with transiting seismic surface waves from large distant earthquakes can dynamically trigger crevasse-attributed seismicity in critically stressed brittle Antarctic glaciers (Peng *et al* 2014) (figure 17), expanding the field of dynamically triggered remote seismicity, previously recognized in the earthquake system, e.g. Brodsky and van der Elst (2014), into the cryosphere.

5. Seismicity at marine glacial termini

Iceberg calving from marine and freshwater glacial termini is a complex process that is influenced by glacial strain, gravity waves, tides, currents, surface processes, thermal transport and phase changes associated with both ocean water and glacial ice, sub- and en-glacial hydrology, and by pre- and syn-calving fracturing processes. Calving (and subsequent melting of produced icebergs) is a predominant component of present ice mass loss from Antarctica (Depoorter *et al* 2013), and also makes up approximately 1/3 of ice mass loss from Greenland (Enderlin *et al* 2014). Calving is a primary process affecting ice loss and sea level rise that has recently accelerated in many large terminating glacial systems (Thomas *et al* 2011). This trend has been accompanied by accelerating ice mass loss due to direct melting in Antarctica and Greenland. In Greenland, the predominant process is surface melting and runoff (Enderlin *et al* 2014). However, in most of Antarctica there is very limited or no surface melting, and accelerated direct melting has recently been driven by warmer ice-shelf water, circulating circumpolar deep water, and by tidal and wind mixing beneath and at the edges of ice shelves (Depoorter *et al* 2013, Paolo *et al* 2015).

Calving results from a complex and sensitive interplay of ice dynamics and fracture with associated basal, surface, and terminus thermal and mechanical boundary conditions. This, coupled with its fundamental importance to the behavior and stability of glacial systems, makes the calving regime of historic interest in understanding glacial dynamics. First proposed as seismic source over a half-century ago (Hatherton and Evison 1962), during the past approximately two decades,

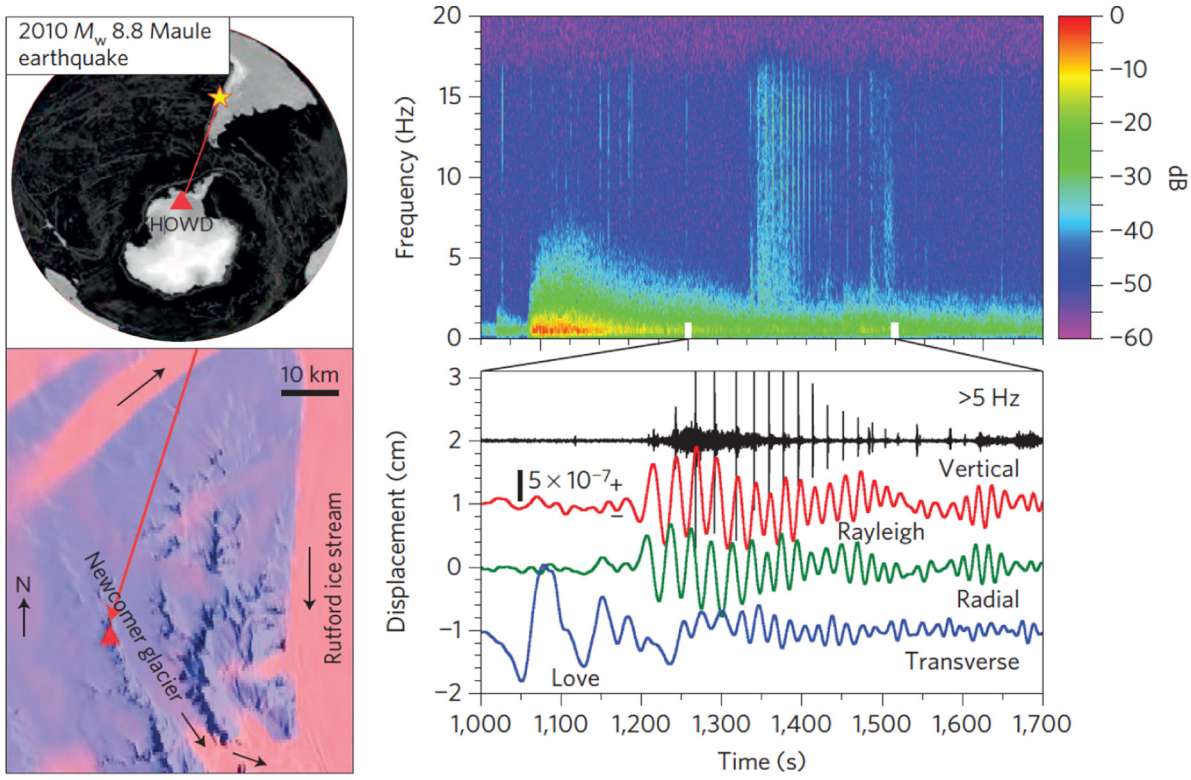

Figure 17. Shallow critically-stress crevasse field-attributed icequakes, dynamically triggered in the Newcomer Glacier region of West Antarctica by teleseismic surface waves from a large (M_w 8.8; ≈4691 km-distant) Chilean earthquake (left). At right is shown a vertical-component spectrogram (top) and associated low-pass filtered (colors) seismograms (bottom) showing the arrival of the Love (transversely-polarized) and Rayleigh (vertically-radially polarized) surface waves from the earthquake. The vertically polarized, high-pass filtered seismogram in black shows triggered shallow icequakes induced by the passage of the Rayleigh wave, with timing approximately phase-locked to the maximum Rayleigh wave vertical displacement (and maximum strain dilitation). Reprinted by permission from Macmillan Publishers Ltd: Nature Geoscience Peng *et al* (2014). Copyright (2014).

seismic and other geophysical method have increasingly been applied to studying the calving system.

5.1. Iceberg calving seismicity in Greenland and Antarctica

The Greenland ice sheet, surrounded by coastal mountains, is primarily drained by a small number of very large and fast moving marine-terminating outlet glaciers, some with terminus thicknesses of up to 1 km or more. Enderlin *et al* (2014) recently estimated that calving from only five Greenland glaciers accounted for approximately 50% (just 15 accounted for 77% and a single glacier, Jakobshavn Isbrae, drains approximately 5 to 8%; Bindshadler (1984)) of icecap mass delivered to the ocean by glacial flow (739 ± 29 Gt) between 2000 and 2014.

The past decade has witnessed dramatic changes in the Greenland ice sheet due to atmospheric and oceanic forcings attributed to climate change. The proportion of ice delivered to the ocean by surface melt and sub- and en-glacial flow has been estimated by Enderlin *et al* (2014) to now be comparable or greater to the glacial (calving) flux, and to be increasing, (32% to 58% between 2010 and 2014) primarily in response to a climate-change driven increase in surface temperature. Another recent change to the Greenland cryosphere has been the thinning, acceleration and terminus retreat, punctuated by ice mélange and other seasonally variations (Amundson *et al* 2010) and of large outlet glaciers (for example, over 10 km of recent retreat at Jakobshavn Isbrae; e.g. Joughin *et al* (2008)).

Greenland and Antarctic outlet glaciers can generate seismic events with source moment magnitudes of up to M_w 5.1 and source durations of 60 s or longer (by comparison, the typical source duration of an M_w 5.0 tectonic earthquake is around 2 s). These events are globally observable as seismic signals with unusually strong Rayleigh waves for their magnitude between 10 and 150 s period (Ekstrom *et al* 2003, Ekstrom 2006, Ekstrom *et al* 2006, Tsai and Ekstrom 2007, Tsai *et al* 2008, Nettles and Ekstrom 2010, Chen *et al* 2011, Veitch and Nettles 2012). Early source modeling using seismographic data from global distances showed that teleseismic surface waves from these events were inconsistent with tectonic earthquake-like (double couple) source mechanisms, but could be modeled using sub-horizontally directed single-forces applied to Earth's surface in the mass-distance product range (for Greenland) of 0.1 to 2.0×10^{14} kg m (Tsai and Ekstrom 2007). Further global monitoring established their approximate locations at the termini of large tidewater glaciers in both Greenland and Antarctica (but preferentially in Greenland) (e.g. Nettles and Ekstrom (2010)). The spatiotemporal evolution of large Greenland glacial earthquakes show seasonal and secular changes, in particular a northward advancement along the west coast of Greenland over the past two decades, that correlate with atmosphere and ocean

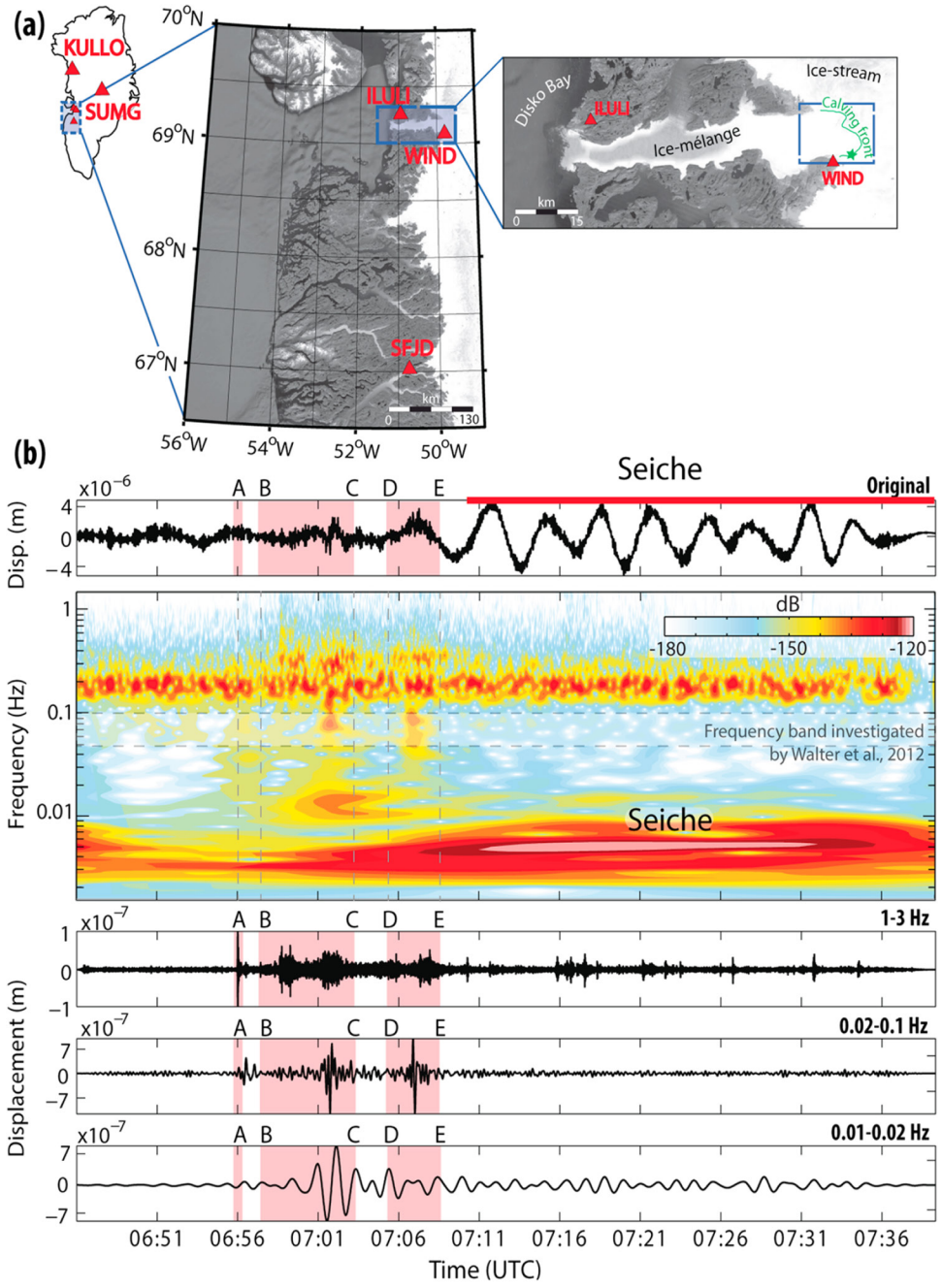

Figure 18. (a) Left: regional seismic stations (red triangles) on the west coast of Greenland used to study megaiceberg calving events at Jakobshavn Isbrae. Right: the glacial fjord and termimus (figure A.1), indicating the source location (Green star). (b) Top: vertical ground displacement at station ILULI and its spectrogram. Bottom: band-pass-filtered seismograms (13, 0.020.1, and 0.010.02 Hz). Attributions of calving event processes, corroborated by video observations, are: (A) ice avalanche at the initiation of calving; ((B) and (C)) initial iceberg capsize; ((D) and (E)) second iceberg calving. Reproduced with permission from Sergeant *et al* (2016). © 2015. American Geophysical Union. All Rights Reserved.

warming, suggesting large-scale glaciological response to changing climate (Ekstrom *et al* 2006, Veitch and Nettles 2012).

Investigations into the source processes of Greenland glacial earthquakes, utilizing seismology, GPS positioning, satellite, and local video observations show that these events arise from glacier, water column, and ocean bed forces applied during the detachment and capsizing of very large ($\approx 1 \times 10^9$ m^3) gravitationally unstable newly calved icebergs (Amundson *et al* 2008, Walter *et al* 2012, Sergeant *et al* 2016, Murray *et al* 2015; (figures 18 and 19). Because larger events are seismically globally observable, their location and magnitudes can be used as valuable proxy measurements to monitor this type of calving. The displacement of large water volumes during these events can additionally generate significant local seiches that apply additional forces to the solid Earth and generate ocean waves that are readily detectable up to 50 km away (Amundson *et al* 2008). Recent seismic modeling at periods between 10 and 100 s by Sergeant *et al* (2016) of a particularly well studied megaiceberg calving event (which incorporated two large icebergs) at Jakobshaven showed that at least four important seismogenic mechanisms occurred during the

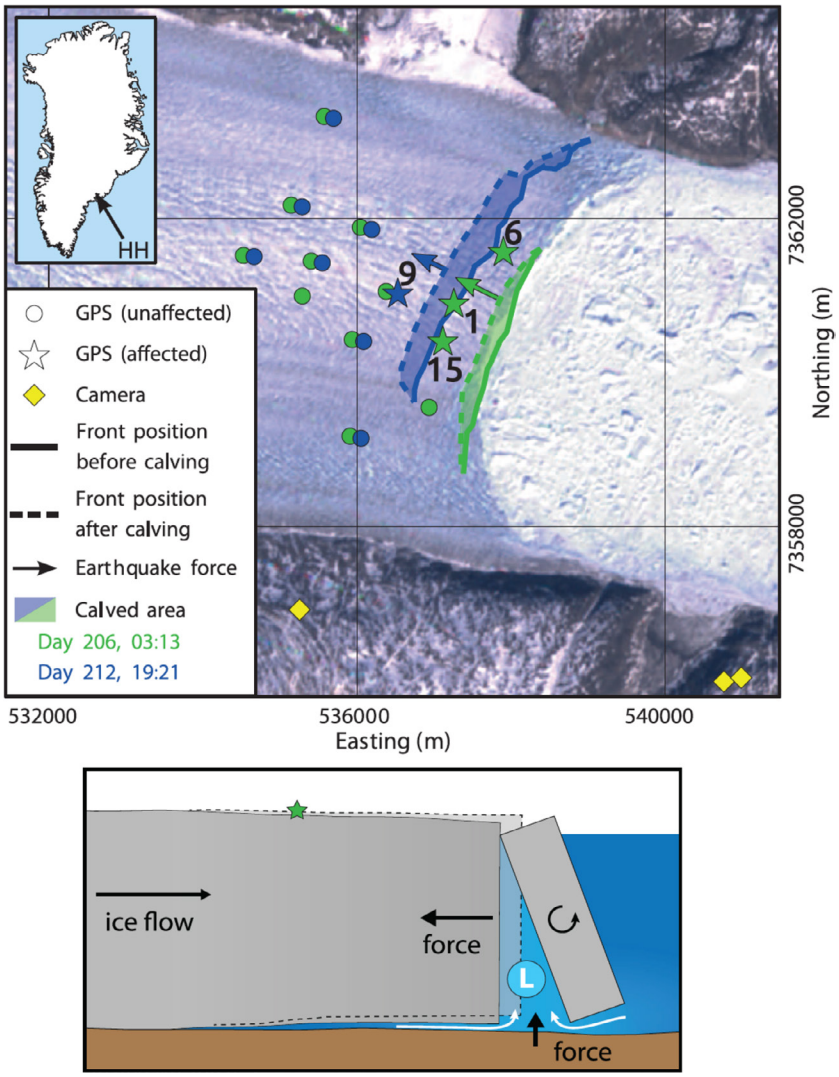

Figure 19. Site and modeling of Helheim Glacier, Greenland megaiceberg calving/capsize glacial earthquake sources during 2013. Map positions are shown in meters in Universal Transverse Mercator zone 24N. The indicated principal force is a reaction force in the up-glacier direction due to the capsizing and rotation of the iceberg. Low pressure behind the rotating iceberg draws water laterally and upwards, which produces a secondary, upward, Earth-normal force. From Murray *et al* (2015). Reprinted with permission from AAAS.

event; collapse initiation, capsizing iceberg-to-terminus contact (distinct for the two associated icebergs), and ice mélange motion (interpreted as sub-horizontal forces generated for 20 min after calving due to collisional or shear forces within the mélange (Amundson *et al* 2010) and/or along the terminus margin). It appears that the complexity and variability of large glacial calving events results in highly variable seismic excitation, and recent studies incorporating video and other corroborative observations indicate that waveform inversions for moment rate functions of these events may have a limited ability to produce reliable estimates of ice loss (Walter *et al* 2012, Sergeant *et al* 2016).

5.2. Glacial rumbling and upstream calving-associated slip

Closer inspection from more locally sited seismographs has further revealed that large fast-moving Greenland glaciers can also produce long-duration (10–40 min) 'glacial rumbling' events, such as observed at Jakobshavn to occur approximately once very two days during the summer melt season by Rial *et al* (2009). These particular events, recorded by a seismographic array at a range near 50 km, were found to commonly culminated in a large-amplitude subevents showing distinct P and S phases that were found to be consistent with fault plane shear (i.e. a double-couple source mechanism) that was geographically associated with a bend in the feeding ice stream. The events had seismic moment magnitudes between approximately 4 and 4.3. However, the sense of slip was not able to be robustly constrained due to a lack of azimuthal source coverage by the available seismic array. Rial *et al* (2009) interpreted these rumbling events as progressive upstream (5–10 km from terminus) ice–ice or ice-bed stick-slip failure, typically induced by calving events at the terminus.

5.3. Glacial calving seismicity in Alaska and Svalbard

In addition to the major outlets of Antarctica and Greenland, large tidewater glaciers are found in other glaciated regions, including Alaska, Arctic Canada, Patagonia, and Svalbard. The stability of many of these glacial systems appears to be

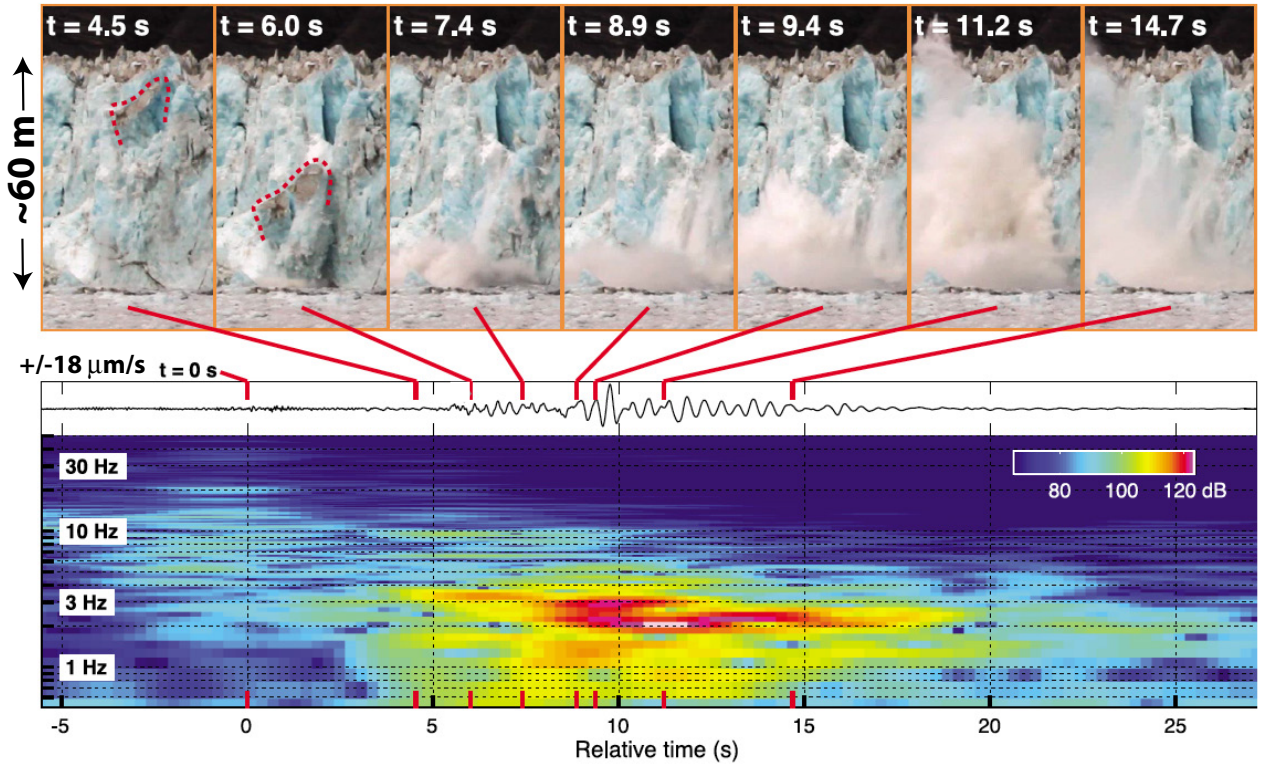

Figure 20. Spectrogram of seismic vertical-component velocity of a calving event from Yahtse Glacier in September 2010. Seismogram was recorded 1.8 km from the source on a rock site at the glacier edge. Images at top show the evolution of the calving event, which was visibly identified as initiating at $t = 0$ s on the indicated time scale. The initial, pre-water-column impact, failure of the ice front is associated with weak seismic energy near 5 Hz. The strong spectral peak near 3 Hz is identified with the occurrence of a Worthington (cavity collapse) jet, which becomes visible beginning near $t = 8.9$ s. The grounded glacier terminus is approximately 170 m thick and the ice front height extends approximately 60 m above the ocean surface. Reproduced with permission from Bartholomaus *et al* (2012).

dominated by surface mass balance (Larsen *et al* 2015), but exceptions exist, including examples of surging mediated by hydrothermodynamic feedback process linked to summer melt noted in Svalbard (Schellenberger *et al* 2017). Calving dynamics are essential to understanding the full range of tidewater systems on all scales. Particularly well-documented in southeast Alaska, e.g. O'Neel *et al* (2007), it has long been recognized that calving seismicity may be a useful proxy for calving rate (Qamar 1988, Bartholomaus *et al* 2012, 2015b, Köhler *et al* 2015, Köhler *et al* 2016). Longer term records have been used to understand seasonal fluctuations, surge-type behavior, and dynamic changes during retreat (Walter *et al* 2010). The seismic and hydroacoustic source mechanisms associated iceberg calving are complex, and include shear and normal forces during detachment and gravitationally driven slip, impact forces of falling ice with the water surface, drag and buoyancy forces associated with ice deceleration, and air/water cavity collapse.

Significant recent progress in understanding seismogenic calving processes has been achieved through simultaneous video/time lapse imagery and seismic observations. Moderate sized calving events involving calved ice volumes of tens to hundreds of thousands of m^3 (i.e. much smaller than the mega-calving events of Greenland; figures 18 and 19), and source durations of several to 1000 s), generate local to regionally detectable seismic energy between 0.5 to tens of Hz, that may be strongly peaked in the short period (e.g. 1–3 Hz; O'Neel *et al* (2007) and Richardson *et al* (2010)) band (figure 20). A common phenomenon observed to be associated with the generation of this narrowband energy is the generation of air cavity collapse-driven subvertical Worthington jets occurring several seconds after the iceberg impacts the water column (Bartholomaus *et al* 2012).

A long-term goal of glacial seismology is to quantitatively estimate calving rates of marine terminating glaciers at temporal resolution that is not possible with remote-sensing observations. However, at the present state of knowledge, complexity and diversity of calving events (e.g. events with a high degree of subareal fragmentation versus those that are largely submarine) makes the inference of calved ice volumes from purely seismological observables challenging. Calibration for specific glaciers and glacial settings may substantially improve accuracy of these estimates. For example, recent work has shown that relatively simple approaches (generalized linear models) can be used to develop scaling relationships between calving observations (either visual (Bartholomaus *et al* 2015b) or satellite-derived (Köhler *et al* 2016)) and seismic attributes, in particular the duration of seismic signal associated with a discrete calving event. Once calibrated, seismic records can then be used to study calving variability over time-windows (daily, seasonal, yearly) during which other observations are not available.

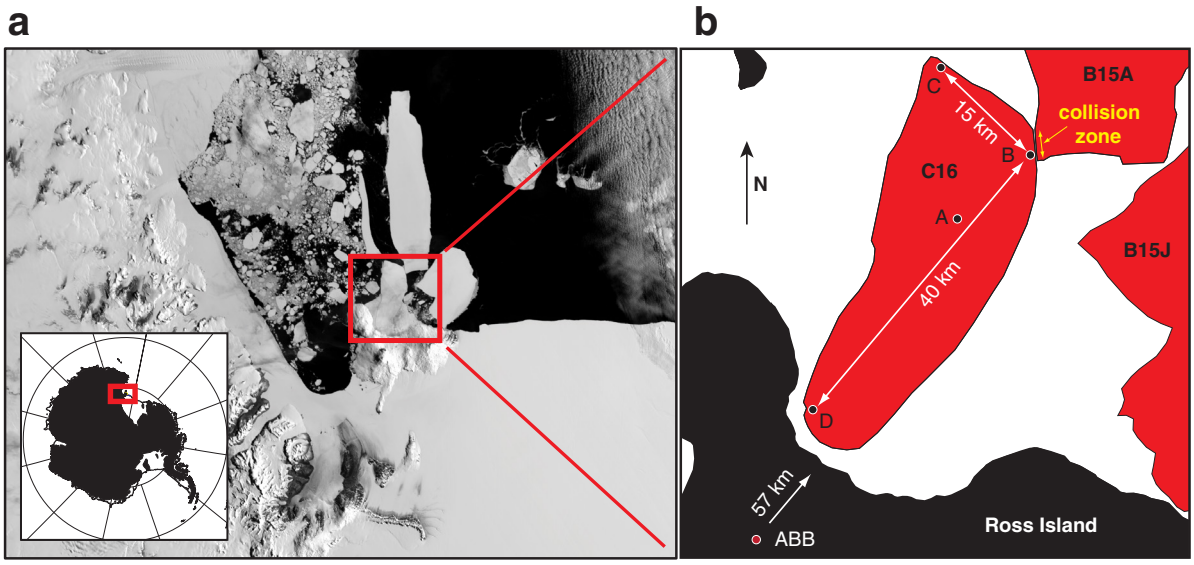

Figure 21. Seismic station locations and icebergs (MODIS satellite image) near Ross Island, Antarctica on 26 December 2003 Iceberg C16 was immobilized against the northern coast of Ross Island, and the icebergs B15A, B15J, and B15K were adrift at this time. (b) Seismograph sites on C16 (AD) and a land-sites seismograph on Mount Erebus (ABB) (Aster *et al* 2004) are shown. The collision zone between B15A and C16 was determined to be the source location of prominent iceberg harmonic tremor events. Reproduced with permission from MacAyeal *et al* (2008). © 2008. American Geophysical Union. All Rights Reserved.

6. Iceberg seismicity

Iceberg collisions and mass wasting processes, e.g. Scambos *et al* (2008), Glowacki *et al* (2015) and Scambos *et al* (2008), are notable contributors to the global oceanic hydroacoustic noise field (Matsumoto *et al* 2014) and have, more recently, been found to produce significant seismic signals that can be recorded by seismographs at distances of hundreds or even thousands of km (Talandier *et al* 2006, Martin *et al* 2010a, 2010b, Pirli *et al* 2015), where the signals propagate to teleseismic distances as hydroacoustic phases in the oceanic sound channel. Collisions or disintegration of isolated icebergs is also a recognized source of atmospheric infrasound (Richardson *et al* 2010). The largest marine icebergs originate from Antarctic ice shelves. For example, B15 (calved in March of 2000 from the Ross Ice Shelf), had an extent approximately 120 by 40 km, a thickness between approximately 180–250 m, and a mass of 10^{15} kg (Dowdeswell and Bamber 2007). The effects of iceberg–iceberg and iceberg grounding contact and seabed scouring are of significant interest in paleoclimatology, biology, marine geology, and a number of other fields (Dowdeswell and Bamber 2007, Martin *et al* 2010b).

6.1. Iceberg harmonic tremor

Highly harmonic spectral characteristics of some iceberg-associated seismic signals were initially noted from seismic data recorded at Mount Erebus Volcano, Ross Island (MacAyeal *et al* 2008), in seismic signals recorded on Pacific islands (Talandier *et al* 2002, 2006) created by coupled hydroacoustic (T) phases (Talandier and Okal 1998, Hanson and Bowman 2006), and in seismograms recorded near the Neumayer Antarctic research station on the Princess Martha Coast of Queen Maud Land (Müller *et al* 2005). Müller *et al* (2005) noted the highly harmonic seismic signals (figure 22) associated with the local passage of drifting tabular icebergs, and hypothesized a mechanism involving forced fluid flow and excited resonances. The true mechanism of iceberg harmonic tremor was determined by MacAyeal *et al* (2008), who exploited a multi-year assemblage of wind and tidally driven, repeatedly colliding large tabular icebergs calved from the Ross Ice Shelf near Ross Island and McMurdo (U.S.) and Scott (New Zealand) Stations (figure 21). This situation facilitated the deployment of iceberg-sited seismographs and GPS positioning instruments to establish both relative iceberg motions and to record associated near-source seismic signals. Iceberg harmonic tremor signals were revealed to arise from repetitive stick-slip events occurring at ice–ice or ice-ground contacts (MacAyeal *et al* 2015) (figure 22). The harmonic features of these signals arise because impulsive subevents, sufficiently regularly spaced in time, produce harmonic spectra with a fundamental frequency that is equal to the subevent frequency (i.e. a periodic sequence of delta functions has a Fourier spectrum that is a sequence of delta functions in the frequency domain (Bracewell 2000)). The repetitive stick-slip nature of this source process was only revealed when iceberg-sited seismographs were deployed very close (several km or less) to the source zone, because multipathing and attenuation obscure the individual subevents in more distantly recorded seismograms (figure 22).

6.2. Iceberg grounding seismicity

Complex seismic and hydroacoustic signals have also been found to be generated during sustained iceberg-seafloor collisions. Martin *et al* (2010b) analyzed iceberg-sited and remote seismographic recordings of the grounding and breakup of B15A in October 2015 as it collided with an undersea shoal

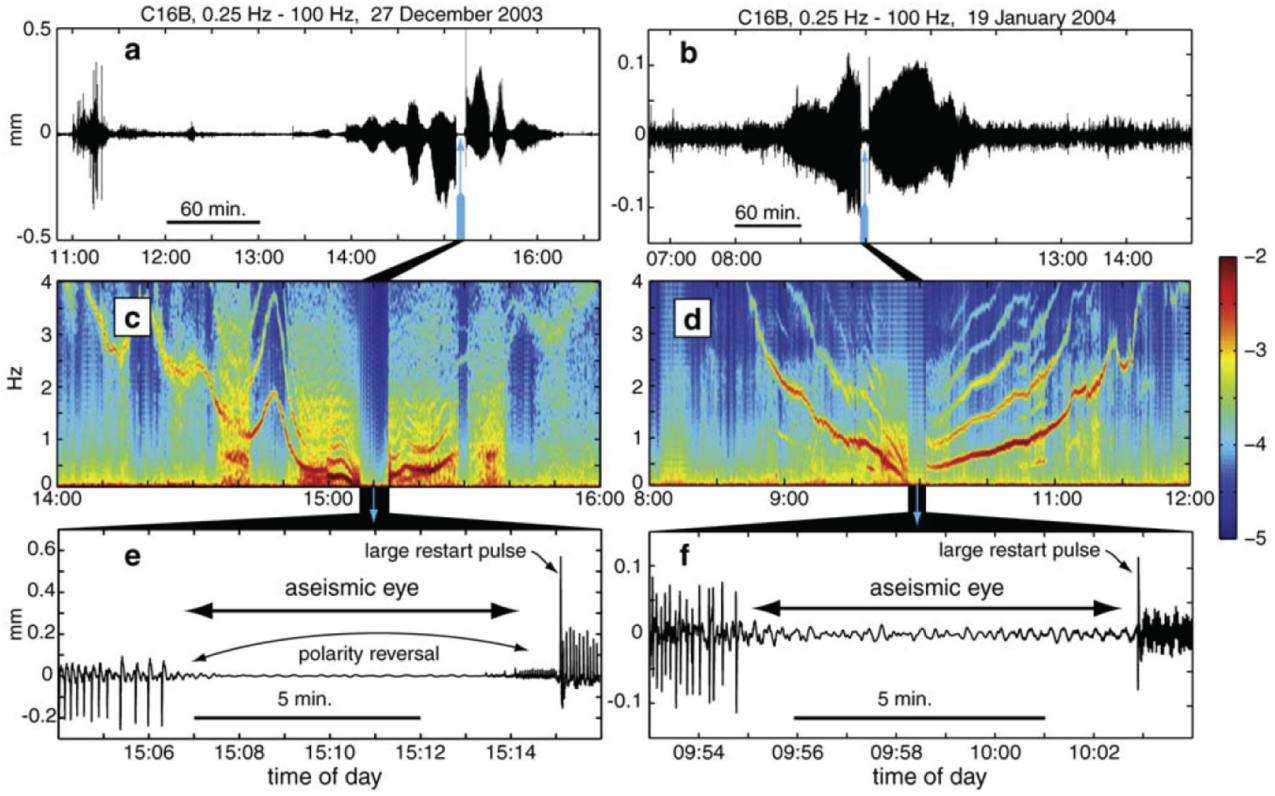

Figure 22. Iceberg harmonic tremor generated by colliding icebergs in the Ross Sea, Antarctica, showing two vertical-component episodes recorded on iceberg C16 seismic station B (figure 1). Respective spectrograms are shown in (c) and (d), where the color bar indicates the $\log_{10}$ of signal power spectral density in units of dB relative to m^2s^2 per Hz. Seismic polarity and iceberg motion reversal across seismic gaps, tracking of signal fundamental frequency with the GPS-constrained velocity of B15A, and the polarities of radiated P waves ((e) and (f)) established the source mechanism as repeated strike-slip, stick-slip, subevents occurring at the C16/B15A contact, and driven by reversing relative iceberg motion. Reproduced with permission from MacAyeal *et al* (2008). © 2008. American Geophysical Union. All Rights Reserved.

near Cape Adare, Antarctica (figures 23 and 24). This relatively well-studied grounding and breakup event generated powerful harmonic and chaotic signals that were observed as far away as South Pole station (≈17.9° distant; Martin *et al* (2010b)).

7. Seismological studies of ice shelves

7.1. Ice shelf seismology

Ice shelves and ice tongues, the floating extensions of ice sheets and glaciers, exert fundamental control on the grounded ice through buttressing. A reduction in buttressing due to collapse or weakening of ice shelves results in the acceleration of inland grounded ice, e.g. Scambos *et al* (2004), thus accelerating sea level rise. The structural integrity of ice shelves is regulated by the distribution and size of crevasses and rifts (a full depth fracture on an ice shelf). Recent catastrophic ice shelf collapses have been observed to be abetted by the pooling of supra-glacial melt water that promotes hyrofracturing through preexisting fractures and subsequent gravitationally driven disintegration (MacAyeal *et al* 2003, Scambos *et al* 2009, Pollard *et al* 2015), and ice shelves are presently thinning globally in response to changes in ocean temperatures (Paolo *et al* 2015, Furst *et al* 2016, Marsh *et al* 2016, Jeong *et al* 2016).

Because of importance to glacial stability and sea-level rise, significant efforts are being undertaken to improve understanding of ice shelf structure, dynamics, and stability, including focused seismic studies that illuminate controls on their strain and fracture (rifting and calving) evolution. Ocean swells from distant storms create flexural elastic waves and attendant strains in ice shelves (Bromirski *et al* 2015) and large icebergs (MacAyeal *et al* 2006, 2015) that may in some cases promote fracturing (Sergienko 2010). Tsunamis from distant earthquakes have also been observed to spur the calving of large tabular icebergs from ice shelves (Brunt *et al* 2011). While external environmental factors appear secondary in influencing ice shelf rift propagation (Bassis *et al* 2007, 2008, Bassis *et al* 2005), near grounding lines tidal stresses have been shown to exert significant control on fracture rates (Osten-Woldenburg 1990, Barruol *et al* 2013, Lombardi *et al* 2016, Hulbe *et al* 2016) and microseismicity (Podolskiy *et al* 2016). This is significant, since many ice shelf crevasses originate at grounding lines and are then advected seaward with flow of the ice shelf, where they are increasingly influenced by the ocean.

Recent seismographic deployments atop ice shelves and tabular icebergs (Nicolas *et al* 1973, Okal and MacAyeal 2006, Bassis *et al* 2008, MacAyeal *et al* 2009, Bromirski and Stephen 2012, Zhan *et al* 2014, Bromirski *et al* 2015, Diez *et al* 2016, Bromirski *et al* 2017), and, in a few cases, on Arctic

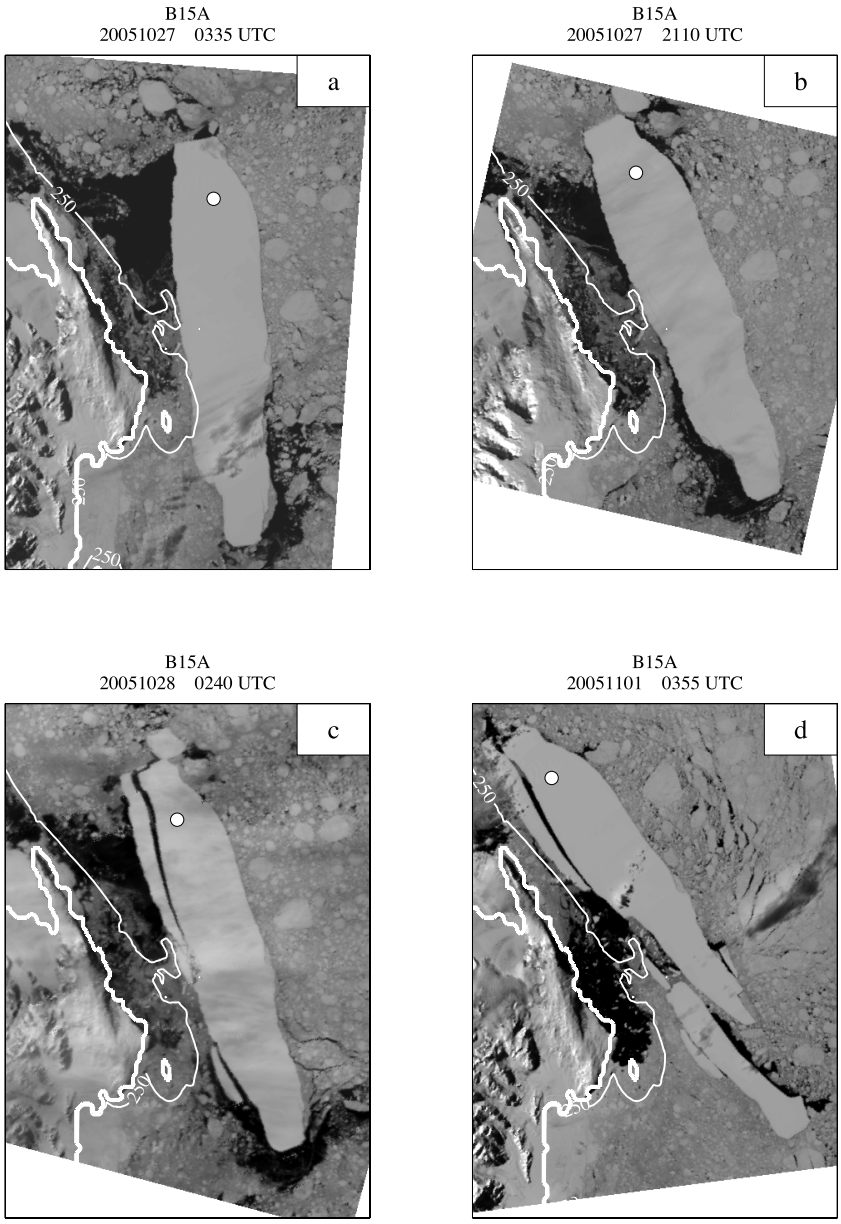

Figure 23. Four successive MODIS images of B15A iceberg breaking up near Cape Adare, northern Victoria Land, Antarctica (250 m resolution). The 250 m depth contour and coast are shown by thin and thick white contours, respectively. The white dot shows the location of a seismograph that was deployed atop the iceberg and recorded its breakup. Reproduced with permission from Martin *et al* (2010a).

sea ice (Läderach and Schlindwein 2011) have observed elastic and gravity wave phenomena over periods from thousands of seconds to frequencies of many Hz. Mechanical and other perturbations to ice shelves are of significant importance to assessing the stability of these features. It has recently been discovered that ice shelf displacements also couple into acoustic-gravity atmospheric waves in the 3–10 h period range (Godin and Zabotin 2016).

Harmonic strain from ocean gravity waves may be important to ice shelf stability, e.g. Sergienko (2010), Bromirski and Stephen (2012) Oceanographic mechanical forcings include wind-driven waves and ocean swell, infragravity waves (ocean gravity waves with periods longer than 100 s), tides, ocean gravity wave signals from regional calving events MacAyeal *et al* (2009), and tsunamis (Brunt *et al* 2011). Ocean waves (Paolo *et al* 2015) and tides (Bromirski *et al* 2015) couple with the sub-ice shelf ocean water column and overlying floating shelf to produce a propagating elastic (compressional, shear, and flexural; e.g. Press *et al* (1951) and Sergienko (2010)) strain field within the floating glacial ice. Recent large-scale deployment of broadband seismographs across the Ross Ice Shelf has shown that coupled gravity wave/flexural wave strains can penetrate the ice shelf/water cavity system to the ice shelf grounding line (Bromirski *et al* 2015) (figure 25).

8. Subglacial and englacial fluvial seismology

Substantial extents of temperate glaciers may be near the melting point, and may thus include liquid inclusions that interact with a melt-containing firn aquifer (Forster *et al* 2013)

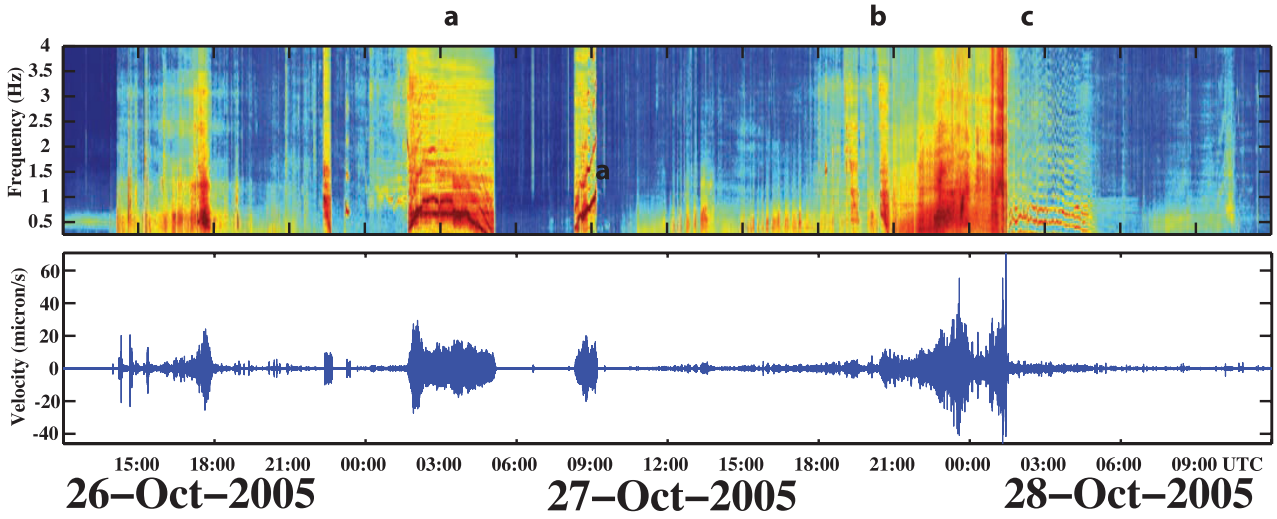

Figure 24. Spectrogram and corresponding vertical-component seismogram, showing harmonic and non-harmonic signals recorded atop B15 iceberg during its shoaling and breakup, which occurred between October 26 (12:00 UTC) and 28 October (12:00 UTC), 2005. Iceberg tremor events (a)–(c) correspond to the first three panels of figure 23, where events a and b are interpreted as hard grounding events which precipitated iceberg breakup, and event c is interpreted as iceberg harmonic tremor from sideswiping iceberg fragments. Reproduced with permission from Martin *et al* (2010a). © 2010. American Geophysical Union. All Rights Reserved.

and englacial channels affected by melt, crevasse formation, and linked conduits, Fountain and Walder (1998), Irvine-Fynn *et al* (2011) and Bradford *et al* (2013). The surface or subsurface transport of water under the influence of gravity or pressurization creates transient forces on the solid Earth that generate seismic waves, e.g. Cole *et al* (2009), Burtin *et al* (2010), Schmandt *et al* (2013) and Burtin *et al* (2016). Water storage and flow through the surface and subsurface hydrologic pathways of glaciers are central to the transport of heat, to dynamics (e.g. by influencing bed friction; Damsgaard *et al* (2016)), to erosion, and to mass balance. The flow of fresh water exiting glaciers also strongly impacts the physical and biological state of downstream fluvial, lake, and marine systems. Dynamic glacial processes also create scenarios for meltwater storage and drainage, which may manifest episodically as glacial outburst floods (GLOFs; e.g. Walter *et al* (2008), Heeszel *et al* (2014b) and Jacquet *et al* (2016)) that pose a significant and increasing natural hazard to communities in glaciated regions. Although long recognized for its potential, e.g. St. Lawrence and Qamar (1979), the routine use of seismic methods to explore the glacial hydrologic system has become common only recently, e.g. Bartholomaus *et al* (2015a). Much of the seismic phenomenology of sub- and englacial flow systems awaits further data collection and study, but recent work point to its potential for monitoring and quantifying the transport of both water and sediment. Terminal flow of subglacial water into the ocean is also a contributor to the hydroacoustic noise field (Glowacki *et al* 2016). The seismic signature of water movement in glacial systems can be generated by one of two general processes: the resonance of fluid-filled cavities and turbulent water-flow.

In temperate glacial systems, water near the surface is commonly focused into relatively constricted conduits that may take the form of moulins in the englacial environment or basal channels in the subglacial environment mediated by melt and or fracture systems that may be highly seasonally variable (Dalban Canassy *et al* 2016). This has led many workers to draw parallels between the tremor-like excitation mechanisms of glacial systems and volcanic systems, where the resonance of magma filled conduits is a mechanism for generating band-limited harmonic tremor. If the properties of conduit wall and fluid can be estimated, models of conduit resonance allow the dominant frequency to be related to conduit thickness and width. For example, long duration (6 min) narrow-band (near 3 Hz) tremor recorded in West Antarctica associated with two distinct events of episodic propagation (estimated using array back projection) were linked to the movement of water within sub-ice lake and drainage systems at the MacAyeal Ice Stream (Winberry *et al* 2009a) (figure 26). Tremor observed on the margin of the Greenland ice sheet has been attributed to the resonance of water-filled moulins, allowing constraints on water depth (Röösli *et al* 2014). In addition to tremor, the harmonic character of discrete glaciers events (duration of a few seconds) has been related to the transient hydraulic resonant stimulation of fluid-filled fractures at or near the base of glaciers (Métaxian *et al* 2003, West *et al* 2011, Heeszel *et al* 2014b), and within ice shelves (Hammer *et al* 2015). Some glacial tremor signals exhibit frequency gliding that bears spectral similarity to volcanic and iceberg tremor (Helmstetter *et al* 2015a). Such frequency-shifting features may result from rapid changes in flow forcing and/or fracture geometry. Ongoing theoretical advances (Lipovsky and Dunham 2015) continue to improve the ability to quantitatively interpret these signals.

The flux of both water and sediments through both englacial and subglacial conduits will vary at both daily and seasonal time-scales. However, continuous high-quality digital seismograms of fluvial systems have only recently been utilized to study seismic signals generated by flow in rivers, e.g. Burtin *et al* (2010), Schmandt *et al* (2013) and Burtin *et al* (2016) and in glacial systems. Bartholomaus *et al* (2015a) monitored subglacial discharge at the large Mendenhall and Yahtse tidewater glaciers in southeastern Alaska and noted discharge-correlated glaciohydraulic tremor (figure 27). Gimbert *et al*

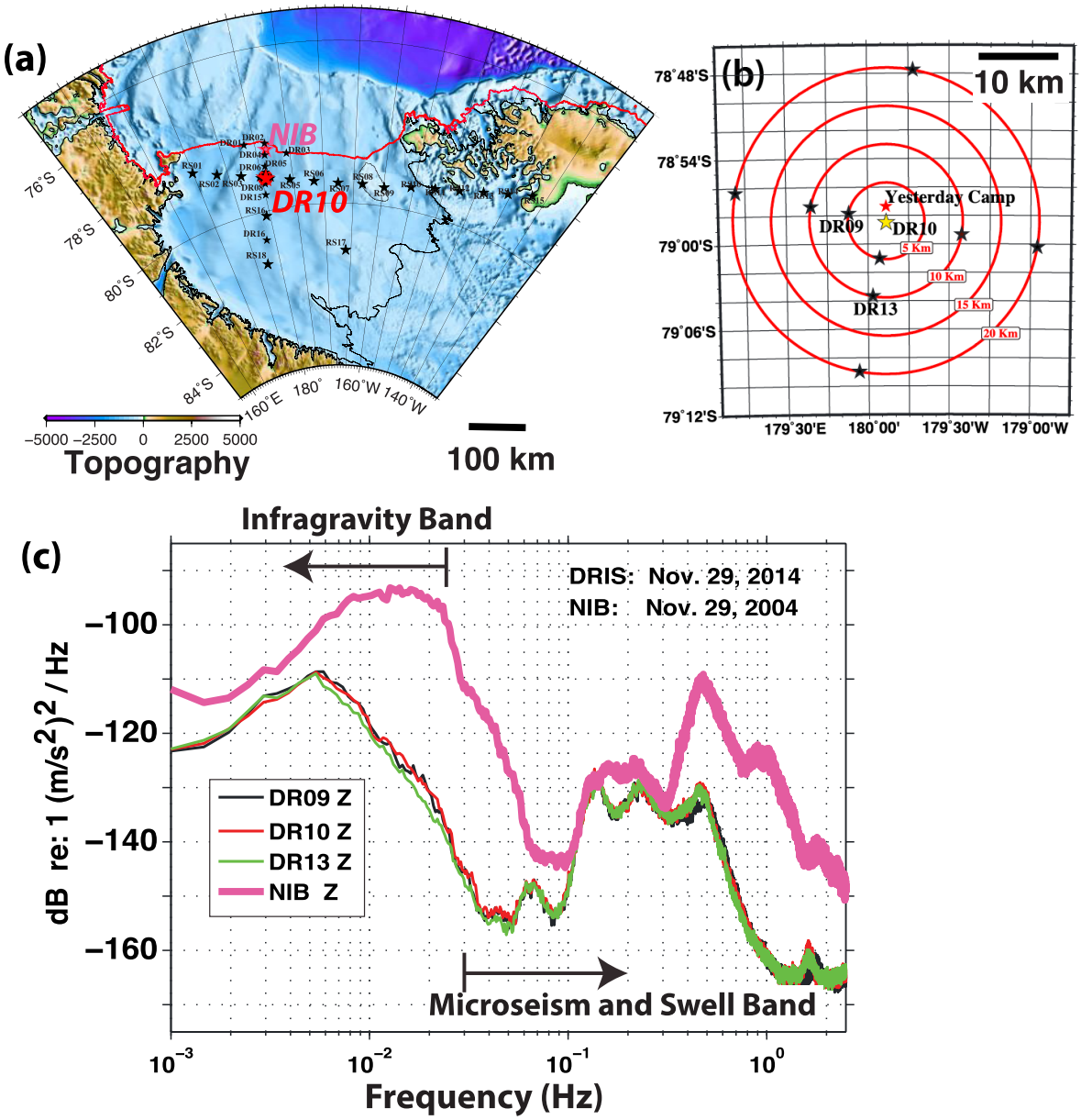

Figure 25. Seismic excitation of the Ross Ice Shelf by ocean waves. (a) Broadband seismograph sites deployed across the ice shelf in the RIS experiment 2014–2016 and from 2004–2006 as part of the pioneering SouthBerg experiment (Cathles *et al* 2009) (ice-front proximal station NIB). Background color scale shows uncompensated topography with ice removed (Fretwell 2013). (b) RIS broadband array (red star in (a)), showing broadband seismographic stations DR09, DR10, and DR13 for which spectra are calculated. (c) Representative vertical-component acceleration power spectral densities observed at ice front station NIB, DR09, DR10, and DR13, showing the propagation of oceanic-generated flexural wave energy into the ocean cavity and interior of the ice shelf in both the microseism and dwell, and the infragravity wave bands. Reproduced with permission from Bromirski *et al* (2015). © 2015. American Geophysical Union. All Rights Reserved.

(2016) studied the relationship between discharge and seismic power at Mendenhall glacier and noted episodic excursions that were successfully modeled using analytical power-law relationships derived for turbulent subglacial conduit flow (figure 28).

Seismic signals from flowing water generally arise from time-varying forces associated with turbulent flow, applied to surrounding ice or rock boundaries and/or by the seismic coupling of acoustic sources within the fluid. Such processes may include pressure fluctuations due to gravity waves, tractions applied due to frictional/impact interactions between water and topographic features of the channel, and via the seismoacoustic coupling of cavitation events and breaking waves. The theory of seismic wave generation by flowing water is still in development and proposed processes and models still await full development and testing. Under simplifying stochastic and physical assumptions, useful analytic expressions for expected seismic power spectral density have recently been derived for turbulent flow in rivers (Gimbert *et al* 2014) and in confined englacial channels (Gimbert *et al* 2016), and have been corroborated with data. Seismic radiation from fluvial systems may also exhibit time-varying response (hysteresis) as the channel is modified by rising and lowering flow levels and as the transportation or disposition of sediment changes, e.g. Schmandt *et al* (2013). The presence of sediment may create additional and distinct (e.g. in a distinct frequency band)

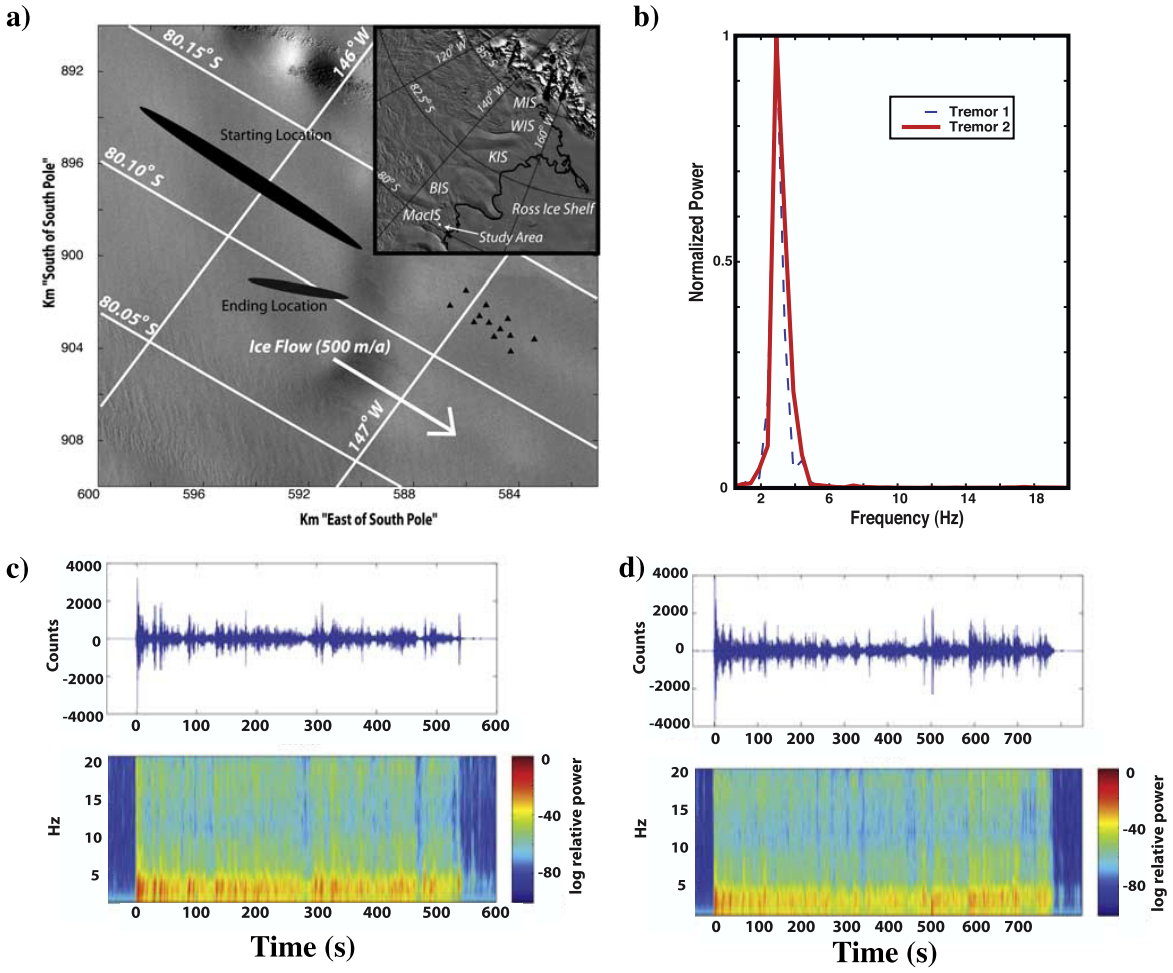

Figure 26. Glaciohydraulic tremor originating beneath the MacAyeal Ice Stream, West Antarctica near its grounding line. The signal is interpreted as a resonating water-ice crack-like conduit with a horizontal dimension on the order of tens of m, draining a small subglacial lake system in episodes lasting approximately 10 min. (a) Location of the MacAyeal Ice Stream (MacIS). Starting and Ending location ellipses show the changing source location of the tremor, estimated using array analysis of seismic energy recorded on the seismographic array indicated by small black triangles. (b) Power spectral density of two tremor episodes, showing narrow-band energy centered near 3 Hz. (C) and (d) show spectrograms (log color scale) showing the sustained, band-limited, and surging nature of the signal with time for two events recorded at a single station. Digitizer counts are proportional to vertical-component seismic velocity. Reproduced with permission from Winberry *et al* (2009a). © 2009. American Geophysical Union. All Rights Reserved.

signals via additional traction and/or impact forces generated by transported bed load constituents (Tsai *et al* 2012, Burtin *et al* 2016).

9. Future directions in glacial seismology

During the past two decades, synoptic scale observations that have become available due to a range of satellite observations, including altimetry, gravimetry, and InSAR, have revealed large secular trends in the behavior and mass balance of the Earth's cryosphere. However, space-borne observations of the physical processes that control these trends (i.e. calving) are often temporally aliased due to their relatively low temporal sampling (typically greater than once per day). Dense temporal sampling provided by terrestrial based observations, including seismic observations, thus remains essential to understanding the processes and future evolution of the cryosphere. Continued advances in glacial seismology can be expected to be strongly driven by continually improving seismological instrumentation and methodologies, theoretical developments that enhance modeling and hypothesis testing, inversion advances, and new interpretations of seismic observables (e.g. using seismic attenuation as a proxy for temperature, Peters *et al* (2012)), and by progress in the further identification and directed interdisciplinary study of critical processes affecting the dynamics of glacial systems.

Broadband and short-period seismographs can now be deployed in extreme polar and alpine glacial environments worldwide, and low-Earth-orbit satellite and other real-time data telemetry options are increasingly available (although in some cases remain expensive or draw intractable amounts of power for year-round operation). However, the dynamic surface environment in areas experiencing large degrees of snowfall, ablation, melting, crevassing, calving, and other processes also limits the degree to which stable and recoverable instrumentation can be deployed. Improved capabilities to deploy seismometers in ice boreholes from the near surface to basal, or potentially sub-basal depths, offer exciting prospects to

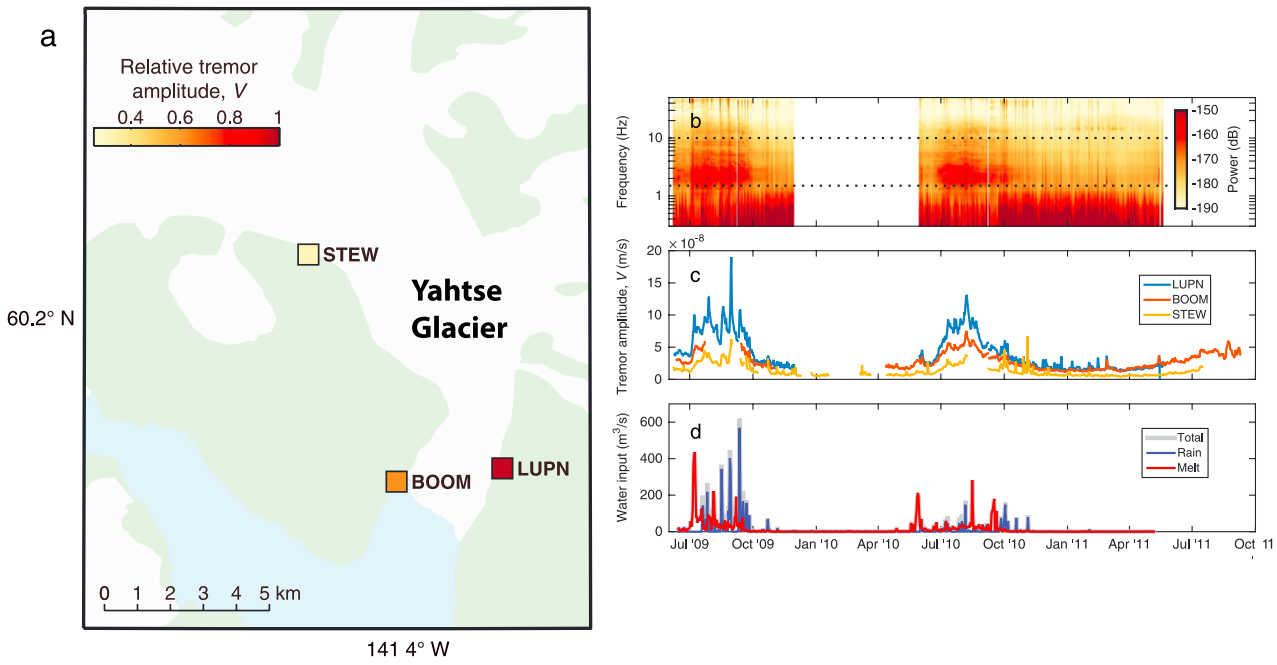

Figure 27. Seasonal glaciohydraulic tremor interpreted as being due to near-terminus subglacial flow at Yahtse Glacier, Alaska between July 2009 and October 2011 (a) selected station locations and color-coded relative tremor amplitude. (b) Vertical-component velocity seismic spectrogram for station LUPN (c) Vertical-component seismic velocity amplitude of tremor for the three indicated stations shown in (a). (d) Estimated total, rain, and glacial melt water input to the system for the same time period. Reproduced with permission from Bartholomaus *et al* (2015a). © 2015. American Geophysical Union. All Rights Reserved.

establish more stable and lower noise observational environments. Such deployments enable measurements of seismic wavefields, material properties and, pressure/temperature states in close proximity to seismic sources, including the critical glacial bed environment. A presently evolving new generation of cheaper and easier to deploy seismographs should result in much denser (in some cases functionally spatially unaliased) short-period recordings of the seismic wavefield on glaciers to advance both seismic source and propagation-related studies, e.g. Aster and Simons (2015).

Photogrammetry, satellite and airborne remote sensing, radar, electromagnetic, and other sensing methods will continue to grow in capabilities and importance, both inherently and as multidisciplinary capabilities that may be partnered with seismological studies. Surface, airborne and space-based ice penetrating radar is a key glaciological tool with very wide use in glaciology for surface and internal imaging, e.g. Arcone (2004). Co-evolving advances in instrumentation, and their greater deployment and integration, can be expected to continue to expand understanding of glacial structure and dynamics, and at greater resolution, as greater numbers of multi-observational studies in areas of particular interest can be realized. Larger numbers of focused studies will also be essential to better understand and characterize the general, as opposed to particular, behavior of glacial systems. In addition to focused studies, denser, wider-ranging, and longer duration deployment of seismographs in glaciated regions can be expected to continue to broadly improve understanding of glacially associated seismogenic regions and their seasonal and longer-term evolution. A number of advanced seismic methodologies that have been widely employed in other environments (e.g. in volcano seismology and shallow Earth imaging) currently still await commensurate realization in glaciological applications.

One such promising methodology is the use of ambient or seismic coda correlation for imaging, and/or near-continuous monitoring of distributed seismic properties, e.g. Duputel *et al* (2009), Zhan *et al* (2014), Larose *et al* (2015) and MacAyeal *et al* (2015). Such methods could provide continuous measurements of the bulk strength and evolution of glacial features. Ambient noise correlation-based methodologies hold great potential for resolving bulk or localized property changes as well as their bounding basal, morainal or other features. Seismological study of mixed rock/snow/ice/permafrost systems, e.g. Overduin *et al* (2015) and Dafflon *et al* (2016) will see significant geophysical attention in the context of increased thaw conditions and associated hazards, such as glacial outburst floods. Seismology is also seeing increasingly routine use in the management of snow avalanche hazards, e.g. van Herwijnen and Schweizer (2011) and Pérez-Guillén *et al* (2016). Subglacial hydrology and sediment properties of glacial systems is similarly primed for greater study, and may be particularly important to the future dynamical behavior of glacial systems with large amounts of surface melt, including Greenland (Walter *et al* 2014, Mordret *et al* 2016), and to ice shelves that are responding rapidly to changes in ocean circulation and temperature that can produce underside melt e.g. Paolo *et al* (2015) and Truffer and Motyka (2016). These systems bear key importance to immediate future sea level rise (Scambos *et al* 2004, Meier *et al* 2007, Yi *et al* 2015). Perhaps the most significant promise of ambient noise correlation seismic methods for imaging is the ability to continuously monitor temporal variability in physical properties, and

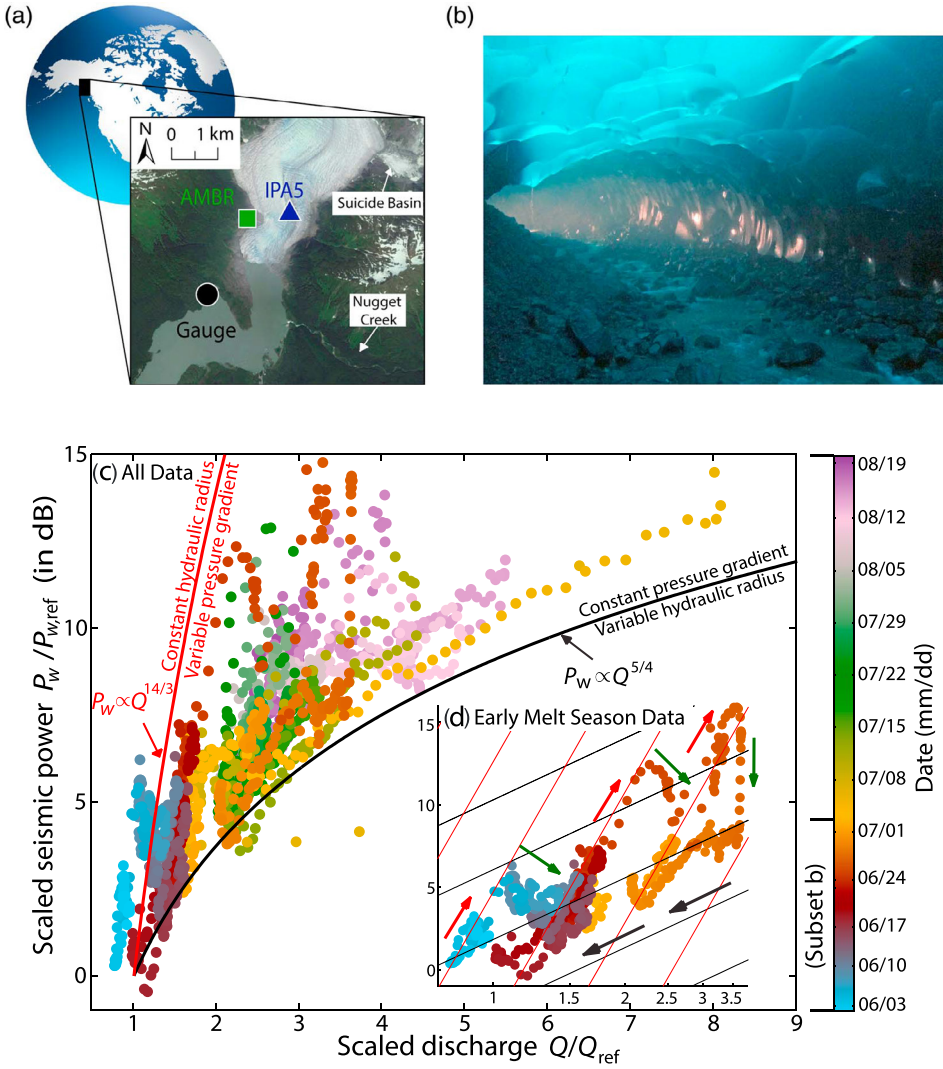

Figure 28. Subglacial water transport generated seismic noise at Mendenhall Glacier, Alaska. (a) Site map, showing the location of (rock-sited) seismograph (AMBR) 50–100 m W of the edge of the glacier and 2 km from the glacier terminus. A nearby gauge at proglacial Mendenhall Lake used for net water discharge monitoring, and a glacier-sited GPS geodetic site (IPA5) were used to monitor glacial motion. (b) Representative photograph of a subglacial conduit (several m in diameter). (c) Scaled short-period (2–5 Hz) seismic velocity power (P/P_{ref}, in db) versus scaled discharge (Q/Q_{ref}), with time of measurement indicated by the color bar at right, Reference power and discharge are representative of minimum power and minimum discharge. (d) detail of (c) for the early season (early June through early July), showing multi-day excursions interpreted as displaying episodic pressurization of the conduit under constant hydraulic radius (red arrows), followed by depressurization (green arrows). Predicted power law relationships between seismic power and discharge from the conduit-specific formulation of the power law derived in Gimbert *et al* (2014) for pressurization of a constant-radius conduit and a constant pressure, variable radius, conduit are shown as red and black curves, respectively. Reproduced with permission from Gimbert *et al* (2016).

to thus infer changes in glacier dynamics and/or conditions that drive glacial behavior or integrity, such as fracture growth or englacial water content (Walter *et al* 2015a). Additionally, emerging results are demonstrating that many passive source techniques developed to image the seismic structure of the solid Earth can be widely applied to glacial environments. Seismic imaging in glacial environments has a long history, e.g. Roethlisberger (1972), but has historically relied on artificial sources such as an explosions or hammer strikes, although recent work has highlighted the viability of on-ice vibroseis sources as well (Hofstede *et al* 2013). However, active source seismic surveys are often laborious, thus limiting the amount of data can be collected during a field project. Passive seismic imaging that leverages both discrete natural sources as well as the ambient seismic wavefield is a promising avenue for complimenting traditional active source seismic surveys. For example, the rheology of ice is highly dependent on *c*-axis fabric orientation (Budd and Jacka 1989). As noted in section 2, seismic wave speeds in single crystal ice are strongly anisotropic, being approximately several percent faster for polarizations that are parallel to, as opposed to perpendicular to, the *c*-axis (Blankenship and Bentley 1987). This makes seismic waves valuably suited for imaging the bulk crystal fabric of glacial ice in regions that lack direct ice core measurements (Horgan *et al* 2008). Thus, shear waves generated by a microseismic basal event will show differential arrival times

(i.e. shear-wave splitting) if the crystalline fabric or layering is highly anisotropic and suitably oriented (Harland *et al* 2013, Smith *et al* 2017). Additional information can be inferred about englacial structure (firn depth, fabric, fracture density) by using surface waves generated by shallow events to map depth-dependent seismic velocity structure (Lough *et al* 2015, Walter *et al* 2015a, Diez *et al* 2016).

Active source seismic studies have also shown the importance of subglacial geology to glacial behavior (Blankenship *et al* 1986, Anandakrishnan *et al* 1998). While natural or ambient sources will likely never supersede the need for very high frequency (> 100 Hz) seismic imaging of the ice-bed interface (Smith 2007) and other short-wavelength critical features of glacial systems, passive methods, such as horizontal to vertical spectral ratios (Pratt *et al* 2016, Picotti *et al* 2017), and receiver function methods, e.g. Chaput *et al* (2014) and Walter *et al* (2014), hold promise for enhanced imaging the large-scale (>100s of meters) sedimentary structure beneath glaciers and ice sheets.

Glacial and regionally sited seismological observations in Greenland and Antarctica are key to constraining mean and spatially varying viscoelastic properties of the crust and mantle at icecap scales. These properties control the rate of glacial isostatic adjustment (GIA) of the solid Earth to ice loading and unloading, which occurs across time scales from years to millennia. Accurate understanding and modeling of GIA is critically important to the dynamic stability of some large glacial systems, such as in West Antarctica, and to the accuracy of space-based or airborne gravimetric, elevation, and other estimations of ice mass change (van der Wal *et al* 2015) and sea level rise (Bromwich and Nicolas 2010). Mantle-scale seismic tomography is also seeing application to estimating the geothermal heat flow boundary conditions that are important to subglacial melting, frictional, and hydrologic environments (Schroeder *et al* 2014, An *et al* 2015, Fisher *et al* 2015, Heeszel *et al* 2016, O'Donnell *et al* 2017). Improved observations and modeling of seismological signals due to englacial and subglacial water transport offer considerable potential for the monitoring and study of the dynamic, and in some cases karst-like, interiors and basal environments of glacial systems. Finally, continuing geophysical studies of Earth's cryosphere, including seismology, will inform structure and dynamic processes investigations of Mars, and for icy bodies elsewhere in the solar system (Cammarano *et al* 2006, Panning *et al* 2006, Kofman *et al* 2010, Vance *et al* 2016).

Acknowledgments

We thank two reviewers for substantive comments that improved the quality and completeness of this manuscript. The authors acknowledge support from the National Science Foundation for their research, including POLENET, which is supported by NSF Office of Polar Programs grants 0632230, 0632239, 0652322, 0632335, 0632136, 0632209, and 0632185. JPW was also supported by NSF Office of Polar Program grant 1141889. This paper benefited from comments from students attending the 2017 Glacial Seismology Summer School held at Colorado State University, which was sponsored by NSF (POLENET), the Scientific Committee on Antarctic Research (SCAR), the International Glaciological Society (IGS) and the International Association of Cryospheric Sciences (IACS).

Appendix. Seismology fundamentals

Below, we summarize seismological fundamentals relevant to this review article. For much more detailed treatment of elastic wave propagation and seismological principles, we refer the reader to one of the excellent general seismology texts that are available, including (Stein and Wysession 1991, Aki and Richards 2002, Shearer 2006).

A.1. P and S waves in isotropic and homogeneous elastic media

Expressing the strain tensor elements (8) in terms of the displacement vector, $\mathbf{u}$ and expanding in terms of displacement terms lead to the general equation of motion for isotropic media, expressed in vector formulation as

$$\begin{aligned}\partial^2\mathbf{u}/\partial t^2 &= (\lambda+2\mu)\nabla(\nabla\cdot\mathbf{u})+\mu\nabla^2\mathbf{u}\\ &= (\lambda+2\mu)\nabla(\nabla\cdot\mathbf{u})-\mu\nabla\times\nabla\times\mathbf{u}.\end{aligned} \tag{A.1}$$

Decomposing the displacement field $\mathbf{u}(x,\ t)$ into the sum of the gradient of a (zero curl) scalar potential and the curl of a (zero divergence) vector potential via a Helmholtz decomposition gives

$$\begin{aligned}\rho\frac{\partial^2}{\partial t^2}(\nabla\Phi+\nabla\times\Psi) &= (\lambda+2\mu)\nabla(\nabla\cdot(\nabla\Phi+\nabla\times\Psi))\\ &\quad-\mu\nabla\times(\nabla\times(\nabla\Phi+\nabla\times\Psi))\\ &= (\lambda+2\mu)\nabla(\nabla\cdot\nabla\Phi)-\mu\nabla\times(\nabla\times\nabla\times\Psi).\end{aligned} \tag{A.2}$$

We can simplify this expression by noting that

$$\begin{aligned}-\nabla\times(\nabla\times\nabla\times\Psi) &= -\nabla(\nabla\cdot(\nabla\times\Psi))\\ &\quad+\nabla^2(\nabla\times\Psi)=\nabla^2(\nabla\times\Psi)\end{aligned} \tag{A.3}$$

and

$$\nabla\cdot(\nabla\Phi)=\nabla^2\Phi \tag{A.4}$$

so that

$$\rho\frac{\partial^2}{\partial t^2}(\nabla\Phi+\nabla\times\Psi)=(\lambda+2\mu)\nabla(\nabla^2\Phi)+\mu\nabla^2(\nabla\times\Psi). \tag{A.5}$$

Grouping the potential terms in (A.5) gives

$$\nabla\left((\lambda+2\mu)\nabla^2\Phi-\rho\frac{\partial^2\Phi}{\partial t^2}\right)=\nabla\times\left(\mu\nabla^2\Psi-\rho\frac{\partial^2\Psi}{\partial t^2}\right). \tag{A.6}$$

The left hand side of (A.6) is the gradient of a function of Φ, while the right hand side is the curl of a function of Ψ. Setting the two bracketed terms to a constant separates the elastodynamic equation of motion into two wave equations. Choosing a constant of zero (i.e. no source terms) gives the wave equations

$$\nabla^2\Phi(\mathbf{x},\ t)=\frac{\rho}{\lambda+2\mu}\frac{\partial^2\Phi(\mathbf{x},\ t)}{\partial t^2} \tag{A.7}$$

and

$$\nabla^2\Psi(\mathbf{x},\ t) = \frac{\rho}{\mu}\frac{\partial^2\Psi(\mathbf{x},\ t)}{\partial t^2}. \tag{A.8}$$

that characterize the two fundamental (P and S) seismic body waves in an isotropic, homogeneous elastic medium.

Because wave fields are most often observed in the far field, plane wave modeling is frequently employed for studying seismic phenomena. A harmonic Helmholz potential plane-wave scalar displacement potential is

$$\Phi(\mathbf{x},\ t) = \Phi_0(\mathbf{x},\ t) = A\mathrm{e}^{\imath(\omega t \pm \mathbf{k}\cdot\mathbf{x})}. \tag{A.9}$$

$$= A\mathrm{e}^{\imath(\omega t \pm (k_x,\ k_y,\ k_z)\cdot(x,\ y,\ z))}.$$

where $\mathbf{k}$ is the vector (propagation direction) wave number. The P wave displacement field due to the displacement potential (A.9) is thus

$$\mathbf{u} = \nabla\Phi = \pm \mathrm{i}A(k_x\Phi\hat{x} + k_y\Phi\hat{y} + k_z\Phi\hat{z}) \equiv B\mathrm{e}^{\imath(\omega t \pm \mathbf{k}\cdot\mathbf{x})}\hat{k}. \tag{A.10}$$

where $B = \pm iA|\mathbf{k}|$. This is a harmonic displacement disturbance with all displacement in the propagation direction $\mp\hat{k}$ and an amplitude proportional to $A|\mathbf{k}|$. The P wave displacement field thus consists of once-per-wavelength compressions and rarefactions. The dilatation of the P wave as a function of space and time is given by

$$\nabla\cdot\mathbf{u} = \mp A|\mathbf{k}|^2\mathrm{e}^{\imath(\omega t \mp \mathbf{k}\cdot\mathbf{x})}, \tag{A.11}$$

which does not vary perpendicular to the $\hat{k}$ direction. Volumetric strain propagating in the P wave is thus caused by shortening in the $\hat{k}$ direction.

The corresponding displacement field from a harmonic Helmholtz potential plane-wave vector displacement potential Ψ is

$$\mathbf{u} = \nabla\times\Psi = \nabla\times(A_x,\ A_y,\ A_z)\mathrm{e}^{\imath(\omega t \pm \mathbf{k}\cdot\mathbf{x})} \tag{A.12}$$

$$= \left(\frac{\partial\Psi_z}{\partial y} - \frac{\partial\Psi_y}{\partial z}\right)\hat{x} + \left(\frac{\partial\Psi_x}{\partial z} - \frac{\partial\Psi_z}{\partial x}\right)\hat{y} + \left(\frac{\partial\Psi_y}{\partial x} - \frac{\partial\Psi_x}{\partial y}\right)\hat{z}$$

$$= \pm\,\mathrm{i}\,((A_zk_y - A_yk_z)\hat{x} + (A_xk_z - A_zk_x)\hat{y} + (A_yk_x - A_xk_y)\hat{z})\,\mathrm{e}^{\imath(\omega t \pm \mathbf{k}\cdot\mathbf{x})}$$

The displacement in the S wave is perpendicular to the propagation direction, $\hat{k}$, and the dilatation, consistent with infinitessimal shear strain, is zero everywhere and at all times

$$\nabla\cdot\mathbf{u} = \nabla\cdot(\nabla\times\Psi) = 0 \tag{A.13}$$

so that the S wave propagates solely shear strain.

A.2. Coupling of P, S, and surface waves

A horizontally layered medium of uniform elastic layers is often usefully employed in seismology, Reflection and transmission (scattering) coefficients for like (P–P and S–S) and converted (P-S and S-P) plane seismic waves for this case are readily derivable by matching displacement and traction boundary conditions at media interfaces for ansatz plane harmonic wave solutions (obeying Snell's Law, as dictated by associated wave speeds defined by (12) and (13)). In the case of plane isotropic layers and plane waves, the seismic wavefield can decomposed into two independent wave systems. The first of these wave system is a system of S waves with particle motions that are perpendicular to the ray plane (referred to as S_H). The second wave system is the coupled system of P and S waves with particle motions lying within the ray plane (referred to as $P-S_V$). Seismic transmission and reflection coefficients can be expressed algebraically in closed forms in terms of Snell's law angles and material density and elastic parameters, and a complete set of reflection and transmission coefficient relationships for isotropic media can be found in Aki and Richards (2002). However, in elastically anisotropic media $P-S_V$ and S_H are no longer decoupled, and are thus not generally separable in this manner. Transmission and reflection coefficients for VTI media may be found in Graebner (1992), and linearized expressions for more general anisotropic media can be found in Behura and Tsvankin (2009).

An important system of coupled P and S waves is the phenomenon of seismic surface and other boundary waves associated with a free surface or other inhomogeneous interface. Such waves can be theoretically derived as coupled propagating and evanescent components of the wavefield. The interface between the solid Earth and the atmosphere can be practically considered as a free surface under most circumstances, and for horizontally layered media, surface waves can be derived using the stress-free boundary condition and corresponding reflection coefficients for a free surface, e.g. Stein and Wysession (1991). Coupled P and S surface waves polarized in the $P-S_V$ (ray) plane are generically referred to as Rayleigh waves, and surface waves comprised of S waves with particle motions perpendicular to the ray plane are generically referred to as Love waves. As with systems of non-evanescent waves, the Rayleigh (P-SV) and Love wave (S_H) components of the seismic wavefield are fully decoupled only in the case of horizontally layered isotropic media. Surface waves in layered media will exhibit dispersion, which is commonly utilized for structural inversion on all scales. Surface waves are also preferentially excited by shallower sources, and may serve as a discriminant for depth.

A.3. Seismic sources

Seismic waves are excited when transient forces are applied at the boundaries of or internally within an elastic medium. Important sources in the cryospheric environment include examples of both types. Internal localized (so that they may be approximated by a point) sources within an elastic medium are typically characterized by a second-order seismic moment tensor, $\mathbf{M}$, where they corresponding scalar moment is

$$M_0 = \sqrt{\frac{\Sigma_{ij}M_{ij}^2}{2}}. \tag{A.14}$$

The seismic moment tensor elements M_{ij} represent the relative magnitudes and signs of opposing force couples oriented

in the x_i directions operating in plane specified by the normal vector x_j. Diagonal moment tensor elements thus represent opposing normal forces that are applied normal to principal planes, and off-diagonal elements represent shear couples. Because internal source process (e.g. collapse, explosion, or fault slip) cannot impart a net change in angular momentum, the moment tensor is symmetric. M_0 has units of force times distance (i.e. N-m in SI units).

A practically important moment tensor type is that of a double-couple, which describes equivalent force couples corresponding to a slipping mode II (in-plane shear) crack and is thus appropriate for slip on a fault or at a glacier bed. The scalar moment of a double couple source can be usefully calculated as

$$M_0 = \mu A d \tag{A.15}$$

where A is the slip patch area, d is the average fault slip, and μ is the rigidity of the surrounding elastic medium. Isotropic volumetric expansion (e.g. explosion) and force couple components of a point seismic source can be represented by a diagonal moment tensor. Additionally, single (non-couple) forces, not represented in the moment tensor, can also be important elements of a seismic source characterizations, such as in modeling reaction forces related to the advection of gas or fluid, or gravitational or otherwise externally driven boundary force, such as may occur during glacial calving processes.

Seismic source sizes are commonly reported using magnitude scales, which are calculated from an appropriately scaled logarithmic formula that incorporates geometric spreading and otherwise appropriately corrected seismic amplitude or other robust observables, e.g. Shearer (2006). Magnitude estimates are typically constrained by a network of seismic stations that measure the seismic radiation over an appropriate angular extent. There are many magnitude scales in historical usage, each derived from different observables (e.g. amplitudes of body waves or surface waves within particular period bands). The most physically fundamental magnitude scale is one based on the scalar moment, referred to *moment magnitude*, which is now in wide general use. For a scalar moment M_0 in SI units, the corresponding moment magnitude is given by Hanks and Kanamori (1979)

$$M_w = \frac{2}{3}\left(\log_{10} M_0 - 9.05\right). \tag{A.16}$$

(A.16) provides reasonable consistency with historic magnitude scales over a wide range of sources sizes, but does not exhibit saturation or other technical problems at very large magnitudes, as can occur with other magnitude scales, e.g. Shearer (2006). For example, fault slip of 0.01 m on a fault plane measuring 100 by 100 m in ice with a medium rigidity characterized as 2×10^{10} Pa corresponds to a scalar seismic moment of 2×10^{12} N m and a corresponding moment magnitude of $M_w \approx 2.17$.

For a general double-couple seismic source representation with $\hat{n} = (n_x,\ n_y,\ n_z)$ specifying the normal to the fault plane and $\hat{d} = (d_x,\ d_y,\ d_z)$ specifying the unit fault slip vector, the moment tensor is given by

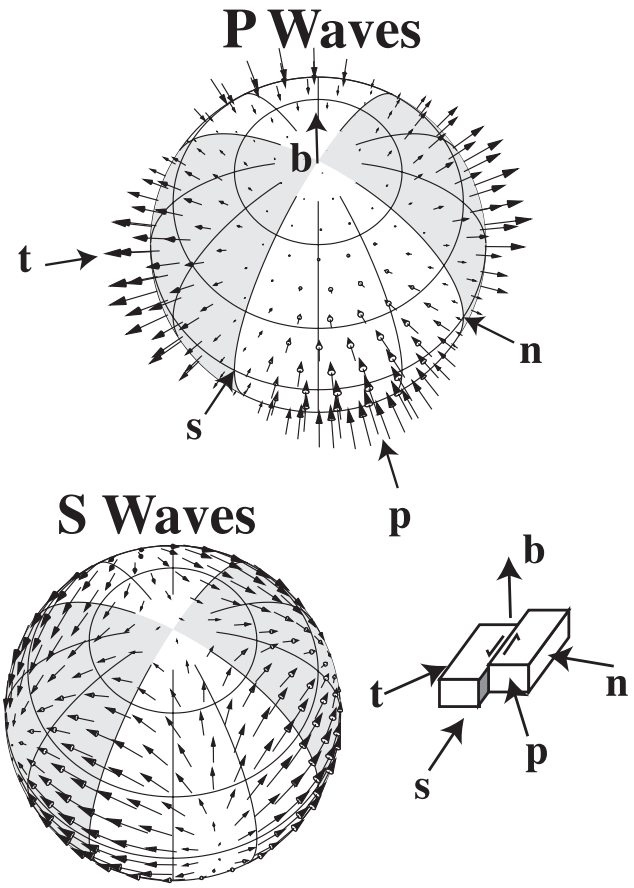

Figure A1. Schematic depiction the relative amplitudes and medium displacement directions of P and S wave far-field seismic waves (arrows) created by a slipping fault (indicated) embedded within an isotropic elastic medium. The slip vector, **s** lies in the fault plane and the fault normal, **n** lies in the (perpendicular) auxiliary plane, each indicated. The intersection of the fault and auxiliary planes defines the **b** axis (which is also orthogonal to the **t** and **p** axes). The far-field seismic radiation from an orthogonal fault, slipping in the opposite sense so that the auxiliary and fault planes are interchanged (i.e. by rotating the fault 90° about the **b** axis and reversing the slip direction), is identical. This fault/auxiliary plane ambiguity can often be resolved with additional seismological observations or from geological/glaciological context (e.g. when it is known that the source is slip on a glacial bed). Adapted from Shearer (2006).

$$\begin{aligned}\mathbf{M} &= M_0(n_i d_j + n_j d_i) \\ &= M_0 \begin{pmatrix} 2n_x d_x & n_x d_y + n_y d_x & n_x d_z + n_z d_x \\ n_y d_x + n_x d_y & 2n_y d_y & n_y d_z + n_z d_y \\ n_z d_x + n_x d_z & n_z d_y + n_y d_z & 2n_z d_z \end{pmatrix}.\end{aligned} \tag{A.17}$$

Seismic sources induce both near-field (non-propagating, static) and far-field (propagating as elastic waves and transitory) strain within an elastic medium. Near-field strain terms may become important when seismographic or other measurements of strain are recorded very close to a source region and/or for large seismic events, and may best be observed geodetically due to their static and sometimes large-amplitude components (e.g. using GPS or other positional instrumentation). In the more commonly relevant situation for glacial seismology, far-field, case, P and S wave displacement amplitudes will decay due to geometric spreading as the inverse of distance and

be proportional to applied force amplitudes for single forces and proportional to the time derivative of applied couple amplitudes (or to the moment rate function in the case of extended time sources) for force couples (Aki and Richards 2002).

The orthogonal eigenvectors of (A.17) are referred to as the **t** (tension), **p** (pressure), and **b** (null) axes, and have eigenvalues M_0, $-M_0$, and 0, respectively. The **t** and **p** axes are the centers of the compressional and dilitational quadrants of the P wave radiation pattern from the double couple source (the maximum and minimum P wave amplitude radiation directions). Conversely, the **b** axis is the axis of zero radiated P- and S- wave energy, which occurs at the intersection of the fault plane and its (indistinguishable from P wave polarity information) counterpart, the *auxiliary plane*. The fault and auxiliary planes of a double-couple solution lie at 45° to the **p** and **t** axes, and the intersection of the fault and auxiliary plane denotes the **b** axis (figure A1). Analytic expressions for seismic radiation terms for isotropic media can be found in Aki and Richards (2002).

ORCID iDs

R C Aster https://orcid.org/0000-0002-0821-4906
J P Winberry https://orcid.org/0000-0003-1205-0745

References

Aki K and Richards P 2002 *Quantitative Seismology* (Sausalito: University Science Books)
Albert D and Bentley C 1998 Seismic studies on the grid eastern half of the ross ice shelf: RIGGS III and RIGGS IV, in the ross ice shelf *Glaciol. Geophys.* **25** 87–108
Albert D G 1998 Theoretical modeling of seismic noise propagation in firn at the south pole, Antarctica *Geophys. Res. Lett.* **25** 4257–60
Alley R 1993 In search of ice-stream sticky spots *J. Glaciol.* **39** 447–54
Allstadt K and Malone S 2014 Swarms of repeating stick-slip icequakes triggered by snow loading at mount rainier volcano *J. Geophys. Res.: Earth Surf.* **119** 1180–203
Amundson J, Truffer M, Luthi M, Fahrenstock M, West M and Motyka R 2008 Glacier, fjord and seismic response to recent large calving events, Jakobshavn Isbrae Greenland *Geop. Res. Lett.* **35** L22501
Amundson J M, Fahnestock M, Truffer M, Brown J, Lthi M P and Motyka R J 2010 Ice melange dynamics and implications for terminus stability, Jakobshavn Isbrae, Greenland *J. Geophys. Res.: Earth Surf.* **115** F01005
An M, Wiens D, Zhao Y, Feng M, Nyblade A, Kanao M, Li Y, Maggi A and Leveque J J 2015 Temperature, lithosphere-asthenosphere boundary, and heat beneath the Antarctic plate inferred from seismic velocities *J. Geophys. Res.* **120** 8720–42
Anandakrishnan S and Alley R 1997 Tidal forcing of basal seismicity of Ice Stream C, West Antarctica, observed far inland *J. Geophys. Res.* **102** 15,183–96
Anandakrishnan S and Bentley C 1993 Micro-earthquakes beneath Ice Streams B and C, West Antarctica: observations and implications *J. Glaciol.* **39** 455–62
Anandakrishnan S, Blankenship D, Alley R and Stoffa P 1998 Influence of subglacial geology on the position of a West Antarctic ice stream from seismic observations *Nature* **394** 62–5
Anandakrishnan S, Voigt D E, Alley R B and King M A 2003 Ice stream D flow speed is strongly modulated by the tide beneath the Ross Ice Shelf *Geophys. Res. Lett.* **30** 1361
Anthony R, Aster R and McGrath D 2017 Links between atmosphere, ocean and cryosphere from two decades of microseism observations on the Antarctic Peninsula *J. Geophys. Res. Earth Surf.* **121**
Anthony R, Aster R, Wiens D, Anandakrishan S, Huerta A D, Winberry J P, Wilson T and Rowe C 2015 The seismic noise environment of Antarctica *Seismol. Res. Lett.* **86** 89–100
Arcone S A 2004 Snow and ice research with ground penetrating radar *Ground Penetrating Radar* (*IEE Radar, Sonar and Navigation Series* vol 15) 2nd edn, ed D J Daniels (London: The Institution of Electrical Engineers) ch 11, pp 439–55
Ardhuin F, Gualtieri L and Stutzmann E 2015 How ocean waves rock the Earth: two mechanisms explain microseisms with periods 3 to 300 s *Geop. Res. Lett.* **42**
Ardhuin F, Stutzmann E, Schimmel M and Mangeney A 2011 Ocean wave sources of seismic noise *J. Geophys. Res.* **116** C09004
Aster R, Beaudoin B, Hole J, Fouch M J, Fowler J and James D 2005 IRIS PASSCAL program marks 20 years of scientific discovery *EOS* **86** 171–2
Aster R *et al* 2004 Real-time data received from Mount Erebus Volcano, Antarctica *EOS* **85** 97–104
Aster R and Simons M 2015 Future geophysical facilities required to address grand challenges in the earth sciences *Technical Report* Community Report to the National Science Foundation
Aster R, Thurber C and Borchers B 2013 *Parameter Estimation and Inverse Problems* 2nd edn (Amsterdam: Elsevier)
Aster R C, McNamara D E and Bromirski P D 2008 Multidecadal climate-induced variability in microseisms *Seismol. Res. Lett.* **79** 194–202
Aster R C, McNamara D E and Bromirski P D 2010 Global trends in extremal microseism intensity *Geophys. Res. Lett.* **37** L14303
Aalgeirsdóttir G, Smith A M, Murray T, King M, Makinson K, Nicholls K W and Behar A 2008 Tidal influence on Rutford Ice Stream, West Antarctica: observations of surface flow and basal processes from closely spaced GPS and passive seismic stations *J. Glaciol.* **54** 715–24
Bannister S *et al* 2002 Seismic activity in the Transantarctic mountains—results from a broadband array deployment *Terra Antarctica* **9** 41–6
Barruol G, Cordier E, Bascou J, Fontaine F R, Legrésy B and Lescarmontier L 2013 Tide-induced microseismicity in the Mertz Glacier grounding area, East Antarctica *Geophys. Res. Lett.* **40** 5412–6
Bartholomaus T, Amundson J, Walter J, O'Neel S, West M and Larsen C 2015a Subglacial discharge at tidewater glaciers revealed by seismic tremor *Geop. Res. Lett.* **42**
Bartholomaus T, Larsen C, O'Neel S and West M 2012 Calving seismicity from iceberg-sea surface interactions *J. Geophys. Res.* **117** F04029
Bartholomaus T C, Larsen C F, West M E, O'Neel S, Pettit E C and Truffer M 2015b Tidal and seasonal variations in calving flux observed with passive seismology *J. Geophys. Res.: Earth Surf.* **120** 2318–37
Bassis J N, Coleman R, Fricker H and Minster J 2005 Episodic propagation of a rift on the Amery Ice Shelf, East Antarctica *Geophys. Res. Lett.* **32**
Bassis J N, Fricker H A, Coleman R, Bock Y, Behrens J, Darnell D, Okal M H and Minster B 2007 Seismicity and deformation associated with ice-shelf rift propagation *J. Glaciol.* **53** 523–36
Bassis J N, Fricker H A, Coleman R and Minster B 2008 An investigation into the forces that drive ice-shelf rift propagation on the Amery Ice Shelf, East Antarctica *J. Glaciol.* **54** 17–27

Behura J and Tsvankin I 2009 Reflection coefficients in attenuative anistorpoic media *Geophysics* **74** WB193–202

Benn D and Evans D 2014 *Glaciers and Glaciation* 2nd edn (London/New York: Routledge Taylor & French Group)

Bentley C 1987 Antarctic ice streams: a review *J. Geophys. Res.: Solid Earth* **92** 8843–58

Bindschadler R A, King M A, Alley R B, Anandakrishnan S and Padman L 2003 Tidally controlled stick-slip discharge of a West Antarctic ice stream *Science* **301** 1087–9

Bindshadler R 1984 Jakobshavn's glacier drainage basin: a balance assessment *J. Geophys. Res. Oceans* **89** 2066–72

Blankenship D, Anandakrishnan S and Kempf J 1987 Microearthquakes under and alongside ice stream b, Antarctica, detected by a new passive seismic array *Ann. Glaciol.*

Blankenship D D and Bentley C R 1987 The crystalline fabric of polar ice sheets inferred from seismic anisotropy *The Physical Basis of Ice Sheet Modelling Proc. Vancouver Symp. (August 1987)* IAHS Publ. 170 pp 17–28

Blankenship D D, Bentley C R, Rooney S T and Alley R B 1986 Seismic measurements reveal a saturated porous layer beneath an active Antarctic ice stream *Nature* **322** 54–7

Bogorodsky V, Bentley C and Gudmandsen P 1985 *Radioglaciology* (Dordrecht: D. Reidel Publishing Company)

Boulton G S, Dobbie K E and Zatsepin S 2001 Sediment deformation beneath glaciers and its coupling to the subglacial hydraulic system *Quat. Int.* **86** 3–28

Brace W F and Byerlee J D 1966 Stick-slip as a mechanism for earthquakes *Science* **153** 990–2

Bracewell R 2000 *The Fourier Transform and its Applications* (Boston: McGraw–Hill)

Bradford J H, Nichols J, Harper J T and Meierbachtol T 2013 Compressional and EM wave velocity anisotropy in a temperate glacier due to basal crevasses, and implications for water content estimation *Ann. Glaciol.* **54** 168–78

Brodsky E E and van der Elst N 2014 The uses of dynamic earthquake triggering *Ann. Rev. Earth Planet. Sci.* **42** 317–39

Bromirski P D, Chen Z, Stephen R A, Gerstoft P, Arcas D, Diez A, Aster R C, Wiens D A and Nyblade A 2017 Tsunami and infragravity waves impacting Antarctic ice shelves *J. Geophys. Res.: Oceans* **122**

Bromirski P D, Diez A, Gerstoft P, Stephen R A, Bolmer T, Wiens D, Aster R and Nyblade A 2015 Ross Ice Shelf vibrations *Geop. Res. Lett.* **42** 7589–97

Bromirski P D and Stephen R A 2012 Response of the Ross Ice Shelf, Antarctica, to ocean gravity-wave forcing *Ann. Glaciol.* **53** 163–72

Bromwich D H and Nicolas J P 2010 Sea-level rise: Ice-sheet uncertainty *Nat. Geosci.* **3** 596–7

Brune J N 1970 Tectonic stress and the spectra of seismic shear waves from earthquakes *J. Geophys. Res.* **75** 4997–5009

Brunt K M, Okal E and MacAyeal D 2011 Antarctic ice-shelf calving triggered by the Honshu (Japan) earthquake and tsunami, March 2011 *J. Glaciol.* **57** 785–8

Budd W and Jacka T 1989a A review of ice rheology for ice sheet modelling *Cold Reg. Sci. Technol.* **16** 107–44

Burtin A, Hovius N and Turowski J M 2016 Seismic monitoring of torrential and fluvial processes *Earth Surf. Dyn.* **4** 285–307

Burtin A, Vergne J, Rivera L and Dubernet P 2010 Location of river-induced seismic signal from noise correlation functions *Geophys. J. Int.* **182** 1161–73

Butler R *et al* 2004 The global seismographic network surpasses its design goal *EOS* **85** 223–9

Cammarano F, Lekic V, Manga M, Panning M and Romanowicz B 2006 Long-period seismology on Europa: 1. Physically consistent interior models *J. Geophys. Res.: Planets* **111** E12009

Carmichael J D, Joughin I, Behn M D, Das S, King M A, Stevens L and Lizarralde D 2015 Seismicity on the western Greenland ice sheet: surface fracture in the vicinity of active moulins *J. Geophys. Res.: Earth Surf.* **120** 1082–106

Carmichael J D, Pettit E C, Hoffman M, Fountain A and Hallet B 2012 Seismic multiplet response triggered by melt at Blood Falls, Taylor Glacier, Antarctica *J. Geophys. Res.: Earth Surf.* **117** 2156–202

Cathles L M, Okal E A and MacAyeal D R 2009 Seismic observations of sea swell on the floating Ross Ice Shelf, Antarctica *J. Geophys. Res.: Earth Surf.* **114** 2156–202

Chaput J, Aster R, Huerta A D, Sun X, Lloyd A, Wiens D, Nyblade A, Anandakrishan S, Winberry J P and Wilson T 2014 The crustal thickness of West Antarctica *J. Geophys. Res.* **119** 1–18

Chaput J, Campillo M, Aster R, Roux P, Kyle P, Knox H and Czoski P 2015 Multiple scattering from icequakes at Erebus volcano, Antarctica: implications for imaging at glaciated volcanoes *J. Geophys. Res.* **120** 1129–41

Chen X, Shearer P, Walter F and Fricker H 2011 Seventeen Antarctic seismic events detected by global surface waves and a possible link to calving events from satellite images *J. Geophys. Res.: Solid Earth* **116** 2156–202

Clark P U, Dyke A S, Shakun J D, Carlson A E, Clark J, Wohlfarth B, Mitrovica J X, Hostetler S W and McCabe A M 2009 The last glacial maximum *Science* **325** 710–4

Clarke G 1987 A short history of scientific investigations on glaciers *J. Glaciol.* **33b** 4–24

Clarke G K 2005 Subglacial processes *Annu. Rev. Earth Planet. Sci.* **33** 247–76

Cole S, Cronin S, Sherburn S and Manville V 2009 Seismic signals of snow-slurry lahars in motion: 25 September 2007, Mt Ruapehu, New Zealand *Geophys. Res. Lett.* **36** L09405

Colgan W, Rajaram H, Waleed A, McCutchan C, Mottram R, Moussavi M and Grigsby S 2016 Glacier crevasses: observations, models and mass balance implications *Rev. Geophys.* **54** 119–61

Cuffey K and Paterson W 2010 *The Physics of Glaciers* (New York: Academic) (glacier depth average velocity)

Dafflon B, Hubbard S, Ulrich C, Peterson J, Wu Y, Wainwright H and Kneafsey T 2016 Geophysical estimation of shallow permafrost distribution and properties in an ice-wedge polygon-dominated Arctic tundra region *Geophysics* **81** WA247–63

Dalban Canassy P, Röösli C and Walter F 2016 Seasonal variations of glacier seismicity at the tongue of Rhonegletscher (Switzerland) with a focus on basal icequakes *J. Glaciol.* **62** 18–30

Damsgaard A, Egholm D L, Beem L H, Tulaczyk S, Larsen N K, Piotrowski J A and Siegfried M R 2016 Ice flow dynamics forced by water pressure variations in subglacial granular beds *Geophys. Res. Lett.* **43** 12,165–73

Danesi S, Bannister S and Morelli A 2007 Repeating earthquakes from rupture of an asperity under an Antarctic outlet glacier *Earth Planet. Sci. Lett.* **253** 151–8

Depoorter M A, Bamber J L, Griggs J A, Lenaerts J T M, Ligtenberg S R M, van den Broeke M R and Moholdt G 2013 Calving fluxes and basal melt rates of Antarctic ice shelves *Nature* **502** 89–92

Dìaz J 2016 On the origin of the signals observed across the seismic spectrum *Earth Sci. Rev.* **161** 224–32

Diez A, Bromirski P D, Gerstoft P, Stephen R A, Anthony R, Aster R, Cai C, Nyblade A and Wiens D 2016 Ice shelf structure derived from dispersion curve analysis of ambient seismic noise, Ross Ice Shelf, Antarctica *Geophys. J. Int.* **205** 785–95

Diez A and Eisen O 2015 Seismic wave propagation in anisotropic ice—part 1: elasticity tensor and derived quantities from ice-core properties *Cryosphere* **9** 367–84

Diez A, Eisen O, Weikusat I, Eichler J, Hofstede C, Bohleber P, Bohlen T and Polom U 2014 Influence of ice crystal anisotropy on seismic velocity analysis *Ann. Glaciol.* **55** 97–100

Douglas A 1977 Seismology in oceanic microseism band *Geophys. J. R. Astron. Soc.* **49** 303–4

Dowdeswell J and Bamber J 2007 Keel depths of modern Antarctic icebergs and implications for sea-floor scouring in the geological record *Mar. Geol.* **243** 120–31
Duputel Z, Ferrazzini V, Brenguier F, Shapiro N, Campillo M and Nercessian A 2009 Real time monitoring of relative velocity changes using ambient seismic noise at the piton de la fournaise volcano (la reunion) from January 2006 to June 2007 *J. Volcanol. Geotherm. Res.* **184** 164–73
Ekstrom G 2006 Global detection and location of seismic sources by using surface waves *Bull. Seism. Soc. Am.* **96** 1201–12
Ekstrom G, Nettles M and Abers G 2003 Glacial earthquakes *Science* **302** 622–4
Ekstrom G, Nettles M and Tsai V C 2006 Seasonality and increasing frequency of Greenland glacial earthquakes *Science* **311** 1756–8
Enderlin E, Howat I, Jeong S, Noh M-J, van Angelen J and van den Broeke M 2014 An improved mass budget for the Greenland ice sheet *Geophys. Res. Lett.* **41** 866–72
Fischer U and Clarke G 1997 Stick-slip sliding behaviour at the base of a glacier *Ann. Glaciol.* **24** 390–6
Fisher A, Mankoff K, Tulaczyk S, Tyler S and Foley N 2015 High geothermal heat flux measured below the West Antarctic ice sheet *Sci. Adv.* **1** e1500093
Forster R R *et al* 2013 Extensive liquid meltwater storage in firn within the Greenland ice sheet *Nat. Geosci.* **7** 95–8
Forsyth D W, Lay T, Aster R and Romanowicz B 2009 Grand challenges for seismology *Eos Trans. AGU* **90** 361–3
Fountain A and Walder J 1998 Water flow through temperate glaciers *Rev. Geophys.* **36** 299–328
Fountain A G, Campbell J L, Schuur E A G, Stammerjohn S E, Williams M W and Ducklow H W 2012 The disappearing cryosphere: impacts and ecosystem responses to rapid cryosphere loss *BioScience* **62** 405
Fountain A G, Jacobel R, Schlichting R and Jannson P 2005 Fractures as the main pathways of water flow in temperate glaciers *Nature* **433** 618–21
Fretwell P *et al* 2013 Bedmap2: improved ice bed, surface and thickness datasets for Antarctica *Cryosphere* **7** 375–93
Fricker H A, Scambos T, Bindschadler R and Padman L 2007 An active subglacial water system in West Antarctica mapped from space *Science* **315** 1544–8
Furst J, Durand G, Gillet-Chaulet G, Tavard L, Rankl M, Braun M and Gagliardini O 2016 The safety band of Antarctic ice shelves *Nat. Clim. Change* **6** 479–82
Gimbert F, Tsai I and Lamb M 2014 A physical model for seismic noise generation by turbulent flow in rivers *J. Geophys. Res.: Earth Surf.* **119** 2209–38
Gimbert F, Tsai V C, Amundson J, Bartholomaus T and Walter J 2016 Subseasonal changes observed in subglacial channel pressure, size and sediment transport *Geophys. Res. Lett.* **43** 3786–94
Glen J 1955 The creep of polycrystalline ice *Proc. R. Soc.* **229** 519–38
Glowacki O, Deane G, Moskalik M, Blondel P, Tegowski J and Blaszczyk M 2015 Underwater acoustic signatures of glacier calving *Geophys. Res. Lett.* **42** 804–12
Glowacki O, Moskalik M and Deane G 2016 The impact of glacier meltwater on the underwater noise field in a glacial bay *J. Geophys. Res. Oceans.* **121** 8455–70
Godin O and Zabotin N 2016 Resonance vibrations of the Ross Ice Shelf and observations of persistent atmospheric waves *J. Geophys. Res. Space Phys.* **121** 157–71
Graebner M 1992 Plane-wave reflection and transmission coefficients for a transversely isotropic solid *Geophysics* **57** 1512–9
Gregory J M, Huybrechts P and Raper S C B 2004 Climatology: threatened loss of the Greenland ice-sheet *Nature* **428** 616–6
Gudmundsson G H 2011 Ice-stream response to ocean tides and the form of the basal sliding law *Cryosphere* **5** 259–70
Haberland C and Ritter O 2016 Gipp: geophysical instrument pool potsdam *J. Large Scale Res. Facil.* **2** A64
Hammer C, Ohrnberger M and Schlindwein V 2015 Pattern of cryospheric seismic events observed at Ekström Ice Shelf, Antarctica *Geophys. Res. Lett.* **42** 3936–43
Hanks T C and Kanamori H 1979 Moment magnitude scale *J. Geophys. Res.* **84** 2348–50
Hanson J A and Bowman J R 2006 Methods for monitoring hydroacoustic events using direct and reflected T waves in the Indian ocean *J. Geophys. Res.* **111** 1–18
Harland S, Kendall J-M, Stuart G, Lloyd G, Baird A, Smith A, Pritchard H and Brisbourne A 2013 Deformation in Rutford Ice Stream, West Antarctica: measuring shear-wave anisotropy from icequakes *Ann. Glaciol.* **54** 105–14
Harper J T, Bradford J, Humphrey N F and Meierbachtol T 2010 Vertical extension of the subglacial drainage system into basal crevasses *Nature* **467** 579–82
Harper J T, Humphrey N F, Pfeffer W T, Fudge T and O'Neel S 2005 Evolution of subglacial water pressure along a glacier's length *Ann. Glaciol.* **40** 31–6
Harrison W 1975 Temperature measurements in a temperate glacier *J. Glaciol.* **14** 23–30
Hatherton T and Evison F F 1962 A special mechanism for some Antarctic earthquakes *New Zealand J. Geol. Geophys.* **5** 864–73
Heeszel D, Fricker H A, Bassis J N, O'Neel S and Walter F 2014a Seismicity within a propagating ice shelf rift: the relationship between icequake locations and ice shelf structure *J. Geophys. Res. Earth Surf.* **119** 731–44
Heeszel D, Walter F and Kilb D 2014b Humming glaciers *Geology* **42** 1099–102
Heeszel D S, Wiens D A, Anandakrishnan S, Aster R C, Dalziel I W D, Huerta A D, Nyblade A A, Wilson T J and Winberry J P 2016 Upper mantle structure of central and West Antarctica from array analysis of Rayleigh wave phase velocities *J. Geophys. Res. Solid Earth* **121** 1758–75
Helmstetter A, Moreau L, Nicolas B, Comon P and Gay M 2015a Intermediate-depth icequakes and harmonic tremor in an Alpine glacier (Glacier d'Argentière, France): evidence for hydraulic fracturing? *J. Geophys. Res.: Earth Surf.* **120** 402–16
Helmstetter A, Nicolas B, Comon P and Gay M 2015b Basal icequakes recorded beneath an Alpine glacier (Glacier d'Argentière, Mont Blanc, France): evidence for stick-slip motion? *J. Geophys. Res.: Earth Surf.* **120** 379–401
Hofstede C, Eisen O, Diez A, Jansen D, Kristoffersen Y, Lambrecht A and Mayer C 2013 Investigating englacial reflections with vibro-and explosive-seismic surveys at Halvfarryggen ice dome, Antarctica *Ann. Glaciol.* **54** 189–200
Horgan H, Anandakrishnan S, Alley R, Peters L, Tsoflias G P, Voigt D and Winberry J 2008 Complex fabric development revealed by englacial seismic reflectivity: Jakobshavn Isbræ, Greenland *Geophys. Res. Lett.* **35**
Hulbe C, Klinger M, Masterson M, Catania G, Cruikshank K and Bugni A 2016 Tidal bending and strand cracks at the Kamb Ice Stream grounding line, West Antarctica *J. Glaciol.* **62** 816–24
Irvine-Fynn T, Hodson A, Moorman B, Vatne G and Hubbard A 2011 Polythermal glacier hydrology: a review *Rev. Geophys.* **49** RG4002
Ishihara Y, Kanao M, Yamamoto M-Y, Toda S, Matsushima T and Murayama T 2015 Infrasound observations at Syowa station, East Antarctica: implications for detecting the surface environmental variations in the polar regions *Geosci. Frontiers* **6** 285–96
Iverson N 2010 Shear resistance and continuity of subglacial till: hydrology rules *J. Glaciol.* **56** 11
Iverson N R, Baker R W, Hooke R L, Hanson B and Jansson P 1999 Coupling between a glacier and a soft bed: I. A relation

between effective pressure and local shear stress determined from till elasticity *J. Glaciol.* **45** 31–40
Iverson N R, Hooyer T S and Baker R V 1998 Ring-shear studies of till deformation: Coulomb-plastic behavior and distributed strain in glacier beds *J. Glaciol.* **44** 634–42
Jacquet J, McCoy S W, McGrath D, Nimick D A, Fahey M, Okuinghttons J, Friesen B A and Leidich J 2016 Hydrologic and geomorphic changes resulting from episodic glacial lake outburst floods: Rio Colonia, Patagonia, Chile *Geophys. Res. Lett.* **44** 854–64
Jeong S, Howat I M and Bassis J N 2016 Accelerated ice shelf rifting and retreat at Pine Island Glacier, West Antarctica *Geophys. Res. Lett.* **43** 11,720–5
Joughin I, Howat I, Alley R B, Ekstrom G, Fahnestock M, Moon T, Nettles M, Truffer M and Tsai V C 2008 Ice-front variation and tidewater behavior on Helheim and Kangerdlugssuaq Glaciers, Greenland *J. Geophys. Res.: Earth Surf.* **113**
Joughin I and MacAyeal D R 2005 Calving of large tabular icebergs from ice shelf rift systems *Geophys. Res. Lett.* **32** L02501
Kavanaugh J and Clarke G 2001 Abrupt glacier motion and reorganization of basal shear stress following the establishment of a connected drainage system *J. Glaciol.* **47** 472–80
Knight J 2002 Glacial sedimentary evidence supporting stick-slip basal ice flow *Quat. Sci. Rev.* **21** 975–83
Kofman W, Orosei R and Pettinelli E 2010 Radar signal propagation and detection through ice *Space Sci. Rev.* **153** 249–71
Köhler A, Nuth C, Kohler J, Berthier E, Weidle C and Schweitzer J 2016 A 15 year record of frontal glacier ablation rates estimated from seismic data *Geophys. Res. Lett.* **43** 155–64
Köhler A, Nuth C, Schweitzer J, Weidle C and Gibbons S J 2015 Regional passive seismic monitoring reveals dynamic glacier activity on Spitsbergen, Svalbard *Polar Res.* **34** 26178
Kohnen H 1974 The temperature dependence of seismic waves in ice *Glaciology* **13** 144–7
Läderach C and Schlindwein V 2011 Seismic arrays on drifting ice floes: experiences from four deployments in the Arctic Ocean *Seismol. Res. Lett.* **82**
Larose E *et al* 2015 Environmental seismology: what can we learn on Earth surface processes with ambient noise? *J. Appl. Geophys.* **116** 62–74
Larsen C, Burgess E, Arendt A, O'Neel S, Johnson A and Kienholz C 2015 Surface melt dominates Alaska glacier mass balance *Geophys. Res. Lett.* **42** 5902–8
Lide D 2004 *CRC Handbook of Chemistry and Physics* (*CRC Handbook of Chemistry and Physics* vol 85) 85th edn (London: Taylor and Francis)
Lipovsky B and Dunham E 2016 Tremor during ice-stream stick slip *Cryosphere* **10** 385–99
Lipovsky B P and Dunham E M 2015 Vibrational modes of hydraulic fractures: inference of fracture geometry from resonant frequencies and attenuation *J. Geophys. Res.: Solid Earth* **120** 1080–107
Lombardi D, Benoit L, Camelbeeck T, Martin O, Meynard C and Thom C 2016 Bimodal pattern of seismicity detected at the ocean margin of an Antarctic Ice Shelf *Geophys. J. Int.* **206** 1375–81
Longuet-Higgins M 1950 A theory of the origin of microseisms *Phil. Trans. R. Soc.* A **243** 1–35
Lough A, Barcheck C G, Wiens D, Nyblade A and Anandakrishan S 2015 A previously unreported type of seismic source in the firn layer of the east Antarctic ice sheet *J. Geophys. Res. Earth Surf.* **120** 2237–52
MacAyeal D, Scambos T, Hulbe C L and Fahnestock M 2003 Catastrophic ice-shelf break-up by an ice-shelf-fragment-capsize mechanism *J. Glaciol.* **49** 22–36
MacAyeal D, Wang T and Okal E 2015 Ambient seismic, hydroacoustic and flexural gravity wave noise on a tabular iceberg *J. Geophys. Res.: Earth Surf.* **120**
MacAyeal D R, Okal E A, Aster R C and Bassis J N 2008 Seismic and hydroacoustic tremor generated by colliding icebergs *J. Geophys. Res.: Earth Surf.* **113** F03011
MacAyeal D R, Okal E A, Aster R C and Bassis J N 2009 Seismic observations of glaciogenic ocean waves (micro-tsunamis) on icebergs and ice shelves *J. Glaciol.* **55** 193–206
MacAyeal D R *et al* 2006 Transoceanic wave propagation links iceberg calving margins of Antarctica with storms in tropics and northern hemisphere *Geophys. Res. Lett.* **33** L17502
Macdonald F A, Schmitz M D, Crowley J L, Roots C F, Jones D S, Maloof A C, Strauss J V, Cohen P A, Johnston D T and Schrag D P 2010 Calibrating the Cryogenian *Science* **327** 1241–3
Man C-S and Huang M 2011 A simple explicit formula for the Voigt-Reuss-Hill average of elastic polycrystals with arbitrary crystal and texture symmetries *J. Elast.* **105** 29–48
Marone C 1998 Laboratory-derived friction laws and their application to seismic faulting *Annu. Rev. Earth Planet. Sci.* **26** 643–96
Marsh O, Fricker H A, Siegfried M, Christianson K, Nicolls K, Corr H and Catania G 2016 High basal melting forming a channel at the grounding line of Ross Ice Shelf, Antarctica *Geop. Res. Lett.* **43** 250–5
Martin S, Drucker R, Aster R, Davey F, Okal E, Scambos T and MacAyeal D 2010a Kinematic and seismic analysis of giant tabular iceberg breakup at Cape Adare, Antarctica *J. Geophys. Res.: Solid Earth* **115** B06311
Martin S, Drucker R, Aster R, Davey F J, Okal E, Scambos T and MacAyeal D R 2010b Kinematic and seismic analysis of giant tabular iceberg breakup at Cape Adare, Antarctica *J. Geophys. Res.* **115** B06311
Matsumoto H, Bohnenstiehl D R, Touradre J, Dziak R, Haxel J, Lau T-K, Fowler M and Salo S 2014 Antarctic icebergs: a significant natural ocean sound source in the southern hemisphere *Geochem. Geophys. Geosys.* **15** 3448–58
McCarthy C, Savage H and Nettles M 2017 Temperature dependence of ice-on-rock friction at realistic glacier conditions *Phil. Trans. R. Soc.* A **375** 20150348
Meier M F, Dyurgerov M B, Rick U K, O'Neel S, Pfeffer W T, Anderson R S, Anderson S P and Glazovsky A F 2007 Glaciers dominate eustatic sea-level rise in the 21st century *Science* **317** 1064–7
Métaxian J-P, Araujo S, Mora M and Lesage P 2003 Seismicity related to the glacier of Cotopaxi Volcano, Ecuador *Geophys. Res. Lett.* **30**
Mikesell T, van Wijk J, Haney M, Bradford J, Marshall H P and Harper J T 2012 Monitoring glacier surface seismicity in time and space using Rayleigh waves *J. Geophys. Res.* **117** R02020
Mordret A, Mikesell T, Harig C, Lipovsky B and Prieto G A 2016 Monitoring southwest Greenland's ice sheet melt with ambient seismic noise *Sci. Adv.* **2** e1501538
Müller C, Schlindwein V, Eckstaller A and Miller H 2005 Singing icebergs *Science* **310** 1299–9
Murray T *et al* 2015 Reverse glacier motion during iceberg calving and the cause of glacial earthquakes *Science* **349** 305–8
Neave K and Savage J 1970 Icequakes on the Athabasca Glacier *J. Geophys. Res.* **75** 1351–62
Nettles M and Ekstrom G 2010 Glacial earthquakes in Greenland and Antarctica *Annu. Rev. Earth Planet. Sci.* **38** 467–91

Nicolas A, Boudier F and Boullier A M 1973 Mechanisms of flow in naturally and experimentally deformed peridotites *Am. J. Sci.* **273** 853–76
Nyblade A, Amundsen J, Hansen S, Ivins E R M L, Nettles M, Raymond C and Stearns L 2012 A facility plan for polar seismic and geodetic science: joint IRIS/UNAVCO workshop report *Technical Report* IRIS Consortium
O'Donnell J, Selway K, Nyblade A, Brazier R, Wiens D, Anandakrishan S, Aster R, Huerta A, Wilson T and Winberry J P 2017 The uppermost mantle seismic velocity and viscosity structure of central West Antarctica *Earth Planet. Sci. Lett.* **472** 38–49
Okal E A and MacAyeal D R 2006 Seismic recording on drifting icebergs: catching seismic waves, tsunamis and storms from Sumatra and elsewhere *Seismol. Res. Lett.* **77** 659–71
O'Neel S, Marshall H P, McNamara D E and Pfeffer W T 2007 Seismic detection and analysis of icequakes at Columbia Glacier, Alaska *J. Geophys. Res.: Earth Surf.* **112** F03S23
Osten-Woldenburg H 1990 Icequakes on Ekström Ice Shelf near Atka Bay, Antarctica *J. Glaciol.* **36** 31–6
Overduin P P, Haberland C, Ryberg T, Kneier F, Jacobi T, Grigoriev M N and Ohrnberger M 2015 Submarine permafrost depth from ambient seismic noise *Geophys. Res. Lett.* **42** 7581–8
Panning M, Lekic V, Manga M, Cammarano F and Romanowicz B 2006 Long-period seismology on Europa: 2. Predicted seismic response *J. Geophys. Res.: Planets* **111** E12008
Paolo F, Fricker H A and Padman L 2015 Volume loss from Antarctic ice shelves is accelerating *Science* **348** 327–31
Park J *et al* 2005 Performance review of the Global Seismographic Network for the Sumatra-Andaman megathrust earthquake *Seismol. Res. Lett.* **76** 331–43
Peng Z, Walter J, Aster R, Nyblade A, Wiens D and Anandakrishan S 2014 Antarctic icequakes triggered by the 2010 maule earthquake in Chile *Nat. Geosci.* **7** 677–81
Pérez-Guillén C, Sovilla B, Suriñach E, Tapia M and Köhler A 2016 Deducing avalanche size and flow regimes from seismic measurements *Cold Reg. Sci. Technol.* **121** 25–41
Peters L E, Anandakrishnan S, Alley R B and Voigt D E 2012 Seismic attenuation in glacial ice: a proxy for englacial temperature *J. Geophys. Res.* **117** F02008
Peterson J 1993 Observations and modeling of seismic background noise *USGS Open-File Report* 93-322 p 94
Picotti S, Francese R, Giorgi M, Pettenati F and Carcione J M 2017 Estimation of glacier thicknesses and basal properties using the horizontal-to-vertical component spectral ratio (HVSR) technique from passive seismic data *J. Glaciol.* **63** 229–48
Pirli M, Matsuoka K, Schweitzer J and Moholdt G 2015 Seismic signals from large, tabular icebergs drifting along the Dronning Maud Land coast, Antarctica and their significance for iceberg monitoring *J. Glaciol.* **61** 481–92
Podolskiy E and Walter F 2016 Cryoseismology *Rev. Geophys.* **54** 708–58
Podolskiy E A, Sugiyama S, Funk M, Walter F, Genco R, Tsutaki S, Minowa M and Ripepe M 2016 Tide-modulated ice flow variations drive seismicity near the calving front of Bowdoin Glacier, Greenland *Geophys. Res. Lett.* **43** 2036–44
Pollard D, DeConto R and Alley R B 2015 Potential Antarctic ice sheet retreat driven by hydrofracturing and ice cliff failure *Earth Planet. Sci. Lett.* **412** 112–21
Pratt M, Shen W, Wiens D, Winberry J and Anandakrishnan S 2016 Constraints on the variable subglacial structure of Whillans Ice Stream from ambient noise Rayleigh wave h/v ratios *AGU Fall Meeting Abstracts*
Pratt M, Winberry J P, Wiens D, Anandakrishan S and Alley R B 2014 Seismic and geodetic evidence for grounding-line control of Whillans Ice Stream stick-slip events *J. Geophys. Res. Earth Surf.* **119** 333–48
Press F, Crary A, Oliver J and Katz S 1951 Air-coupled flexural waves in floating ice *Trans. AGU* **32** 166–72
Qamar A 1988 Calving icebergs: a source of low-frequency seismic signals from Columbia Glacier, Alaska *J. Geophys. Res.* **93** 6615–23
Rathbun A P, Marone C, Alley R B and Anandakrishnan S 2008 Laboratory study of the frictional rheology of sheared till *J. Geophys. Res.: Earth Surf.* **113**
Raymond C F and Malone S 1986 Propagating strain anomalies during mini-surges of Variegated Glacier, Alaska, USA *J. Glaciol.* **32** 178–91
Rial J, Tang C and Steffen K 2009 Glacial rumblings from Jakobshavn Ice Stream, Greenland *J. Glaciol.* **55** 389–99
Richardson J, Waite G P, FitzGerald K and Pennington W 2010 Characteristics of seismic and acoustic signals produced by calving, Bering Glacier, Alaska *Geophys. Res. Lett.* **37** L03503
Richardson J, Waite G P, Pennington W, Turpening R and Robinson J 2012 Icequake locations and discrimination of source and path effects with small aperture arrays, Bering Glacier terminus, AK *J. Geophys. Res.* **117** F04013
Roethlisberger H 1972 Seismic exploration in cold regions *Sci. Eng. Monogr. II-A2a* U.S. Army Cold Regions Research and Engineering Laboratory, Hanover, NH
Röösli C, Helmstetter A and Walter F 2016a Meltwater influences on deep stick-slip icequakes near the base of the Greenland ice sheet *J. Geophys. Res.* **121** 5838–58
Röösli C, Walter F, Ampuero J-P and Kissling E 2016b Seismic moulin tremor *J. Geophys. Res.: Solid Earth* **121** 5838–58
Röösli C, Walter F, Husen S, Andrews L C, Lüthi M P, Catania G A and Kissling E 2014 Sustained seismic tremors and icequakes detected in the ablation zone of the Greenland ice sheet *J. Glaciol.* **60** 563–75
Roult G *et al* 2010 The GEOSCOPE program: progress and challenges during the past 30 years *Seismol. Res. Lett.* **81** 427–52
Roux P, Marsan D, Metaxian J-P, O'Brien G and Moreau L 2008 Microseismic activity within a serac zone in an alpine glacier (Glacier dArgentière, Mont Blanc, France) *J. Glaciol.* **54** 157–68
Roux P-F, Walter F, Riesen P, Sugiyama S and Funk M 2010 Observation of surface seismic activity changes of an alpine glacier during a glacier-dammed lake outburst *J. Geophys. Res.: Earth Surf.* **115** F03014
Rowe C, Aster R, Kyle P and Eschebacher A 2005 Seismic observations at Mount Erebus Volcano Observatory: 1997–1998 *Antarct. J. USA* **33** 335–9
Scambos T, Fricker H A, Liu C-C, Bohlander J, Fastook J, Sargent A, Massom R and Wu A-M 2009 Ice shelf disintegration by plate bending and hydro-fracture: satellite observations and model results of the 2008 Wilkins Ice Shelf break-ups *Earth Planet. Sci. Lett.* **280** 51–60
Scambos T, Ross R, Bauer R, Yermolin Y, Skvarca P, Long D, Bohlander J and Haran T 2008 Calving and ice-shelf break-up processes investigated by proxy: Antarctic tabular iceberg evolution during northward drift *J. Glaciol.* **54** 579–91
Scambos T A, Bohlander J A, Shuman C A and Skvarca P 2004 Glacier acceleration and thinning after ice shelf collapse in the Larsen B embayment, Antarctica *Geophys. Res. Lett.* **31** L18402
Schellenberger T, Dunse T, Kaab A, VSchuler T, Hagen J and Reijmer C 2017 Multi-year surface velocities and sea-level

rise contribution of the Basin-3 and Basin-2 surges, Austfonna, Svalbard *Cryosphere Discuss.* (https://doi.org/10.5194/tc-2017-5)
Schmandt B, Aster R C, Scherler D, Tsai V C and Karlstrom K 2013 Multiple fluvial processes detected by riverside seismic and infrasound monitoring of a controlled flood in the Grand Canyon *Geophys. Res. Lett.* **40** 4858–63
Scholz C H 1998 Earthquakes and friction laws *Nature* **391** 37–42
Schoof C, Rada C, Wilson N, Flowers G and Haseloff M 2014 Oscillatory subglacial drainage in the absence of surface melt *Cryosphere* **8** 959–76
Schroeder D, Blankenship D D, Young D and Quartini E 2014 Evidence for elevated and spatially variable geothermal flux beneath the West Antarctic ice sheet *Proc. Natl Acad. Sci.* **111** 9070–2
Sergeant A, Mangeney A, Stutzmann E, Montagner J-P, Walter F, Moretti L and Castelnau O 2016 Complex force history of a calving-generated glacial earthquake derived from broadband seismic inversion *Geophys. Res. Lett.* **43** 1055–65
Sergienko O 2010 Elastic response of floating glacier ice to impact of long-period ocean waves *J. Geophys. Res.: Earth Surf.* **115**
Sergienko O V, Macayeal D R and Bindschadler R A 2009 Stick-slip behavior of ice streams: modeling investigations *Ann. Glaciol.* **50** 87–94
Shearer P 2006 *Introduction to Seismology* 2nd edn (Cambridge: Cambridge University Press)
Smith A 2006 Microearthquakes and subglacial conditions *Geophys. Res. Lett.* **33** L24501
Smith A M 2007 Subglacial bed properties from normal-incidence seismic reflection data *J. Environ. Eng. Geophys.* **12** 3–13
Smith E, Smith A and White R 2015 Mapping the ice-bed interface characteristics of Rutford Ice Stream, West Antarctica, using microseismicity *J. Geophys. Res.* **120** 1881–94
Smith E C, Baird A F, Kendall J M, Martin C, White R S, Brisbourne A M and Smith A M 2017 Ice fabric in an Antarctic ice stream interpreted from seismic anisotropy *Geophys. Res. Lett.* **44** 3710–8
St. Lawrence W and Qamar A 1979 Hydraulic transients: a seismic source in volcanoes and glaciers *Science* **203** 654–6
Stein S and Wysession M 1991 *An Introduction to Seismology, Earthquakes and Earth Structure* (New York: Wiley)
Stuart G, Murray T, Brisbourne A, Styles P and Toon S 2005 Seismic emissions from a surging glacier: Bakaninbreen, Svalbard *Ann. Glaciol.* **42** 151–7
Sullivan W 1961 *Assault on the Unknown; the International Geophysical Year* 1st edn (New York: McGraw-Hill)
Talandier J, Hyvernaud O, Okal E A and Piserchia P F 2002 Long-range detection of hydroacoustic signals from large icebergs in the Ross Sea, Antarctica *Earth Planet. Sci. Lett.* **203** 519–34
Talandier J, Hyvernaud O, Reymond D and Okal E A 2006 Hydroacoustic signals generated by parked and drifting icebergs in the southern Indian and Pacific Oceans *Geophys. J. Int.* **165** 817–34
Talandier J and Okal E A 1998 On the mechanism of conversion of seismic waves to and from T waves in the vicinity of island shores *Bull. Seismol. Soc. Am.* **88** 621–32
Thomas R, Frederick E, Li J, Krabill W, Manizade S, Paden J, Sonntag J, Swift R and Yungel J 2011 Accelerating ice loss from the fastest Greenland and Antarctic glaciers *Geophys. Res. Lett.* **38** L10502
Thomason J and Iverson N 2008 A laboratory study of particle ploughing and pore-pressure feedback: a velocity-weakening mechanism for soft glacier beds *J. Glaciol.* **54** 169–81
Truffer M and Motyka R 2016 Where glaciers meet water: subaqueous melt and its relevance to glaciers in various settings *Rev. Geophys.* **54** 220–39
Tsai V C and Ekstrom G 2007 Analysis of glacial earthquakes *J. Geophys. Res.: Earth Surf.* **112** F03S22
Tsai V C, Minchew B, Lamb M and Ampuero J-P 2012 A physical model for seismic noise generation from sediment transport in rivers *Geophys. Res. Lett.* **39** L02404
Tsai V C, Rice J R and Fahnestock M 2008 Possible mechanisms for glacial earthquakes *J. Geophys. Res.: Earth Surf.* **113**
Tulaczyk S, Kamb W B and Engelhardt H F 2000 Basal mechanics of ice stream B, West Antarctica: 1. Till mechanics *J. Geophys. Res.: Solid Earth* **105** 463–81
van den Broeke M 2008 Depth and density of the Antarctic firn layer *Arctic. Antarct. Alpine Res.* **40** 432–8
van der Wal W, Whitehouse P and Schrama E 2015 Effect of GIA models with 3D composite mantle viscosity on GRACE mass balance estimates for Antarctica *Earth Planet. Sci. Lett.* **414** 134–43
van Herwijnen A and Schweizer J 2011 Monitoring avalanche activity using a seismic sensor *Cold Reg. Sci. Technol.* **69** 165–76
Vance S *et al* 2016 Vital signs: seismology of icy ocean worlds (arXiv:1610.10067v5 [astro-ph.EP])
VanWormer D and Berg E 1970 Seismic evidence for glacier motion *J. Glaciol.* **12** 259–65
Veitch S and Nettles M 2012 Spatial and temporal variations in Greenland glacial-earthquake activity 1993–2010 *J. Geophys. Res.* **117** F04007
Walker R T, Parizek B R, Alley R B, Anandakrishnan S, Riverman K L and Christianson K 2013 Ice-shelf tidal flexure and subglacial pressure variations *Earth Planet. Sci. Lett.* **361** 422–8
Walter F, Amundson J, O'Neel S, Truffer M, Fahnestock M and Fricker H 2012 Analysis of low-frequency seismic signals generated during a multiple-iceberg calving event at Jakobshavn Isbrae, Greenland *J. Geophys. Res.: Earth Surf.* **117** F01036
Walter F, Chaput J and Luthi M 2014 Thick sediments beneath Greenland's ablation zone and their potential role in future ice sheet dynamics *Geology* **42** 487–90
Walter F, Clinton J, Deichmann N, Dreger D, Minson S and Funk M 2009 Moment tensor inversions of icequakes on Gornergletscher, Switzerland *Bull. Seismol. Soc. Am.* **99** 852870
Walter F, Deichmann N and Funk M 2008 Basal icequakes during changing subglacial water pressures beneath Gornergletscher, Switzerland *J. Glaciol.* **54** 511–21
Walter F, O'Neel S, McNamara D, Pfeffer W, Bassis J N and Fricker H A 2010 Iceberg calving during transition from grounded to floating ice: Columbia Glacier, Alaska *Geophys. Res. Lett.* **37** L15501
Walter F, Roux P, Roeoesli C, Lecointre A, Kilb D and Roux P-F 2015a Using glacier seismicity for phase velocity measurements and Green's function retrieval *Geophys. J. Int.* **201** 1722–37
Walter J, Brodsky E, Tulaczyk S, Schwartz S and Pettersson R 2011 Transient slip events from near-field seismic and geodetic data on a glacier fault, Whillans ice plain, West Antarctica *J. Geophys. Res.* **116** F01021
Walter J I, Svetlizky I, Fineberg J, Brodsky E E, Tulaczyk S, Barcheck C G and Carter S P 2015b Rupture speed dependence on initial stress profiles: insights from glacier and laboratory stick-slip *Earth Planet. Sci. Lett.* **411** 112–20
Wathelet M 2008 An improved neighborhood algorithm: parameter conditions and dynamic scaling *Geophys. Res. Lett.* **35** L09301
Wathelet M, Jongmans D and Ohrnberger M 2004 Surface-wave inversion using a direct search algorithm and its application to ambient vibration measurements *Near Surf. Geophys.* **2** 211–21

Weertman J 1957 On the sliding of glaciers *J. Glaciol.* **3** 33–8
West M, Larsen C, Truffer M, O'Neel S and LeBlanc L 2011 Glacier microseismicity *Geology* **38** 319–22
Wiens D A, Anandakrishnan S, Winberry J P and King M A 2008 Simultaneous teleseismic and geodetic observations of the stick-slip motion of an Antarctic ice stream *Nature* **453** 770–3
Winberry J, Anandakrishnan S, Wiens D and Alley R 2013 Nucleation and seismic tremor associated with the glacial earthquakes of Whillans Ice Stream, Antarctica *Geophys. Res. Lett.* **40** 312–5
Winberry J P, Anandakrishan S and Alley R B 2009a Seismic observations of transient subglacial water-flow beneath MacAyeal Ice Stream, West Antarctica *Geophys. Res. Lett.* **36** L11502
Winberry J P, Anandakrishnan S, Alley R B, Bindschadler R A and King M A 2009b Basal mechanics of ice streams: insights from the stick-slip motion of Whillans Ice Stream, West Antarctica *J. Geophys. Res.: Earth Surf.* **114**
Winberry J P, Anandakrishnan S, Alley R B, Wiens D A and Pratt M J 2014 Tidal pacing, skipped slips and the slowdown of Whillans Ice Stream, Antarctica *J. Glaciol.* **60** 795–807
Winberry J P, Anandakrishnan S, Wiens D A, Alley R B and Christianson K 2011 Dynamics of stick-slip motion, Whillans Ice Stream, Antarctica *Earth Planet. Sci. Lett.* **305** 283–9
Withers M, Aster R, Young C, Beiriger J, Harris M, Moore S and Trujillo J 1998 A comparison of select trigger algorithms for automated global seismic phase and event detection *Bull. Seismol. Soc. Am.* **88** 95–106
Yi S, Sun W, Heki K and Qian A 2015 An increase in the rate of global mean sea level rise since 2010 *Geophys. Res. Lett.* **42** 3998–4006
Zhan Z, Tsai V C, Jackson J and Helmberger D 2014 Ambient noise correlation on the Amery Ice Shelf, East Antarctica *Geophys. J. Int.* **196** 1796–802
Zhang H J and Thurber C H 2003 Double-difference tomography: the method and its application to the Hayward fault, California *Bull. Seismol. Soc. Am.* **93** 1875–89
Zoet L, Carpenter B, Scuderi M, Alley R, Anandakrishnan S, Marone C and Jackson M 2013 The effects of entrained debris on the basal sliding stability of a glacier *J. Geophys. Res.: Earth Surf.* **118** 656–66
Zoet L K, Anandakrishnan S, Alley R B, Nyblade A A and Wiens D A 2012 Motion of an Antarctic glacier by repeated tidally modulated earthquakes *Nat. Geosci.* **5** 623–6

Richard Aster (PhD Scripps Institution of Oceanography, 1991) is Professor of Geophysics and Department Head of Geosciences at Colorado State University. His work has included multiple field projects and field seasons in Antarctica, working on the Ross Ice Shelf, in multiple locales in West Antarctica, on Mount Erebus, and at South Pole.

J. Paul Winberry (PhD, the Pennsylvania State University, 2008) is a research geophysicist in the Department of Geological Sciences at Central Washington University. His research is focused on glacier physics as well as the interactions between the solid-Earth and ice-sheets. He has conducted field experiments in Antarctica, Greenland, Alaska, and Norway.